A QUEST FOR ARTICULAR CARTILAGE PROGENITOR CELLS LEADS TO TEMPORAL REGULATION OF HYALURONAN REQUIRED FOR 3T3-L1 ADIPOGENESIS

by

Samantha Sue Sellers

June, 2017

Director of Dissertation: Cheryl B. Knudson

Department: Anatomy and Cell Biology

During embryogenesis, mesenchymal progenitor cells exhibit hyaluronan-dependent pericellular matrices as a major component of the extracellular matrix. As connective tissues form by cellular condensations, there is a loss of cell-associated hyaluronan to facilitate cell-to-cell adhesion. The goal of this dissertation is to gain insight into how hyaluronan-associated components of the extracellular/pericellular matrix participate in directing differentiation fates of mesenchymal cells. This work began with attempts to isolate and study a primary mesenchymal progenitor population from adult bovine articular cartilage and progressed to the use of the adipocyte-favoring mesenchymal progenitor cell line, 3T3-L1. A particle exclusion assay revealed that 3T3-L1 mesenchymal cells exhibited large hyaluronan-dependent pericellular matrices that were displaced by small hyaluronan fragments consisting of 6-8 disaccharides, suggesting retention of the matrix by a cell surface receptor. These pericellular matrices were enhanced with the addition of exogenous aggrecan (prepared from bovine articular cartilage). However, 3T3-L1 cells lost the ability to synthesize or retain a hyaluronan-dependent pericellular matrix during adipogenesis. We observed a reduction in mRNA and protein expression of CD44, the hyaluronan receptor that anchors the pericellular matrix to the cell surface, during adipogenesis, in addition to

a reduction in mRNA expression of *Has2* and *Vcan*. These reductions in pericellular matrix components are likely responsible for the loss of detectable pericellular matrix by 3T3-L1 adipocytes. The importance of CD44's role in pericellular matrix retention was further supported when pericellular matrices could not be formed by 3T3-L1 adipocytes even when exogenous hyaluronan and aggrecan were supplied. Hyaluronan was visualized by staining with a binding protein (HABP) and fluorescent microscopy. Mesenchymal cells exhibited bright cell surface HABP staining whereas adipocytes stained only weakly. However, when the adipocytes were permeabilized with 0.5% Triton-X, hyaluronan was revealed between the lipid droplets of these cells suggesting receptor-mediated endocytosis. When hyaluronan synthesis was blocked with 4-methylumbelliferone, adipogenesis of 3T3-L1 cells was significantly inhibited. Additionally, exogenous aggrecan added to the culture medium during the adipogenic differentiation protocol significantly inhibited adipogenesis. Collectively, these data suggest that 3T3-L1 adipogenesis is dependent upon the temporal regulation of hyaluronan.

A QUEST FOR ARTICULAR CARTILAGE PROGENITOR CELLS LEADS TO TEMPORAL REGULATION OF HYLARUONAN REQUIRED FOR 3T3-L1 ADIPOGENESIS

A Dissertation

Presented to the Faculty of the Department of Anatomy and Cell Biology

East Carolina University

In Partial Fulfillment of the Requirements for the Degree

Doctor of Philosophy in Anatomy and Cell Biology

by

Samantha Sue Sellers

June, 2017

A QUEST FOR ARTICULAR CARTILAGE PROGENITOR CELLS LEADS TO TEMPORAL REGULATION OF HYLARUONAN REQUIRED FOR 3T3-L1 ADIPOGENESIS

by

Samantha Sue Sellers

APPROVED BY:

DIRECTOR OF
DISSERTATION: _____
Cheryl B. Knudson, Ph.D.

COMMITTEE MEMBER: _____
Warren Knudson, Ph.D.

COMMITTEE MEMBER: _____
David Terrian, Ph.D.

COMMITTEE MEMBER: _____
Anthony Capehart, Ph.D.

CHAIR OF THE DEPARTMENT
OF ANATOMY AND CELL BIOLOGY: _____
Cheryl B. Knudson, Ph.D.

DEAN OF THE
GRADUATE SCHOOL: _____
Paul J. Gemperline, Ph.D.

TABLE OF CONTENTS

LIST OF TABLES

LIST OF FIGURES

LIST OF ABBREVIATIONS

^{o}C	degrees Celsius
Δ	delta
3T3-L1	murine mesenchymal pre-adipocyte cell line
Acan, Agg	aggrecan
ADAMTS	a disintegrin and metalloprotease with thrombospondin motif
Adipo	adipogenic media
HABP-B, HABP-b	biotinylated hyaluronan binding protein
BAC	bovine articular chondrocytes
BASC	bovine articular stem cells
bp	base pairs
BSA	bovine serum albumin
C3H10T1/2	murine mesenchymal cell line
CD44	clusters of differentiation forty-four
cDNA	complementary deoxyribonucleic acid
cm	centimeter
CsCl	cesium chloride
CT	cycle threshold

CTL	control
D6, D10	day 6, day10
DAPI	4, 6-diamidino-2-phenylindole, dihydrochloride
DEX	dexamethasone
DMEM	Dulbecco’s modified Eagle’s medium
DNA	deoxyribonucleic acid
ECM	extracellular matrix
EDTA	ethylenediaminetetraacetic acid
ELISA	enzyme-linked immunosorbent assay
Fabp4	fatty acid binding protein four
FBS	fetal bovine serum
FSC	forward scatter channel
g	gravity
Gapdh	glyceraldehyde 3-phosphate dehydrogenase
HA	hyaluronan
HYAL	hyaluronidase
HABP	hyaluronan binding protein
HAS	hyaluronan synthase

HCl	hydrochloric acid
HRP	horseradish peroxidase
JSN	joint space narrowing
kDa	kilodalton
M	molar
MCF-7	human breast carcinoma cell line
MG-63	osteogenic sarcoma cell line
MIX	methylisobutylxanthine
mg	miligram
ml	milliliter
mm	micromass
MM	maintenance media
mM	millimolar
MMPs	matrix metalloprotease
Mono	monolayer
N_2	nitrogen
NaCl	sodium chloride
Na_2SO_4	sodium sulfate

ND	not detected
nm	nanometer
OA	osteoarthritis
oligos	oligosaccharides
PBS	phosphate buffered saline
PCM	pericellular matrix
PI	propidium iodide
Pparγ	peroxisome proliferator-activated receptor gamma
RBC	red blood cell
RCS	rat chondrosarcoma cell line
RNA	ribonucleic acid
rpm	rotations per minute
SSC	side scatter channel
SH	*Streptomyces* hyaluronidase
S. H'dase	*Streptomyces* hyaluronidase
TAE	Tris acetate EDTA
Tris	tris (hydroxymethyl) aminomethane
U	unit

UV	ultraviolet
V	volt
Vcan	versican
µg	microgram
µl	microliter
µM	micromolar

CHAPTER 1: INTRODUCTION

1. Overall Summary

A new cell type isolated from articular cartilage has been described as having progenitor characteristics. This discovery offers new hope for cartilage regeneration therapies that could potentially replace or enhance current cartilage repair techniques that can at times produce structurally inadequate cartilage. The ability to quickly efflux the vital stain Hoechst 33342 is commonly used to isolate these (chondro)progenitor cells, collectively called a "side population". Differential adhesion to fibronectin has been used to enrich the side population and some investigators have used putative mesenchymal progenitor cell markers CD105, CD166, and Notch-1 to isolate these chondroprogenitor cells. However, the use of these markers to isolate the side population from articular cartilage is still debated.

There are several proposed markers for the identification of progenitor cells but induced differentiation into different cell types is a very convincing demonstration of multipotency. Three common lineages to demonstrate multipotency of mesenchymal progenitor cells are chondrocytes, osteocytes, and adipocytes. Three well characterized cell lines were chosen to serve as positive controls for each of these differentiation pathways, C3H10T1/2 for chondrogenic, MG-63 for osteogenic, and 3T3-L1 for adipogenic differentiation. While cells isolated from articular cartilage induced to differentiate into osteocytes is not particularly impressive, those same cells induced to become adipocytes would provide more conclusive evidence of multipotency, therefore the primary focus was to establish a working adipogenesis protocol with 3T3-L1 cells. In addition to

differentiation experiments, these same three cell lines were used to verify that our lab could identify Hoechst 33342 efflux by microscopic observation.

Out of the three cell lines tested for Hoechst 33342 efflux potential via microscopic observation, it was evident that 3T3-L1 cells had the highest Hoechst 33342 efflux capability which was surprising since this cell line is considered unipotent to pre-adipocytes. The 3T3-L1 cell line is a well-established model for studying adipogenesis but could potentially become an even greater asset for researching mesenchymal cell differentiation if multipotency could be established. Even though this was not a primary goal of this dissertation, some preliminary experiments demonstrated that after induction with chondrogenic medium in micromass culture, 3T3-L1 cells showed chondrogenic potential with positive alcian blue staining and increased expression of chondrogenic markers, aggrecan and hyaluronan synthase-2. Much more research is needed to confirm the use of 3T3-L1 cells as a potential model for chondrogenesis but these initial experiments are promising.

For my original goal, I was able to successfully isolate a side population in bovine articular cartilage cells using flow cytometry to detect increased Hoechst 33342 efflux but not in sufficient numbers to make downstream differentiation experiments feasible. Researchers have circumvented low side population numbers by expanding their populations, but this is undesirable since primary chondrocytes maintained in monoculture have been shown to dedifferentiate, developing morphology changes that resemble mesenchymal cells. I attempted to enrich the side population by selecting cells able to adhere to fibronectin, a documented characteristic of

progenitor cells, but was unable to detect a difference in Hoechst 33342 efflux by microscopic observation in fibronectin adherent (progenitor) vs non-adherent cells. However, while additional attempts were made to increase side population cell numbers, I worked to establish an adipogenesis protocol with 3T3-L1 cells.

During adipogenic differentiation of 3T3-L1 cells, the culture medium became notably more viscous. This interesting observation was pursued to find that the increased viscosity was partly attributed to increased hyaluronan in the culture medium as noted by previous researchers. However, there appeared to be a clear gap in knowledge as to how hyaluronan and hyaluronan-associated components of the extracellular matrix contributed to directing differentiation of these 3T3-L1 mesenchymal cells into adipocytes. This led us to investigate changes in the pericellular matrix and its components during adipogenesis while my attempts to increase the side population cell numbers for my original goal went without success.

This study found that mesenchymal 3T3-L1 cells exhibit large hyaluronan-dependent pericellular matrices, but during adipogenesis, 3T3-L1 cells lost the ability to retain a pericellular matrix even when supplemented with exogenous hyaluronan and aggrecan. This could partly be explained by the decrease in the hyaluronan receptor, CD44, which anchors the pericellular matrix to the cell surface. In addition, hyaluronan was visualized mainly on the surface of mesenchymal 3T3-L1 cells whereas the majority of hyaluronan was discovered inside adipocyte 3T3-L1 cells, between lipid droplets. These findings reveal that hyaluronan is removed from the surface of 3T3-L1 cells as they transition from mesenchymal progenitor cells to adipocytes, either by release from

the cell surface or by internalization or likely both. However, whether the reduction of cell surface hyaluronan is required for adipogenesis to occur or is merely a by-product of the differentiation process remained unknown. Our lab and many others have used 4-MU as an inhibitor of hyaluronan biosynthesis. This study found that inhibition of hyaluronan synthesis with 4-MU treatment throughout the adipogenic protocol significantly decreased adipogenesis of 3T3-L1 cells. Others have reported that treatment with hyaluronidase to degrade synthesized hyaluronan during adipogenesis also significantly inhibited 3T3-L1 adipogenesis. These findings suggests the presence of hyaluronan is a requirement for 3T3-L1 adipogenesis to occur.

Our lab has shown the addition of exogenous aggrecan to chondrocytes blocks endocytosis of CD44 and hyaluronan. Treatment of 3T3-L1 mesenchymal cells with exogenous aggrecan caused the pericellular matrix to swell as aggrecan molecules fully decorated hyaluronan. This study found that the addition of exogenous aggrecan to the culture media during the adipogenic protocol led to a significant decrease in adipogenesis of 3T3-L1 cells. The mechanism of this inhibition could be due to blocked hyaluronan endocytosis or blocked release from the cell-surface. These findings indicate that not only the presence of hyaluronan is required for 3T3-L1 adipogenesis, but that hyaluronan molecules bound to the cell surface must not be sterically hindered and available for endocytosis or interaction with other molecules. The major findings of this study reveal that not only is the presence of hyaluronan required but also that hyaluronan must then be removed from the cell surface for 3T3-L1 adipogenesis to occur suggesting that 3T3-L1 adipogenesis is dependent upon the temporal regulation of hyaluronan.

2. Articular Cartilage

2.1. Structure and function

Articular cartilage is a smooth, viscoelastic, connective tissue that lines the surface of articulating bones of diarthrodial joints to provide a low-friction, load-bearing surface that allows joint movement. Articular cartilage offers protection to subchondral bone from mechanical stress by redistributing weight and resisting compression. This ability is afforded by the unique properties of the extracellular matrix (ECM) which comprises over 90% of the total mass of articular cartilage. The ECM is composed of proteoglycans, collagen fibrils, and a variety of other macromolecules [1]. Aggrecan is the predominate proteoglycan in the ECM of articular cartilage and attracts water molecules which allows for shock absorption and compression resistance because of its negative charge [2]. Type II collagen is the most abundant type of collagen in articular cartilage and provides tensile strength and shape for the tissue as well as a framework to resist the swelling pressure of aggrecan [3]. Collagens IX and XI are important in the fibrillary network; mutations in these genes result in chondrodysplasia with early onset osteoarthritis [4]. In addition, collagen-binding receptors, such as integrins and the discoidin domain receptor-2 are essential for mediating cell-matrix interactions in articular cartilage [5]. The remaining percentage of articular cartilage's total mass (estimates range between 1% and 10%) is made up of its cellular component, chondrocytes being the main cell type found in this tissue [6-8].

Articular cartilage is arranged into horizontal, laminar zones that are characterized mainly by chondrocyte shape and collagen orientation. The layer adjacent to the subchondral bone consists of hypertrophic chondrocytes and a calcified matrix called the calcified zone. The deep zone, next to the calcified zone, is characterized by a special distribution of collagen fibrils that form vertical

columns around rapidly proliferating chondrocytes [9, 10]. The middle zone is described as having collagen fibers that twist into circles or intersect into a bent crosshatch network around round chondrocytes [11]. Flat, nearly inactive chondrocytes with collagen fibers parallel to the surface are found in the superficial zone next to the joint space [12]. The arrangement and organization of articular cartilage reflects its purpose. The superficial zone provides a smooth, nearly friction free surface while deeper zones are responsible for shock absorption and compression resistance.

In addition to horizontal zones, the ECM can be further divided into circumferential zones based on proximity to chondrocytes. They are, from farthest to closest to a resident chondrocyte, called the interterritorial, territorial, and pericellular matrices. While they contain many of the same molecular components, there are some distinct differences in the structure and composition between them. The interterritorial matrix is characterized as having a higher concentration of keratan sulfate rich proteoglycans while more chondroitin sulfate rich proteoglycans are found in the territorial matrix [1, 13]. The pericellular matrix is generally characterized as having higher concentrations of fibronectin, proteoglycans, and type VI collagen, when compared to the rest of the ECM [14], but its underlying scaffold is comprised of hyaluronan, a non-sulfated polysaccharide [15]. Through hyaluronan, the pericellular matrix gains another of its defining characteristics which is direct anchorage to the cell surface via hyaluronan binding receptors, such as CD44 [16]. Hyaluronan will be discussed further in section 3. Because of its intimate association with chondrocytes, the pericellular matrix influences many biochemical or biophysical signals they receive and therefore, plays an important role in regulating cell biosynthesis [17]. For example, aggrecan, which is synthesized inside chondrocytes and then secreted, is converted into a form with a higher binding affinity for hyaluronan outside the cell in the matrix [18].

2.2. Articular cartilage cells

Chondrocytes, the main cell type in articular cartilage, either singly or in groups, establish a specialized microenvironment, the pericellular matrix, that together are called the "chondron" and can be thought of as a functional unit of articular cartilage [19]. Unlike the majority of cells found in other tissues, most chondrocytes exist without direct cell-cell contact and have a hypoxic metabolism [20]. Because articular cartilage is an avascular tissue, chondrocytes rely on diffusion from the articular surface for their nutrients and metabolites [13]. Chondrocytes are responsible for synthesis, degradation, and regulation of *all* components of the ECM, including large volumes of collagens, glycoproteins, and proteoglycans. They also maintain homeostasis of the articular cartilage matrix by sustaining a balance between catabolic and anabolic events [8, 21]. The number of chondrocytes in articular cartilage remains relatively unchanged throughout life, although their distribution differs. The superficial zone of articular cartilage shows a decrease of chondrocytes while deeper zones show an increase [22]. This redistribution likely leads to decreased superficial ECM maintenance and a decrease in lubrication of the articular cartilage surface, resulting in decreased proteoglycan aggregates causing increased tissue stiffness and likelihood for injury.

Historically, chondrocytes were thought to be the only cell type in articular cartilage, however, a population of cells recently found in articular cartilage has been shown to have progenitor characteristics such as a high colony formation capacity, mesenchymal stem cell markers, and acquire a chondrogenic phenotype after several passages [23, 24]. These cells, termed chondro-progenitors, have been isolated from bovine, mouse, and even human articular cartilage [24-26]. Both healthy and osteoarthritic articular cartilage contain cells with putative mesenchymal progenitor markers such as CD105, CD166, and Notch-1 but it is heavily

emphasized that widely accepted markers may not be applicable for detection of progenitors in articular cartilage [27, 28]. These cells also respond to transforming growth factors (TGFs) and enhance synthesis of articular cartilage markers, aggrecan and collagen II [25, 26]. Unlike MSCs isolated from bone marrow, these chondroprogenitor cells can maintain chondrocyte phenotype without calcification or expression of hypertrophic traits in 3D culture systems [29, 30]. In other tissues, stem/progenitor cells provide a renewable source of cells capable of replacing damaged differentiated cells. This discovery opens the possibility of targeting a resident progenitor cell population within articular cartilage for not only repair, but regeneration of damaged cartilage.

2.3. Osteoarthritis

2.3.1. Definition and characterization

Due to its avascular nature and low mitotic activity, articular cartilage displays little capacity for self-repair [9]. Any lesions or minor injuries occurring in articular cartilage are unlikely to heal and will frequently lead to degenerative joint diseases such as osteoarthritis (OA) [31]. OA does not affect just the articular cartilage, but rather the whole diarthrodial joint. This is a complex organ consisting of several key components, including articular cartilage, subchondral bone, and synovial membrane lining the inner layer of the fibrous joint capsule. OA results in osteophyte formation, subchondral bone remodeling, and synovial membrane inflammation which may further articular cartilage tissue degradation. Osteoarthritic change starts with the loss of the superficial layer of articular cartilage and as the disease progresses, deeper zones are damaged and lost [10]. The surface of OA cartilage appears frayed and jagged when compared to healthy cartilage. The shearing of cartilage signals a local inflammatory response (without neutrophils or

macrophages) that releases proinflammatory cytokines like interleukin (IL)-1 and tumor necrosis factor (TNF)-α. These catabolic cytokines are needed at low levels for homeostasis and are balanced by anabolic, inhibitory cytokines like those in the bone morphogenetic protein (BMP) family. OA disease is thought to progress when disruption of this balance is tipped in favor of the catabolic cytokines [32].

Catabolic cytokines induce expression of proteinases that breakdown components of the ECM. The main aggrecanase upregulated in OA cartilage is the disintegrin and metalloproteinase with thrombospondin motifs (ADAMTS)-4 [33]. ADAMTS-4 first cleaves aggrecan in the superficial layer and immediately surrounding chondrocytes. This produces a halo around chondrocytes when stained with safranin-O and is considered one of the first histological signs of OA disease. The main collagenase upregulated in OA cartilage is the matrix metalloproteinase (MMP)-13 which cleaves several types of collagen [34]. Collagen cleavage is considered a late response in OA and is not reversible, whereas cleavage of aggrecan is considered an early response and is reversible by *de novo* synthesis of aggrecan by resident chondrocytes [35].

Cartilage defects are traditionally categorized by the four grades of the Outerbridge classification system in which grade I is defined as swollen and softened cartilage, grade II contains fragmentation or fissures 1.27 cm or less. If the defect exceeds this size, it is classified as grade III until the injury reaches the subchondral bone in which case it is then classified as grade IV [36]. However, since OA affects the whole joint and not just the articular cartilage, a different classification system is needed to define its severity and progression.

Today, the most widely used classification tool for the radiographic diagnosis of OA is the five grade scheme developed by Kellgren and Lawrence (KL) in 1957 [37]. The KL classification system distinguishes grades using mainly joint space width and osteophyte formation. Osteophytes are fibrocartilage capped bony outgrowths that originate from the periosteum of cortical bone [38]. Grade 0 is healthy articular cartilage with no signs of joint space narrowing (JSN) or osteophyte formation. Grade 1 has doubtful JSN with possible osteophyte formation while grade 2 has definite osteophyte formation with possible JSN. Grade 3 joints are defined as having moderate osteophytes, definite JSN, and some bone-end deformity. The most severe, grade 4, is characterized by large osteophytes, marked JSN, and definite bone-end deformity. While this system has been criticized for not being entirely appropriate for monitoring the progression of OA, it still remains the most widely used for assessing the initial severity of OA when patients present with pain [39].

2.3.2. Economic burden

The most common cause of chronic disability in older adults is OA, which is considered a 'wear and tear' disease defined as the progressive degeneration of articular cartilage [40]. Clinically, OA is characterized by joint pain, limitation of movement, popping sounds from the affected joint, stiffening after periods of immobilization, and different degrees of inflammation [41]. The main risk factors for developing OA are, age (elderly people), gender (women more than men), prior joint injuries, misalignment of the joint, abnormal biomechanics, genetic predisposition and obesity [42]. OA causes a significant amount of pain and loss of mobility for approximately 12.1% of the entire US population, over 35 million people, and is a significant economic burden [43]. In a study completed with 2011 data, OA patients were found to have a

greater comorbidity burden and spend nearly four times as much on overall healthcare costs per year compared to patients without OA, $8,644 compared to $2,273 [44]. Additionally, OA patients were found to lose almost twice as much time from work due to pain or recovery, which raised their indirect costs even more [45]. Patients with OA incur greater direct and indirect medical costs in addition to decreased quality of life and work productivity compared to those without OA.

2.3.3 Current treatments

Current treatment for focal articular cartilage defects focus on reducing pain while surgical options aim to regenerate or replace damaged articular cartilage. Symptoms of early OA, such as pain, stiffness, and swelling are usually treated non-surgically with oral/topical pharmaceuticals, physical therapy, and/or life-style changes such as increased activity and weight loss. When these are no longer effective, more invasive procedures are available to alleviate symptoms. Intraarticular injections of corticosteroids or hyaluronan have been shown beneficial for reliving acute flare-ups but are not recommended for long term use as they have also been shown to eventually accelerate degradation of articular cartilage [46-48]. In the not so distant past, when OA had become well developed and there was no more hope for re-establishing a healthy cartilage surface, prosthetic joint replacement was the only solution for restoring mobility to the affected joint. However, in recent years, several alternative surgical methods have been developed that aim to regenerate articular cartilage. The three main techniques that are currently employed are microfracture, osteochondral grafts, and autologous chondrocyte implantation.

Steadman *et al.* (2010) describes microfracture as a regenerative technique in which mesenchymal stem cells are recruited from subchondral bone and bone marrow. This method is

recommended for grade III and some IV cartilage defects that do not include loss of the underlying bone and are surrounded by healthy cartilage. A 2-4 mm perforation is made in the subchondral bone to allow migration of bone marrow progenitor cells to the open space. A fibrin clot is formed that remodels into fibrocartilaginous tissue over a period of 12-16 months [49]. Fibrocartilage is inferior to hyaline cartilage and lacks mechanical properties that allow it to withstand mechanical stress over time [50]. In addition, this microfracture technique requires a very long post-operatory period where weight bearing is restricted until mostly healed. Some reports have shown that although patients initially feel significantly improved, the affected joint functionality is not maintained for more than a year and efficacy depends on other factors such as patient age, compliance with post-operative rehabilitation, and size of initial damage.

Osteochondral grafts involve transplantation of full-thickness cartilage samples, including subchondral bone, from either the patient (autograft) or a cadaver (allograft). Allografts allow for a larger area of cartilage to be replaced but come with the increased risk of disease transmission while autografts are considered safer but limit the size of the defect that can be repaired and come with complications at the donor site [51]. Osteochondral grafts have a much shorter post-operative period than microfracture, about 6 weeks, and an even longer efficacy period of about 10 years [52]. However, a shortage of available healthy tissue makes this option for only relatively small defects.

Autologous chondrocyte implantation (ACI) was developed as a two stage process, involving an arthroscopic and surgical step, to treat large cartilage defects [53]. Peterson *et al.* (2000) reports that ACI is generally recommended for patients with grade III and IV cartilage

defects, with preferably intact subchondral bone, and for whom other treatments have not been successful. Normal articular cartilage is harvested from a non-weight bearing area and then expanded *in vitro* before being applied to the damaged area during a second surgery [54]. Articular cartilage is not a cellularly dense tissue, therefore the number of cells harvested is very limited. During expansion, chondrocytes do not maintain their phenotype well and tend to de-differentiate in culture. De-differentiated chondrocytes express fewer markers for hyaline cartilage, collagen II and aggrecan, and more markers for fibrocartilage, collagen I and versican. However, studies have shown that two years after implantation, markers for both hyaline and fibrocartilage can be detected [54, 55]. Currently, the only Food and Drug Administration (FDA) approved method of tissue engineering in the United States is the transplantation of *in vitro* expanded autologous chondrocytes commercialized under the name of Carticel® [56]. This procedure still requires a long post-operative period of limited weight-bearing but good results have been reported, however there is still room for improvement.

The most appropriate cell source for cartilage tissue engineering is one that is either abundant or can be easily expanded and which can produce large amounts of ECM components specific to hyaline cartilage without de-differentiation (or with re-differentiation after *in vitro* expansion of cell numbers). Mesenchymal stem cells (MSCs) can be isolated from numerous tissues and can differentiate into several musculoskeletal lineages, including chondrocytes [57, 58]. While there isn't a perfect solution, the use of MSCs promises significant opportunities for cartilage engineering, but their characterization is still ill-defined and there are currently no established guidelines for MSCs to be used clinically [57]. Additionally, a subpopulation of MSCs

isolated from articular cartilage, chondroprogenitor cells, are a current focus of research efforts to repair articular cartilage defects and inhibit the onset of OA [25-27, 29, 30].

3. Adipose tissue

Adipose tissue is a metabolically dynamic organ that is classified into two types; white and brown [59]. Brown adipose tissue is a specialized thermogenic tissue that converts chemical energy into heat and is protective against metabolic disease. Rodents and other small mammals have copious brown adipose tissue deposits but larger mammals often lose most of their brown adipose tissue after infancy [60]. White adipose tissue is the most abundant type of adipose tissue in large mammals and is defined by its long term energy storage in the form of triacylglycerides in unilocular lipid droplets [61]. While not thermogenic, white adipose tissue does provide thermal insulation and efficient energy storage, as well as having extensive distribution in the body to offer mechanical protection and lower friction for muscle bundles and organs to move without compromising their functional integrity [60].

The predominant cell type in adipose tissue is the adipocyte and there are three types found in mammals; white, brown, and beige (brite). They differ in origin, morphology, number of mitochondria, and thermogenic gene expression [62]. White adipocytes are mainly found in white adipose tissue and are of mesenchymal origin. They have a unilocular lipid droplet, few mitochondria, and a low oxidative rate [63]. Brown adipocytes comprise brown adipose tissue and

are derived from myogenic precursor cells [64]. They have a smaller diameter than white adipocytes, abundant mitochondria, contain multilocular lipid droplets, and dissipate stored energy in the form of heat [65]. There is a second thermogenic type of adipocyte called beige or brite which is a "brown-like" adipocyte with multilocular morphology. Studies have suggested that these cells can arise from *de novo* differentiation of mesenchymal/adipocyte progenitor cells or from transconversion of white adipocytes but underlying molecular mechanisms of this lineage remain unknown [66].

3.1. Cell model for adipogenesis study

The study of pre-adipocyte differentiation *in vivo* is difficult because adipose tissue in adult mammals is roughly only one third adipocytes with the remaining two-thirds a combination of pre-adipocytes, fibroblasts, blood vessels, and nerve tissue [67]. In addition, little work has been completed with primary cultures because distinguishing between fibroblasts and pre-adipocytes is challenging due to their similar morphology, however, significant progress has been made in the last few years separating these two cell types with flow cytometry [68]. Also, since pre-adipocytes constitute such a small portion of adipose tissue, large amounts are required to isolate a relevant amount for experimental purposes. The limited life span of primary cultures also contributes to the difficulty in studying adipogenesis *ex vivo*. Therefore, pre-adipocyte differentiation has been primarily studied using *in vitro* cell models, most notably, the so called "unipotent" pre-adipocyte 3T3-L1 cell line [69, 70].

The 3T3-L1 cell line was derived from the fibroblastic NIH 3T3 cell line which are from disaggregated Swiss 3T3 BALB/c mouse embryos [71]. The parental NIH 3T3 cell line is highly

susceptible to spontaneous transformations that allow it to adapt to a variety of culture conditions [72-75]. The adipogenic ability of 3T3-L1 cells has been demonstrated numerous times and our findings here were repeated with different cell stocks and passage numbers which suggest our results are likely due to the inherent characteristics of the 3T3-L1 cells instead of the pre-neoplastic nature of their parental NIH 3T3 cell line. The 3T3-L1 cell line is one of the most well-characterized and reliable models for studying the conversion of pre-adipocytes to adipocytes [76]. When injected into mice, 3T3-L1 cells differentiate and form fat pads that are indistinguishable from normal adipose tissue [77]. Additionally, in culture, differentiated 3T3-L1 cells possess most of the ultrastructural characteristics of adipocytes from animal tissue with the formation and appearance of developing lipid droplets mimicking live adipose tissue [71, 78]. Because of this, 3T3-L1 cells have been extensively studied to establish the underlying molecular mechanisms of adipogenesis.

3.2. Adipogenesis of 3T3-L1 cells

Differentiation of pre-adipocytes to adipocytes involves a comprehensive network of transcription factors that are responsible for expression of key proteins to induce mature adipocyte formation [79]. The process of adipogenesis also involves significant changes in cell morphology, induction of insulin sensitivity and changes in secretory capacity of cells. Once 3T3-L1 cells reach confluence, the cell-cell contact inhibits replication and induces very early markers of adipocyte differentiation, including lipoprotein lipase and collagen VI [80, 81]. Confluent 3T3-L1 cells can be induced to undergo adipogenesis simultaneously by a defined adipogenic medium that includes a combination of a glucocorticoid, an agent that elevates intracellular cAMP levels, and insulin, all in the presence of fetal bovine serum [82]. Dexamethasone is used to stimulate the

glucocorticoid pathway and methylisobutylxanthine, a cAMP-phosphodiesterase inhibitor, is used to stimulate the cAMP-dependent protein kinase pathway while insulin acts by stimulating cells to take up glucose, which is then stored in the form of triglycerides [83].

About 24 hours after treatment with an adipogenic medium, 3T3-L1 cells undergo a post-confluent mitosis, completing at least one round of DNA replication and cell division. By the second day, the cells complete mitosis and enter growth arrest again, committing the cells to adipogenic differentiation [84]. This mitosis step is believed to be necessary to unwind DNA so that transcription factors can gain access to regulatory response elements present in genes involved in modulating the mature adipocyte phenotype [85]. CCAAT/enhancer binding proteins (C/EBP) β and δ are the first transcription factors induced after exposure to the adipogenic inducers. C/EBPβ and δ activity mediate the expression of transcriptions factors C/EBPα and peroxisome proliferator-activated receptor (PPAR) γ. Expression of either C/EBPα or PPARγ alone leads to the expression of the other (they serve as a positive feed-back loop for each other), suggesting that, at the final stages of adipogenesis, both C/EBPα and PPARγ function in a cooperative manner to induce adipocyte specific genes that establish the mature adipocyte phenotype [86]. The terminal differentiation stage of adipocytes is characterized by induction of genes that are important for insulin action, lipid synthesis, and transport. Many of these genes have promoters that contain regulatory elements for PPARγ, like the fatty acid binding protein (FABP)-4, which is a lipid chaperone and considered a marker for late adipogenesis [87]. PPARγ is capable of promoting adipogenesis in C/EBPα deficient cells but C/EBPα is not able to promote adipogenesis in PPARγ deficient cells. Therefore, even though these two transcription factors mutually induce the expression of each other, only PPARγ is considered the master regulator of adipogenesis [88].

The commitment of pre-adipocytes to adipocytes involves various signaling pathways that influence key regulators of adipogenesis, like C/EBPα and PPARγ. Adipogenic differentiation is governed by sequential activation of a number of other transcription factors that function downstream of signaling pathways leading to adipocyte establishment. One signaling pathway that affects adipocyte differentiation is initiated by transforming growth factor (TGF)-β which has been shown to inhibit adipogenesis in vitro [89]. While the exact mechanism of TGF-β adipogenic inhibition is still unknown, studies have shown that inhibition occurs through a Smad3 dependent pathway in which Smad3, activated by TGF-β, binds to C/EBPβ and C/EBPδ and inhibits their transcriptional activity [89, 90]. This in turns leads to decreased PPARγ transcription, which is the main regulator for adipogenesis.

3.3. Extracellular matrix during adipogenesis

An understanding of the control of cell shape, growth and differentiation requires consideration of interactions between the cell and its environment. Although the transcriptional regulation of adipogenesis has been extensively studied, the role of the extracellular matrix (ECM) microenvironment on the regulation of adipogenesis has not been fully elucidated. However, there is increasing evidence that the ECM strongly influences adipogenesis and that extracellular macromolecules can regulate cell behavior directly to the cell interior through receptor-mediated interactions. In a study of human mesenchymal stem cells (MSC), ECM for adipogenesis and osteogenesis were designed to mimic the stages of differentiation of the two cell types, which was found to regulate the expression of transcription factors effectively controlling the balance of adipogenesis and osteogensis in MCSs [91].

The ECM maintains a very dynamic equilibrium between the synthesis and degradation of ECM proteins for maintenance and remodeling. Matrix metalloproteases (MMPs) contribute to ECM remodeling by degrading ECM and basement membrane components for adipocyte differentiation and expansion [92]. Although comprehensive MMP substrate discovery screens have just begun, it is generally stated that every component of the ECM can be cleaved by one or more of the 23 members of the MMP family [93-95]. Several studies have demonstrated that activity of MMPs are required for adipogenesis to occur and that their inhibition decreases adipocyte differentiation [92, 96]. For example, upon addition of adipogenic inducers, the tissue inhibitor of MMP (TIMP)-3 expression is strongly reduced and is maintained at low levels throughout adipogenesis. In addition, overexpression of TIMP-3 in 3T3-L1 cells inhibits adipocyte differentiation through repressed C/EPBβ expression [97]. This suggests TIMP-3 down regulation is essential for adipocyte differentiation and is specifically involved in the regulation of early adipogenic induction.

The ECM components associated with the cytoskeleton via receptors, like integrins, play an important role in the morphological change during adipogenesis. Integrins are essential to link ECM components, like collagen, to the cell surface. Crosstalk between ECM components and transcription factors, including PPARγ, influence adipocyte differentiation [98]. Signaling through type I collagen has been suggested to be a key regulatory component during adipogenesis because its continued expression decreased expression of PPARγ [99].

The plasma membrane glycoprotein, CD44, is also essential for mediating cell-matrix interactions although very little is known about its role in adipogenesis. CD44 is the principal cell

surface receptor for hyaluronan, an integral part of the ECM that is discussed in the next section. CD44 appears to exhibit a capacity for cell signaling induced by alterations in CD44-HA interactions [100, 101]. In addition, the cytoplasmic domain of CD44 has been shown to interact with cytoskeletal adaptor proteins ezrin, radixin, and moesin (ERM) [102] as well as ankyrin [103, 104]. These interactions may suggest a role for CD44 in the cell shape which is drastically altered as the pre-adipocyte changes from a fibroblast form to the rounded cell shape distinctive in mature adipocytes. Transient knockdown of membrane-cytoskeleton linker proteins ezrin, radixin, and moesin (ERM) caused disassembly of actin fiber and focal adhesions which decreased cell stiffness resulting in inhibited adipogenesis in human MSCs [105]. Several studies have described an increase in cell stiffness with adipocyte differentiation due to the increase in mono- and polysaturated fatty acids in the lipid monolayer surrounding newly formed lipid droplets [106, 107]. Additionally, a decrease in actin and tubulin expression is an early event in adipocyte differentiation that precedes overt changes in morphology and the expression of adipocyte specific genes. These changes in cell shape reflect a distinct process in differentiation and are not the result of accumulated lipid stores [108]. The drastic morphological changes observed during adipocyte differentiation occur even when triglyceride accumulation is blocked [109]. But whether CD44 plays a role is still unknown.

4. Hyaluronan

Hyaluronan was first purified from the vitreous humor of bovine eyes by Karl Meyer in 1934 [110]. In the 1950s, Meyer and colleagues determined that hyaluronan was a linear polysaccharide composed of repeating units of N-acetylglucosamine and D-glucuronic acid. This disaccharide moiety is repeated thousands of times generating a molecule with a molecular mass ranging from 0.5 to 20 million Daltons or more [111]. Hyaluronan has several names which reflect the properties of the molecule under various conditions. When first isolated, hyaluronan behaved like a mild acid and was therefore named "hyaluronic acid" [110]. Under physiological conditions, hyaluronan existed as an electrolyte and associated with cations, often as a sodium salt, which prompted the name sodium hyaluronate. The name was later amended to just hyaluronate in reference to its salt form or hyaluronan to encompass all forms of the molecule and that it is included in the glycosaminoglycan family [112].

Hyaluronan is not branched, it does not contain any sulfate groups and it is not covalently linked to a proteoglycan protein core [113]. This makes hyaluronan an atypical glycosaminoglycan with a very simple chemical composition. Despite this, hyaluronan fulfills several distinct molecular functions that contribute not only to the structural and physiological characteristics of tissues, but also to the mediation of cell behaviors during morphogenesis, tissue remodeling, inflammation and disease [114, 115]. Hyaluronan is extremely hydrophilic and attracts large amounts of water to provide hydration and lubrication to various tissues. Through its interaction with proteoglycans and link proteins, hyaluronan organizes and maintains the structural integrity of extracellular and pericellular matrices. As a signaling molecule, hyaluronan interacts with a

variety of cell surface receptors and hyaluronan-binding proteins to activate intracellular events to mediate cell functions [113, 114]. Even though its concentration and binding partners vary, hyaluronan is ubiquitously found in the ECM of all vertebrate tissues and is evolutionarily conserved across mammalian species which further suggests its biological importance [116].

4.1. Hyaluronan synthesis and degradation

Unlike other glycosaminoglycans that are synthesized in the Golgi apparatus, hyaluronan is synthesized at the inner face of the plasma membrane by the integral membrane glycosyltransferase, hyaluronan synthase (HAS) [117, 118]. There are three eukaryotic isoforms that have been identified that are responsible for all hyaluronan synthesis in mammalian species, HAS1, HAS2, and HAS3 and they all share significant amino acid homology across different species [119]. Each HAS contains two distinct membrane domains, a cytoplasmic loop containing the catalytic site and the binding sites for the two UDP-sugar precursors [120]. Hyaluronan is polymerized as HAS alternatively adds UDP-N-acetylglucosamine and UDP-glucuronic acid monomers to the reducing end of the growing polymer. As polymerization occurs, the non-reducing end of the chain is translocated through the plasma membrane where it can be released into the ECM or retained at the cell surface [121]. A Pore Translocation Model has been proposed to explain how hyaluronan reaches the outside of the cell in which the growing disaccharide chain is translocated through the HAS enzyme itself to the exterior of the cell [122]. The exact mechanism by which hyaluronan synthesis is terminated remains unknown but is partly responsible for varying sizes of hyaluronan chains.

The three individual HAS isoforms also produce hyaluronan of differing sizes [123]. HAS1 and HAS2 are able to produce higher molecular weight hyaluronan while HAS3 produces relatively low molecular weight hyaluronan [124]. Other factors can alter the size of hyaluronan such as hyaluronidases, alterations to the UDP sugar pool, or the action of oxygen radicals which can all can result in fragments of short oligosaccharides that can trigger inflammation or MMP activation [125-128]. Hyaluronan chain size is critical in many cellular process including some pathophysiological conditions. Examples include; angiogenesis, wound repair, proliferation and migration, induction of inflammatory genes, and differentiation [129-133]. When native hyaluronan is displaced by short oligosaccharides, the pericellular matrix is reduced in size [16] and catabolic factors are activated in articular chondrocytes [101]. Native hyaluronan displaced by oligosaccharides significantly decreases proliferation and migration of vascular smooth muscle cells [134]. In addition, high molecular weight hyaluronan was shown necessary for normal cardiac morphogenesis in mice [135].

4-Methylumbelliferone (4-MU) specifically inhibits HAS activity at the post-transcriptional level and results in a significant decrease in both hyaluronan synthesis and extracellular formation. The mechanism of 4-MU inhibition involves the addition of glucuronide to 4-MU by exogenous UDP-glucuronyl transferase (UGT) that transfers glucuronic acid to 4-MU from UDP-glucuronic acid. This results in a depletion of UDP-glucuronic acid, one of the essential precursors for hyaluronan synthesis [136].

As mentioned previously, hyaluronidases can alter the size of hyaluronan. Six hyaluronidase (HYAL) genes have been identified in humans with HYAL-1 and HYAL-2 being

the major players in most tissues [137, 138]. In some cells, HYAL-2 can associate with cells via a glycosylphosphatidyl-inositol anchor [139, 140]. HYAL-2 has also been shown to bind CD44 at the chondrocyte plasma membrane [139]. The activity of HYAL-2 associated with CD44 could be detected at pH 4.8 and only weak hyaluronidase activity was detected at 6.8 [141]. Nevertheless, this would allow HYAL-2 to be internalized along with CD44 to low pH intracellular vesicles. Hyaluronan endocytosis via CD44 to low pH intracellular vesicles participates in hyaluronan turnover [142]. Most internalized hyaluronan is destined for catabolism in the lysosome [143]. HYAL-2 is active under acidic conditions generally in lysosomes, however at least one study has found HYAL-2 to have activity at near neutral pH only when CD44 is also present [144]. Extracellular activity of HYAL-2 is still highly debatable and more research needs to be completed but this would provide for extracellular hyaluronan degradation and promote internalization and remodeling of the ECM. Experimentally, *Streptomyces* hyaluronidase is the most commonly used hyaluronidase for research because it specifically and exclusively degrades hyaluronan [145].

4.2. Hyaluronan receptors

Hyaluronan interacts with cells through cell surface receptors for its structural role in the ECM, to initiate signaling cascades or to be internalized. Described hyaluronan receptors include; CD44, Receptor for Hyaluronan-Mediated Motility (RHAMM), Intracellular Adhesion Molecule (ICAM)-1, Hyaluronan Receptor for Endocytosis (HARE), and Lymphatic Vessel Endothelial Hyaluronan Receptor (LYVE-1). CD44 is the primary and most studied hyaluronan receptor in articular cartilage. CD44 was found to be associated with insulin resistance in adipose tissue but its importance during adipogenesis remains largely unknown [146]. CD44 is a single pass transmembrane receptor that binds to hyaluronan and plays a primary role in the assembly and

maintenance of the pericellular matrix by chondrocytes [147]. In addition to hyaluronan binding, CD44 also participates in cell signaling [148], tumor invasion/metastasis [149], and hyaluronan endocytosis [150]. The cytoplasmic domain of CD44 interacts with cytoskeleton linker proteins ankyrin and ERM (as mentioned previously). ERM proteins crosslink the actin cytoskeleton to CD44 and are important in the regulation of cell migration and cell shape, while the interaction between CD44 and ankyrin was found necessary for the binding of hyaluronan and retention of the pericellular matrix [151, 152].

Hyaluronidase-sensitive pericellular matrices or "coats" have been observed on mesenchymal cells isolated from hyaluronan-enriched regions of the developing embryo [153]. Due to collapse of these coats during aldehyde fixation, the particle exclusion assay [154] has become an important method for visualization of the hydrated coats [155] (Figure 1).

One hyaluronan molecule is able to bind multiple CD44 receptors which increases the likelihood of internalization. The CD44 receptors that assist with hyaluronan endocytosis associate with lipid rafts which are cholesterol and sphingolipid rich domains in the plasma membrane. This association with lipid rafts is necessary for hyaluronan endocytosis but not for binding between CD44 and hyaluronan [156]. Internalization of hyaluronan through CD44 mediated endocytosis has been shown to require acylation of the cytoplasmic tail [156]. There are many variants of CD44 due to alternative splicing of variable exons and post-translational modification which might afford CD44 a few possibilities for facilitating endocytosis.

In both melanoma cells [157] and fibroblasts [158], hyaluronan was able to be internalized via CD44 mediated mechanisms but also micropinocytosis that is independent of CD44. However, hyaluronan internalization in chondrocytes appears to be strictly CD44 dependent [150]. Work with keratinocytes and chondrocytes suggests CD44 mediated hyaluronan internalization is not associated with clathrin-coated vesicles, caveolae, or pinocytosis-which suggest a non-classical mode of uptake regulated by alternative mechanisms [147, 159]. However, when hyaluronan-bound CD44 binds to TGF-β type I receptor in human kidney epithelial cells, both are transported to lipid rafts and associate with caveolin-1, which is a cholesterol binding protein that is required for the formation of caveolae and subsequent clathrin independent endocytosis [160, 161]. Adipocytes harbor more cholesterol than any other tissue and have an abundance of caveolae for constant trafficking between the plasma membrane and lipid droplets [162]. Even though various caveolae/raft pathways largely by-pass fusion with endosomes and lysosomes [163], Choi *et al*. found that mouse fibroblasts, mouse neurons, and human neuroblastoma cells all utilize caveolae-mediated endocytosis to transport a particular ECM protein to lysosomes for degradation [164]. With the extensive remodeling of the ECM, pre-adipocytes undergoing adipogenesis must possess a mechanism for degradation and endocytosis of hyaluronan, particularly hyaluronan present in the pericellular matrix. This could serve as a mechanism for CD44 mediated ECM turnover during adipogenesis.

4.3. Hyaladherins

In addition to cell surface receptors, several other proteins bind hyaluronan such as fibrin, fibronectin, and a family of proteoglycans which are all collectively called hyaluronan binding proteins (HABPs) or hyaladherins [165]. Hyaladherins can be classified based on the binding motif

that is used to bind hyaluronan. The cell surface receptor RHAMM binds hyaluronan with a B(X7)B sequence where B is a basic residue and the Xs contain at least one basic amino acid but the rest can be any other non-acidic amino acids [166]. A second hyaluronan binding motif, called the link module, consist of ~100 amino acids that bind to hyaluronan when folded into the correct tertiary structure [167]. CD44, versican, and aggrecan all use this link module to bind hyaluronan [168]. Both aggrecan and versican are proteoglycans that consist of a core protein decorated with sulfated glycosaminoglycans (Figure 2). Hyaladherins generally interact with a small number of sugar repeats of hyaluronan so a single chain of high molecular weight hyaluronan can theoretically accommodate over 1,000 protein molecules, which explains why many signaling responses induced by hyaluronan/protein interactions are heavily dependent on hyaluronan molecular weight [169, 170].

The first specific hyaladherin discovered was the cartilage proteoglycan, aggrecan [171]. This large aggregating chondroitin sulfate proteoglycan was so named because of its high affinity for hyaluronan, allowing more than 100 molecules to noncovalently bind to a single chain of hyaluronan giving the appearance of a bottle brush. This bond is strengthened further with the presence of link protein, a small glycoprotein that also demonstrates strong, specific binding to hyaluronan [172, 173]. Similar to aggrecan is versican, which is a proteoglycan synthesized by fibroblasts and also aggregates on hyaluronan molecules with a link protein [174]. The repulsion between the highly charged chondroitin sulfates in these proteoglycans can have important effects on the material properties and permeability of the matrix. Proteoglycans allow the hyaluronan chain to remain extended which increases the osmotic swelling of the pericellular matrix which directly contributes to compressive stiffness in a tissue [175]. When excess proteoglycan is added,

the pore size of the pericellular matrix is decreased but the overall size of the pericellular matrix is increased [176, 177].

4.4. The use of hyaladherins fragments to detect hyaluronan.

In the past, hyaluronan was quantified by isolating it from other polysaccharides and then determining the uronic acid concentration by a colometric assay [178]. It was discovered later that hyaluronan could be tightly and specifically bound by a hyaluronan binding protein (HABP) composed of a portion of aggrecan as well as the link protein isolated from bovine cartilage [172, 173, 179]. The addition of a detectable tag on HABP led to the development of new methods for specific quantification and visualization of hyaluronan such as a sandwich ELISA-like assay (Figure 3A) [180] and immunohistochemistry-like fluorescence assay (Figure 3B) [181].

4.5. Hyaluronan during adipogenesis

Hyaluronan was first identified in the culture medium of 3T3-L1 cells undergoing adipogenesis in 1991 by Calvo *et al.* [182]. They observed that as adipogenesis progresses, the culture medium became noticeably more viscous. In addition, a high molecular weight proteoglycan that contributed to the increased viscosity was also described [182] and later identified as versican [183]. This increase in hyaluronan found in the media was partially explained by a brief spike in HAS-2 expression during mid-adipogenesis but was also accompanied by a similar spike in HYAL-2 expression [184]. When hyaluronan was degraded with *Streptomyces* hyaluronidase or synthesis was blocked with 4-MU, adipogenesis of 3T3-L1 cells was significantly inhibited. This suggested that adipogenesis is dependent on the presence of hyaluronan [185].

All these results indicate a possible role for these ECM molecules during adipogenesis and open the field for more thorough study in 3T3-L1 cell differentiation. A thorough understanding of the differentiation process would allow for manipulation of adipocyte cell number and control of certain diseases (non-insulin dependent diabetes mellitus, hypertension, immune dysfunction, certain types of cancer [186]. The study of molecular mechanisms of adipocyte development may suggest important patterns for comparison to other developmental systems which may provide understanding of the physiology of animal and human development.

5. SPECIFIC AIMS

While the overall goal of this dissertation was to gain insight into how hyaluronan and its associated components act in directing differentiation of mesenchymal cells, there was a substantial shift in the approach used to achieve that goal. Three specific aims are presented here. The first specific aim describes the original, abandoned approach in which primary mesenchymal cells were to be isolated from bovine articular cartilage. Even though this aim was not achieved it is included here because work performed attempting to accomplish this aim was paramount in shifting to the approach outlined in the last two specific aims in which a cell line is used to investigate the effects of hyaluronan and its components on mesenchymal cell differentiation

5.1. Isolate a progenitor side population from bovine articular cartilage.

Several alternative surgical methods are under development to regenerate articular cartilage that has been lost or damaged during osteoarthritis disease progression. Chondroprogenitor cells, isolated from articular cartilage, could provide a cellular source for articular cartilage repair. Based on other preliminary studies, the goal of this aim is to determine whether a side population of progenitor cells can be obtained from adult bovine articular cartilage and then used for further analysis of differentiation potential.

5.2. Investigate the hyaluronan-dependent pericellular matrix of 3T3-L1 mesenchymal cells and 3T3-L1 adipocytes.

Like many tissues, adipose tissue is regulated by the physiological interaction between cells and a variety of extracellular matrix components. Previous studies have shown that the pericellular assembly of fibronectin dictates cytoskeletal and extracellular matrix organization which affects 3T3-L1 conversion from mesenchymal cells to adipocytes [187] and that modulation of pericellular collagen was found necessary for adipogenesis [188]. In mesenchymal to chondrocyte differentiation, modulation of hyaluronan dependent pericellular matrices is required for chondrogenesis to occur [153] however little is known about pericellular matrix changes during adipogenesis. The goal of this aim is to test the hypothesis that 3T3-L1 mesenchymal cells have a hyaluronan-dependent pericellular matrix and it is modulated during the course of adipogenesis.

5.3. Investigate the role of hyaluronan during adipogenesis of 3T3-L1.

The maintenance and differentiation of stem cells are intimately mediated by hyaluronan and its interactions with proteins. Hyaluronan has been reported to facilitate differentiation of mesenchymal cells to chondrocytes, fibroblasts, and keratinocytes [189]. Previous studies have implicated a functional role for hyaluronan during 3T3-L1 adipogenesis [182, 184, 185]. The goal of this aim is to test the hypothesis that hyaluronan plays an essential role during 3T3-L1 adipogenesis as part of the pericellular matrix and begin to elucidate the mechanisms involved.

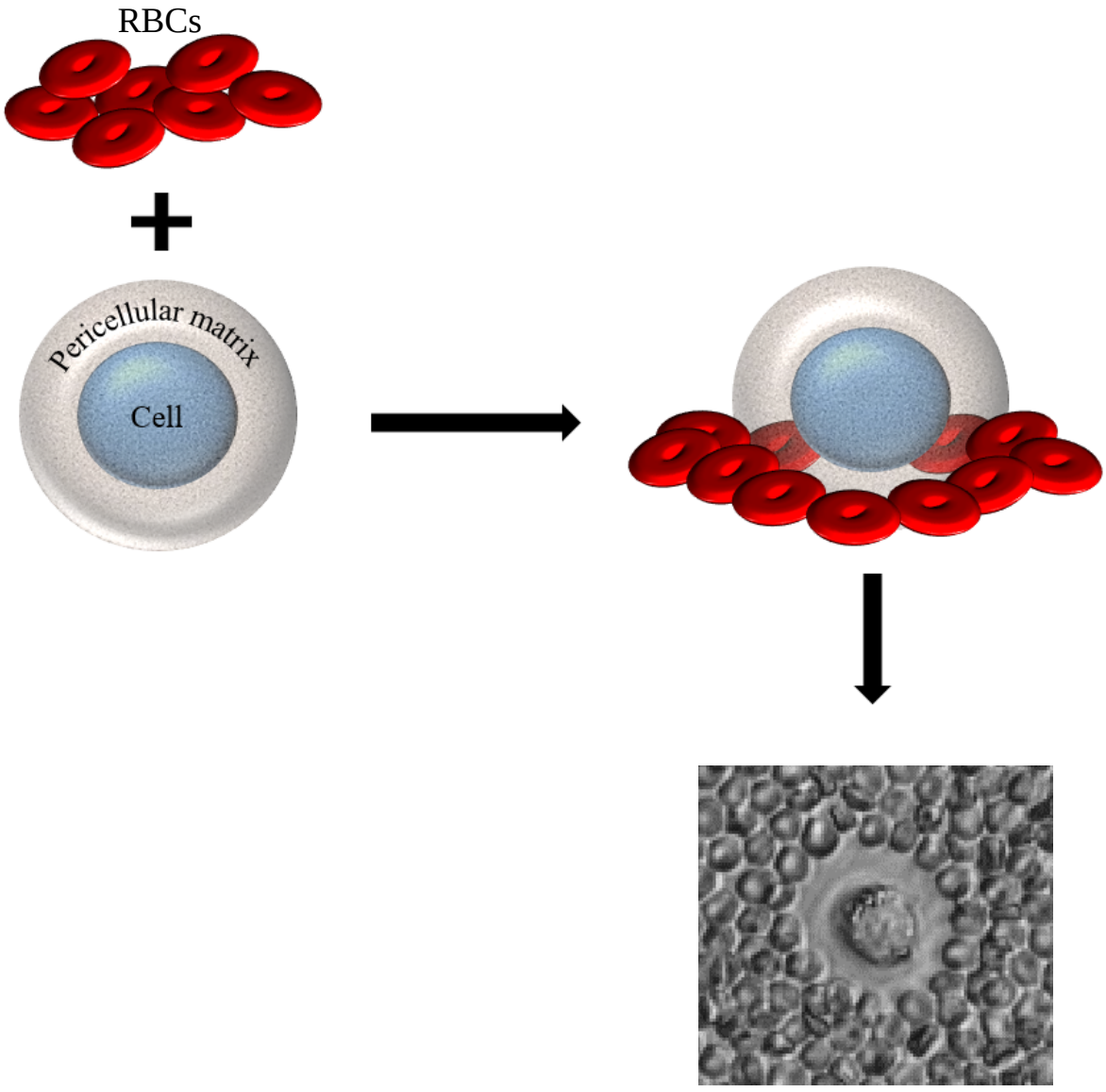
RBCs
Pericellular matrix
Cell

Figure 1. The classical particle exclusion assay to reveal hydrated pericellular matrix. The pericellular matrix assembled by cells is composed largely of water and hard to visualize with traditional staining methods. Adding small inert particles, like formalin fixed equine erythrocytes (red blood cells-RBC), which settle down on the tissue culture plastic and around the living cell, are excluded from its matrix, revealing a halo that represents the cell's pericellular matrix or 'coat'.

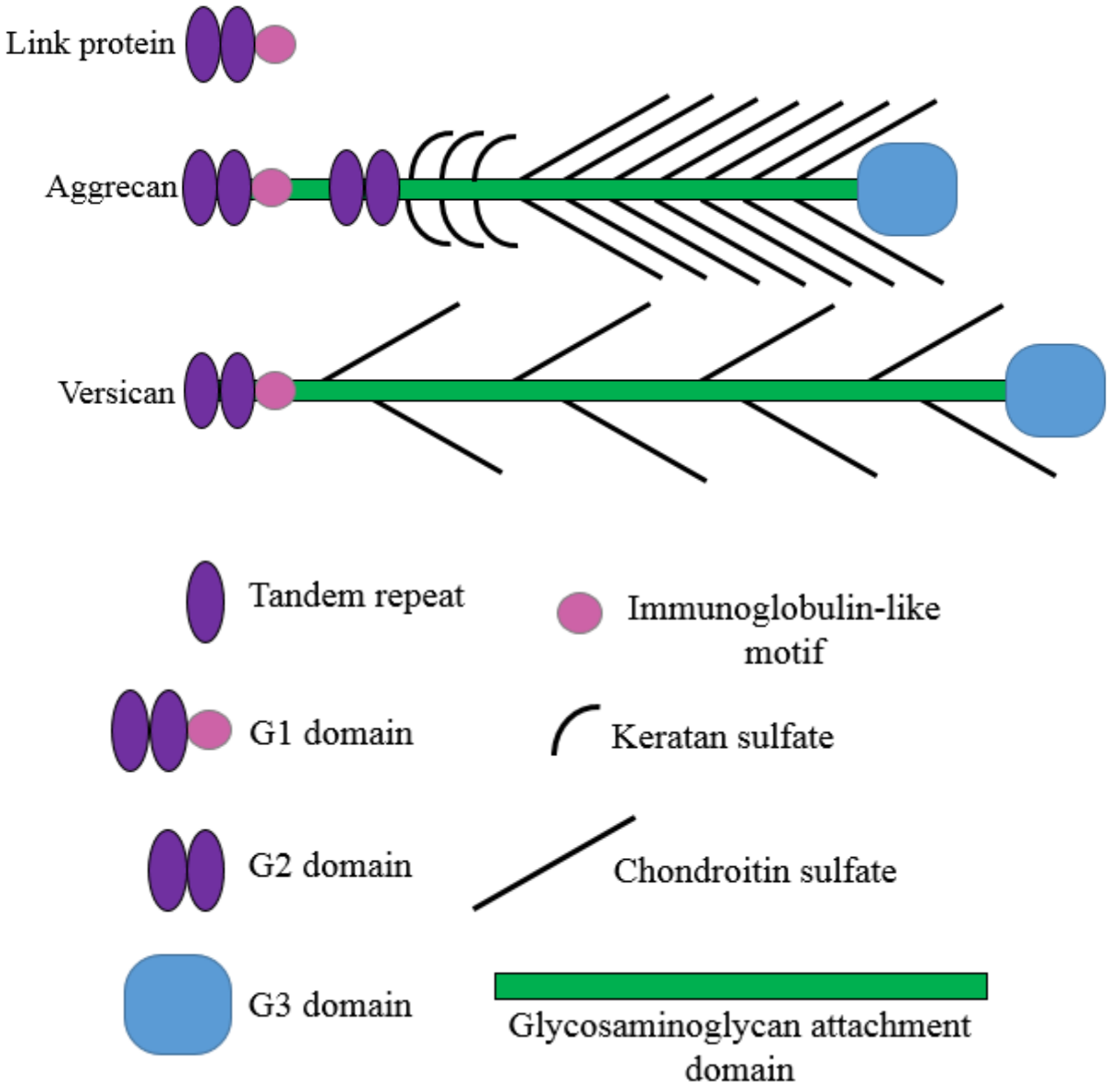
Link protein
Aggrecan
Versican
Tandem repeat
Immunoglobulin-like motif
G1 domain
Keratan sulfate
G2 domain
Chondroitin sulfate
G3 domain
Glycosaminoglycan attachment domain

Figure 2. Structure of link protein, aggrecan, and versican: three extracellular matrix hyaladherins. The N-terminal globular domain (G1) consists of a signal peptide, two hyaluronan-binding repeats (tandem repeats) and an immunoglobulin-like motif. The G1 domain of all three molecules binds to hyaluronan mediated by the two tandem repeats. Link protein is essential just the G1 domain (also called the link module). Only aggrecan contains a second globular domain (G2) that consists of two tandem repeats. Aggrecan and versican have protein cores (represented by the entire green line) of differing amino acid sequence and a C-terminal globular domain (G3). This glycosaminoglycan attachment domain between the G2 and G3 domains of aggrecan is substituted with keratan sulfate and chondroitin sulfate. For versican, the glycosaminoglycan attachment domain between the G1 and G3 domains is substituted with chondroitin sulfate only. The G3 domain consists of a carbohydrate recognition domain and epidermal growth factor-like repeats. This figure was re-drawn based on Figure 1 in [190].

A.

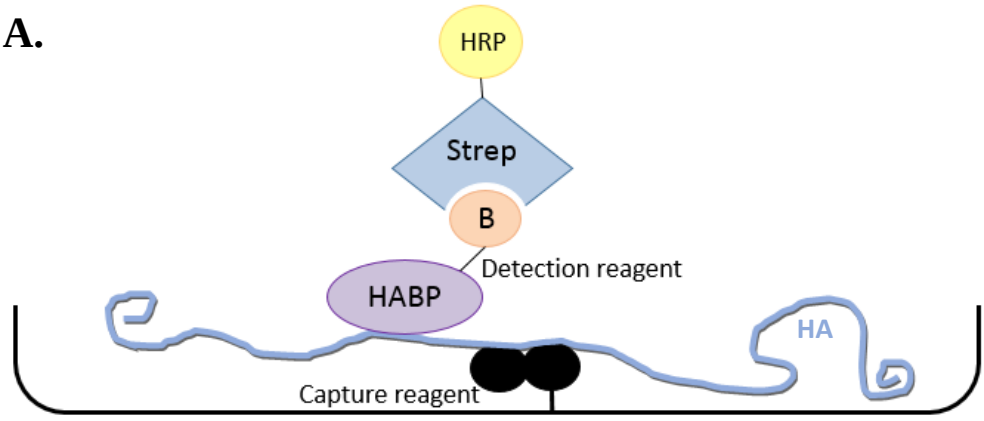
HRP
Strep
B
Detection reagent
HABP
HA
Capture reagent

B.

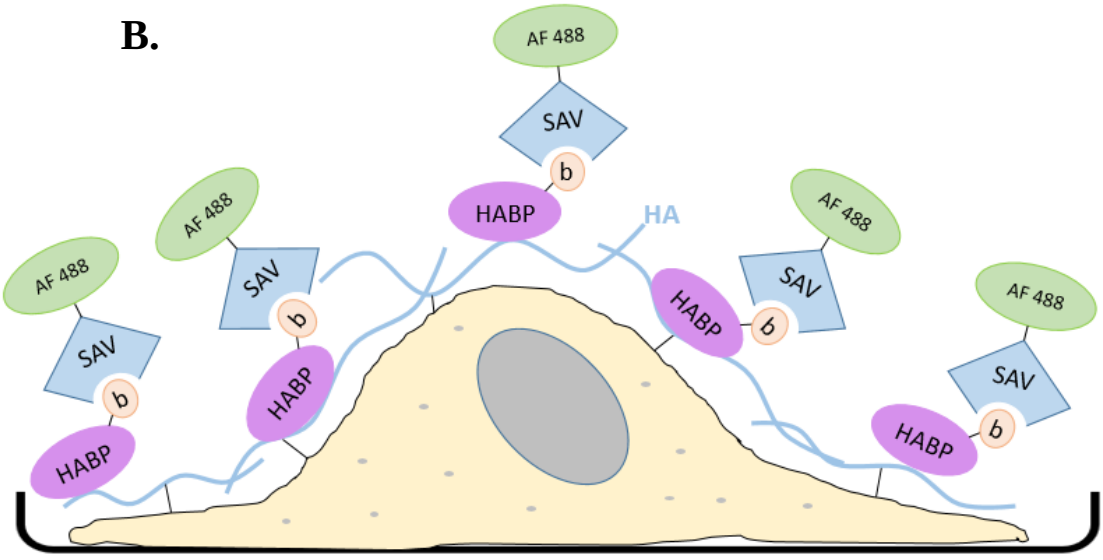
AF 488
SAV
b
HABP
HA

Figure 3. HABP is used for quantifying hyaluronan in an ELISA-like assay and visualizing cell-associated hyaluronan. In the ELISA-like assay, chondroitenase-treated purified proteoglycan (from articular cartilage) is coated to high affinity binding ELISA plates to serve as the capture reagent. Hyaluronan (HA) is then incubated with the capture reagent and allowed to bind. The detection reagent is biotinylated HABP-B (purple oval-"HABP" with peach "B") followed by the addition of streptavidin conjugated to horseradish peroxidase (blue diamond-"Strep" with yellow "HRP") (A). Cell associated hyaluronan (HA) is visualized with biotinylated HABP as well. Surface HA is detected in cells cultured and fixed in chamber slides and incubated with HABP-b (purple oval-"HABP" with peach "b"). Streptavidin (blue diamond-"SAV") conjugated to Alexa-Fluor 488 (green oval-"AF488") binds to the biotin linked to HABP for detection. Cells can be permeabilized with Triton-X-100 to visualize intracellular HA (B).

CHAPTER 2: MATERIALS AND METHODS

1. Cell culture

1.1. Primary bovine articular cartilage cell isolation and cell culture

Cells from bovine articular cartilage were isolated using the previously described method [128]. Articular cartilage was removed from the metacarpophalangeal joints of adult steers (18 months) obtained from a local abattoir [191]. To harvest cells from the superficial layer only, very thin slices were removed from the cartilage. Middle/deep layers were harvested together by removing the remaining cartilage after the superficial layer had been removed. For most experiments, full thickness cartilage was removed in slices. Regardless of originating location, after the cartilage was removed, it was rinsed in sterile phosphate buffered saline (PBS; AMRESCO, Baltimore, MD) and subjected to sequential digestion with 0.2% pronase (EMD Scientific, San Diego, CA) in Dulbecco's Modified Eagle Medium (DMEM; Mediatech, Herndon, VA) containing 10% fetal bovine serum (FBS; Hyclone, South Logan, UT), 1% L-glutamine and 1% penicillin-streptomycin for 1 hour at 37°C, 5% CO_2, followed by 0.0025% collagenase P (Roche, Indianapolis, IN) in the same diluent and incubation conditions as pronase digestion overnight. The next day, the cell suspension was passed through sterile 100 then 40 μm cell sieves to filter out clumps and obtain a single cell suspension, which was then centrifuged at 300 x *g* for 5 minutes at room temperature. The cell pellet was suspended in Hoechst medium for both fibronectin adhesion or flow cytometric analysis.

Hoechst medium consisted of Hanks' balanced salt solution (Sigma) supplemented with 2% FBS and 10 mM HEPES (AMRESCO, Solon, OH).

1.2. MCF-7 cell culture

The MCF-7 cell line is a stable epithelioid cell line derived from free-floating passages of a primary culture of human breast carcinoma cells [192]. They were a gift to the Knudson lab by Dr. Li Yang (East Carolina University, NC). MCF-7 cells were cultured as high density monolayers in DMEM containing 10% FBS, 1% L-glutamine and 1% penicillin-streptomycin and incubated at 37^{o}C in a 5% CO_2 environment. The MCF-7 cells were passaged at confluence using 0.25% trypsin/2.21 mM EDTA.

1.3. 3T3-L1 cell culture

The 3T3-L1 cell line is a pre-adipose line derived from the established mouse fibroblast 3T3 line [71] and was a gift to the Knudson lab by Dr. Philip Pekala (formerly East Carolina University, NC) or was purchased from ZenBio, Inc (Durham, NC). 3T3-L1 cells were cultured as low density monolayers in DMEM containing 10% FBS, 1% L-glutamine and 1% penicillin-streptomycin (defined as maintenance media; MM) and incubated at 37^{o}C in a 5% CO_2 environment. The 3T3-L1 cells were passaged at no more than 80% confluence using 0.25% trypsin/2.21 mM EDTA.

1.4. C3H10T1/2 cell culture

The C3H10 T1/2 cell line was derived from a C3H mouse embryo [193] and was purchased from the American Type Culture Collection (Manassas, VA). C3H10T1/2 cells were cultured as monolayers in DMEM containing 10% FBS, 1% L-glutamine and 1% penicillin-streptomycin and incubated at 37^{o}C in a 5% CO_2 environment. The C3H10T1/2 cells were passaged at confluence using 0.25% trypsin/2.21 mM EDTA.

1.5. MG-63 cell culture

The human MG-63 cell line was derived from an osteogenic sarcoma [194, 195] and was purchased from the American Type Culture Collection (Manassas, VA). MG-63 cells were cultured as monolayers in DMEM containing 10% FBS, 1% L-glutamine and 1% penicillin-streptomycin and incubated at 37^{o}C in a 5% CO_2 environment. The MG-63 cells were passaged at confluence using 0.25% trypsin/2.21 mM EDTA.

1.6. Rat chondrosarcoma cell culture

The rat chondrosarcoma cell line (RCS) is a continuous long-term culture line derived from the Swarm rat chondrosarcoma tumor [196, 197]. The RCS cell line in the Knudson laboratories was a gift of Dr. James H. Kimura (formerly of Rush University Medical Center) and represented an early clone of cells that eventually became known as long-term culture RCS [198]. RCS chondrocytes were cultured as high-density monolayers in DMEM containing 10% FBS, 1% L-glutamine and 1% penicillin-streptomycin, and incubated at 37^{o}C in a 5% CO_2 environment. RCS cells were passaged at confluence using 0.25% trypsin/2.21 mM EDTA.

2. Characterizational assays

2.1. Phase contrast microscopy

Cells were observed using a Nikon TE2000 inverted phase-contrast microscope and images were captured digitally in real time using a Retiga 2000R digital camera (QImaging, Surrey, British Columbia).

2.2. Fluorescent microscopy

Fluorescence was observed with either a Nikon TE2000 inverted microscope using 10, 20, or 40x objectives or a Nikon E600 microscope and a 60x oil objectiveequipped with a Y-Fl Epi-fluorescence attachment (Melville, NY). Images were captured digitally using a Retiga 2000R digital camera and processed using NIS Elements BR version 1.30 imaging software (Nikon, Lewisville, TX)

2.3. Particle exclusion assay

Mesenchymal 3T3-L1 cells were plated at a density of 10^4 cells per cm^2 overnight in DMEM containing 10% FBS, 1% L-glutamine, and 1% penicillin-streptomycin then incubated at 37^{o}C in a 5% CO_2 environment. 3T3-L1 cells undergoing adipogenesis were dislodged with forceful pipetting of PBS and transferred to a new culture well in DMEM + 10% FBS with 1% L-glutamine and 1% penicillin-streptomycin. The next day, the medium was replaced with 74 µl/cm^2 suspension of formalin-fixed equine erythrocytes in DMEM containing 10% FBS [147]. The cultures were allowed to sit for 10 minutes at room temperature before analyses with phase

contrast microscopy. On occasion, 4 μM Calcein AM (Molecular Probes, Eugene, OR) was added with the RBC suspension to increase visibility of cells. In these instances, cultures were analyzed via fluorescent microscopy in addition to phase contrast microscopy.

2.4. Oil Red O stain

Stock solution of 5 mg/ml Oil Red O (Matheson Coleman Bell) in 100% isopropyl alcohol was diluted in water to 3 mg/ml and filtered. Cells were rinsed with PBS and fixed with 3.7% paraformaldehyde for 2 min at 4°C, rinsed again with PBS and stained with filtered Oil Red O for 1 hour at room temperature. Wells were rinsed 3 times with water before images were observed and recorded via phase contrast microscopy or a Canon PowerShot SX700 HS (Tokyo, Japan). For quantification, Oil Red O stain was extracted from cells with 100% ethanol for 10 minutes at room temperature with rocking. Absorbance was measured with a 492 nm wavelength on Multiskan Ascent plate reader (Thermo Scientific).

2.5. Alcian blue stain

Micromass cultures (described in section 7.2) to be stained with alcian blue were rinsed with PBS and then fixed with 3.7% paraformaldehyde for 10 minutes at room temperature. Cultures were rinsed 3 times with PBS then stained with 1% alcian blue/3%acetic acid (Sigma) in deionized water for 30 minutes at room temperature. Wells were rinsed 3 times with water before images were recorded via a Canon PowerShot SX700 HS (Tokyo, Japan). For quantification, alcian blue stain was extracted from micromass cultures with 4 M guanidine HCl (Sigma)

overnight at 4°C with rocking. Absorbance was measured with a 592 nm wavelength Multiskan Ascent plate reader (Thermo Scientific)

2.6. Hoechst 33342 stain and efflux assay

Cells to be analyzed via flow cytometry were counted and suspended in Hoechst medium at 10^6 cells/ml. Hoechst 33342 (Tocris, Bristol, UK) was added to the cells to obtain a final concentration of 5 μg/ml then incubated in a 37°C water bath for 90 minutes, in the dark, with frequent agitation. Cells were centrifuged at 375 x g for 6 minutes at 4°C then re-suspended at 10^6 cells/ml in fresh, cold Hoechst medium with 2 μg/ml propidium iodide (Sigma) but without and with 50 μM verapamil (Sigma) [199]. Cell suspensions were kept on ice and in the dark until cytometric analysis could be completed (less than 1 hour).

Cells to be microscopically analyzed for Hoechst efflux were suspended at 10^6 cells/ml in Hoechst medium then incubated with 5 μg/ml Hoechst 33342 for 5 or 20 minutes at 4 or 37°C [200]. Cells were centrifuged at 375 x g for 6 minutes and re-suspended fresh, cold Hoechst medium then plated at 2.5×10^5 cells/cm^2. Images were recorded by phase contrast and fluorescent microscopy 3 hours after plating unless otherwise specified.

3. Flow Cytometry

Single cell suspensions incubated with Hoechst 33342 and propidium iodide, without and with verapamil, were analyzed for the presence of a side population using the FACSVantage cell sorter (BD Biosciences) fitted with a UV laser for excitation, 675/20 LP filter for Hoechst Red detection, 424/44 BP filter for Hoechst Blue detection and a 640 longpass dichroic mirror for separation of the Blue and Red signals. Forward scatter (FSC) vs side scatter (SSC), FSC vs propidium iodide Red (FL2-H), and Hoechst Red (FL5-H) vs Hoechst Blue (FL4-H) two parameter plots were generated with linear scales. Voltages were adjusted so that all cells were visible on the FSC vs SSC and FSC vs FL2-H plots [199]. Events with high side scatter, low forward scatter, and high propidium iodide fluorescence were excluded on the Hoechst Red vs Hoechst Blue plot because these were likely dead cells or cellular debris. One hundred thousand events were analyzed and the side population was gated at the left side of the plot, indicating low Hoechst Red and Blue and appearing as a tail off the G1 cluster.

4. Fibronectin adhesion assay

Fibronectin coated plates were prepared by allowing 10 μg/ml fibronectin (Sigma) in PBS to dry on sterile, uncoated Corning petri dishes (Becton Dickinson Labware, Franklin Lakes, NJ) overnight at 4°C [201, 202]. Coated plates were stored at 4°C if not used immediately.

Bovine articular cartilage primary cells isolated from one metacarpophalangeal joint were suspended in 10 mls Hoechst medium. The cell suspension was split into two fibronectin coated plates with 5 mls each and incubated for 10 minutes at 37°C with 5% CO2. Non-adhered cells

(called Bovine Articular Chondrocytes-BAC) were collected and the plates were rinsed two times with sterile PBS. Adhered cells (called Bovine Articular Stem Cells-BASC) were detached from the plate with 0.25% trypsin/2.21 mM EDTA. BASCs were rinsed and suspended in Hoechst media to be analyzed for Hoechst 33342 efflux.

5. Isolation of bovine aggrecan monomer

Full thickness slices of bovine articular cartilage were excised from 18-24 month bovine metacarpophalangeal joints obtained from a local abattoir. The cartilage was frozen in liquid nitrogen, ground to a powder and extracted in a dissociative buffer consisting of 4.0 M guanidine HCl, 0.01 M EDTA, and 0.05 M sodium acetate (Sigma), pH 5.8 [173]. After gentle stirring at 4°C for 24 hours, the solution was centrifuged at 13,000 x g for 45 minutes at 4°C then passed through a 100 μM sieve to remove undissociated clumps. The strained solution was brought to a final density of 1.5 g/ml by the addition of 0.5452 g CsCl/ml. Samples were centrifuged at 100,000 x g for 48 h at 4°C under vacuum in a Beckman 50.2Ti rotor. Upon completion, the bottom fifth of each centrifuge tube was isolated, dialyzed against 0.05 M Na_2SO_4 for 24 hours, then water for 48 hours, and then lyophilized [179]. The product was stored at -80°C.

6. Agarose gel electrophoresis

Isolated bovine aggrecan monomer was dissolved in PBS and adjusted to 2 mg/ml. Samples were combined with 1 mg/ml pharmaceutical-grade hyaluronan (ARTZ, Seikagaku, Japan) or

digested with 5 Units/ml *Streptomyces* hyaluronidase (Sigma) for 90 minutes at 37°C. Equal volumes were then electrophoresed on a 1% agarose gel prepared in Tris-acetate-EDTA buffer and cast into 10 x 15 cm trays of a MP-1015 horizontal electrophoresis apparatus (ISI Scientific) [177, 203]. One well was loaded with 5 µl of a 1 kb-PLUS DNA ladder (100– 12,000 bp; Thermo Fisher, Waltham, MA) for size reference. Electrophoresis was carried out for 30 minutes at 150V. Gels were fixed by incubation in 30% ethanol for 1 hour at room temperature, rinsed with water and then stained overnight with Stains-All. The stock Stains-All solution consisted of 0.1% Stains-All (ThermoFisher) dissolved in formamide. Two mls of stock Stains-All was diluted in 2 mls formamide, 10 mls isopropal alcohol, 200 µl 3 M Tris (Sigma), and 25.8 mls water to make the Stains-All working stock. Stained bands were imaged by trans-white light on the Chemi-Doc Imager (Bio-Rad, Hercules, CA).

7. Cell treatments

7.1. Adipogenic induction

3T3-L1 cells were plated at 3 x 10^4 cells/cm^2 in culture plates on Day -4 and incubated at 37°C in 5% CO^2 throughout adipogenesis. This concentration produced a confluent lawn of cells in 48 hours. Two days after reaching visual confluence in culture, 3T3-L1 cells were induced to undergo adipogenesis with 0.5 mM methylisobutylxanthine (Sigma), 1 uM dexamethasone (Sigma), and 1.7 uM insulin (Sigma) in maintenance media (MM) (Day 0; Adipo1 media). Forty-eight hours later, medium was replaced with 1.7 uM insulin in MM (Day 2; Adipo2 media). After another 48 hours, medium was replaced with 0.43 uM insulin in MM (Day 4; Adipo3 media). Finally, after an additional 48 hrs (Day 6), the medium was switched to MM and cultures were

maintained in this medium until at least 10 days post induction [204, 205]. A timeline for 3T3-L1 adipogenesis is depicted in Figure 4. The red arrows represent media changes and when, if any, experimental treatments were administered.

7.2. Chondrogenic induction

A 3T3-L1 cell suspension was made in DMEM + 10% FBS with 1% L-glutamine and 1% penicillin-streptomycin at a concentration of 10^7 cells/ml. Five spots of 10 µl were seeded onto a 35 mm culture dish to form micromass cultures containing 10^5 cells each [206, 207]. Micromass cultures were incubated for 3 hours at 37°C in 5% CO2 to allow cells to adhere to the culture dish. Culture dishes containing micromass cultures were then flooded with control (DMEM + 10% FBS with 1% L-glutamine and 1% penicillin-streptomycin) or chondrogenic medium. Incubation continued for 8 days with media changes every 2-3 days before cultures were either fixed and stained with alcian blue or collected for RNA isolation.

The chondrogenic medium consisted of high glucose DMEM supplemented with 1% ITS (Sigma), 10% FBS, 1% L-glutamine, 1% penicillin-streptomycin, 25 µg/ml ascorbic acid (Sigma), 1 mM sodium pyruvate (ThermoFisher, Waltham, MA) and then filter sterilized before adding dexamethasone to 100 nM. TGF-β1 (R&D Systems, Minneapolis, MN) was added to medium to a concentration of 10 ng/ml immediately before introducing to cultures [208-210].

7.3. 4-Methylumbelleferone treatment

A stock solution of 200 mM 4-methylumbelleferone (4-MU; Sigma) was made in dimethylsulfoxide-DMSO (ThermoFisher). 3T3-L1 cells that were undergoing adipogenic induction were treated by the addition of 200 μM 4-MU to every media change on days 0, 2, 4, and 6 [185], as indicated in Figure 4.

7.4. Exogenous aggrecan treatment

Some 3T3-L1 cultures plated for a particle exclusion assay were treated with 2 mg/ml exogenous bovine aggrecan dissolved in DMEM + 10% FBS with 1% L-glutamine and 1% penicillin-streptomycin 24 hours after plating. Cultures were incubated with the aggrecan for 1 hour at 37°C in 5% CO_2. Exogenous aggrecan was also added to the RBC solution used in the particle exclusion assay to a concentration of 2 mg/ml.

Some 3T3-L1 cells undergoing adipogenic induction were treated with 2 mg/ml exogenous aggrecan dissolved in adipogenic media, Adipo1, Adipo2, Adipo3, and MM at every media change on days 0, 2, 4, and 6. For recovery from exogenous aggrecan treatment, Day 6 were adipogenically induced normally without and with 2 mg/ml exogenous aggrecan and stained with Oil Red O on Day 6. Samples analyzed on Day 10 include 3T3-L1 cells that were adipogenically induced without or with 2 mg/ml exogenous aggrecan but also included cultures where aggrecan was excluded from the media change on Day 6 then stained for Oil Red O on day 10. Samples analyzed on Day 14 and 18 include 3T3-L1 cells that were adipogenically induced without or with

2 mg/ml exogenous aggrecan but also included cultures where aggrecan was excluded from the media change on Day 10 then stained for Oil Red O on Days 14 and 18. Oil Red O was extracted from samples and optical density analyzed per section 2.3.

7.5. Streptomyces hyaluronidase treatment

Some 3T3-L1 cultures were treated with 20 Units/ml *Streptomyces* hyaluronidase dissolved in DMEM + 10% FBS with 1% L-glutamine and 1% penicillin-streptomycin for 3 hours at 37°C in 5% CO_2 before completion of particle exclusion assay or visualizing hyaluronan (section 10.2) [16].

7.6. HA_{oligo} treatment

HA_{oligos} were prepared in our lab by 16 hour treatment of hyaluronan (rooster comb, Sigma or Life Core) with testicular hyaluronidase by Dr. Warren Knudson [211]. Twenty-four hours after 3T3-L1 cultures were plated for a particle exclusion assay, some were treated with 200 μg/ml HA_{oligos} dissolved in DMEM + 10% FBS with 1% L-glutamine and 1% penicillin-streptomycin for 90 minutes at 37°C in 5% CO_2. Additionally, after 90 minutes of incubation with HA_{oligos}, some cultures were also treated with 2 mg/ml exogenous aggrecan for 1 hr at 37°C in 5% CO_2 before completion of particle exclusion assay.

7.7. Exogenous hyaluronan treatment

Twenty-four hours after 3T3-L1 cultures were plated for a particle exclusion assay, some were treated with 1 μg/ml pharmaceutical-grade ARTZ hyaluronan (Seikagaku, Japan) diluted in DMEM + 10% FBS with 1% L-glutamine and 1% penicillin-streptomycin 90 minutes at 37°C in 5% CO_2. Additionally, after 90 minutes of incubation with hyaluronan and rinsing twice with PBS, some cultures were also treated with 2 mg/ml exogenous aggrecan for 1 hr at 37°C in 5% CO_2 before completion on particle exclusion assay.

8. RNA isolation and qRT-PCR

8.1. RNA isolation

3T3-L1 cells cultured for RNA isolation were washed 3 times with cold, sterile PBS then mixed with 400 μl or 800 μl cold TRIzol (Fisher) depending if culture was in a 12- or 6-well culture plate. The monolayer was mixed thoroughly with TRIzol and then the lysate was transferred to a 1.5 ml microfuge tube and kept on ice. An equal volume of 100% ethanol was added to the lysate, briefly vortexed, then transferred to a quick spin column from a Direct-zol™ RNA Miniprep kit (Zymo Research, Irvine, CA). Samples were processed according to the manufacturer's instructions. RNA concentrations were determined by absorbance at 260 and 280 nm using a Nanodrop One spectrophotometer (ThermoScientific).

8.2. Quantitative Reverse Transcriptase Polymerase Chain Reaction (qRT-PCR)

Total RNA from 3T3-L1 cultures were converted to cDNA using the iScript cDNA Synthesis Kit (BioRad, Hercules, CA). Quantitative PCR was performed using the Sso-Advanced SYBR-Green Supermix (BioRad) and amplified on a StepOnePlus Real-Time PCR System (Applied Biosystems, Foster City, CA) to obtain cycle threshold (Ct) values for target levels. Mouse specific primer sequences are listed in Table 1. Real time efficiency (E) was calculated as $E=10^{[-1/slope]}$ [212]. The fold increase in copy numbers of mRNA was calculated as a relative ratio of target gene to *Gapdh* ($\Delta\Delta$Ct) following the mathematical model introduced by Livak et al. [213].

Table 1. Primer Sequences

Target	Forward sequence	Reference
Gapdh	Forward: GGTGAAGGTCGGTGTGAACG	NM_008084.3
	Reverse: CTCGCTCCTGGAAGATGGTG	
Has1	Forward: GAGGCCTGGTACAACCAAAAG	NM_008215.2
	Reverse: CTCAACCAACGAAGGAAGGAG	
Has2	Forward: CGGTCGTCTCAAATTCATCTG	NM_008216.3
	Reverse: ACAATGCATCTTGTTCAGCTC	
Has3	Forward: TGGACCCAGCCTGCACCATTG	NM_008217.4
	Reverse: CCCGCTCCACGTTGAAAGCCAT	
Cd44	Forward: CTTCTATGTCCTCTTCCCAAG	NC_000068,7
	Reverse: TGGTGTCATCAACCCATTCC	
Vcan	Forward: GAAGTATGAGGGAGCTGTTACC	D16263.1
	Reverse: CTGTCTCTGTGCTAGAAACTGG	
Acan	Forward: GTTGGTTACTTCGCCTCCAG	NM_007424.2 [214]
	Reverse: GTCCTCCAAGCTCTGTGACC	
Fabp4	Forward: GAAGTGGGAGTGGGCTTTGCCA	NM_024406.2
	Reverse: CACCAGGGCCCCGCCATCTA	
Pparγ	Forward: GACCTGAAGCTCCAAGAATACC	EF062476.1
	Reverse: TGGAAGCCTGATGCTTTATCC	

Table 1. Primer Sequences. Primers were designed using nucleotide sequences for the listed accession numbers with the PrimerQuest Tool by Integrated DNA Technologies (IDT). Primers were designed so that all amplified products were less than 250 bp.

9. Western Blotting

9.1. Protein isolation

3T3-L1 monolayers were rinsed twice with cold PBS before cold Cell Lysis Buffer (Cell Signaling) supplemented with protease and phosphatase inhibitor set 2 and set 3 (Thermo Scientific and Sigma, respectively) were added to wells over ice. The cells were scraped and transferred to a 1.5 ml microfuge tube then incubated on ice for 30 minutes. Lysates were centrifuged at 13,000 x *g* for 10 minutes at 4°C. Supernatants were transferred to clean tubes and stored at -80°C until they could be analyzed for protein concentration using a Bicinchoninic Acid (BCA) Protein Assay (Pierce, Rockford, IL).

9.2. BCA assay

Following protein extraction from cells, aliquots of each sample were diluted 10-fold in lysis buffer and plated in a 96-well plate along with serial 1:10 dilutions of Bovine Serum Albumin (BSA) in lysis buffer for the standard curve. Two-hundred and fifty microliters of combined BCA protein assay reagents (Reagent A:Reagent B = 50:1) was added to each well. Plates were incubated for 30 minutes at 37°C before absorbance was obtained at 562 nm on a Multiskan Ascent plate reader (Thermo Scientific). Protein concentrations were calculated using the equation for the BSA linear regression.

9.3. Electrophoresis and immunoblotting

Equal micrograms of protein lysate was mixed with 4X NuPAGE LDS Sample Buffer (Invitrogen) and 10X NuPAGE Reducing Agent (Invitrogen). DNase/RNase free water was added to each sample to level volumes. Samples were heated at 70°C for 10 minutes and then loaded into a 4-12% NuPAGE Bis-Tris Mini gel (Novex, Carlsbad, CA) and electrophoresed at 150 volts for 45 minutes. Once separated, protein samples were transferred from the acrylamide gel to nitrocellulose membrane (Bio-Rad Laboratories, Inc.) using a Criterion blotter apparatus (Bio-Rad Laboratories, Inc.). The nitrocellulose membrane was then blocked in blocking buffer (5% non-fat dry milk in Tris buffered saline containing 0.1% Tween 20) for 1 hour at room temperature and rocking. Primary antibodies, either anti-C-terminal CD44 [191] or anti-GAPDH (Santa Cruz Biotechnology, Dallas, Texas), were diluted in blocking buffer and incubated on membranes overnight at 4°C with rocking. After rinsing with Tris buffered saline containing 0.1% Tween 20 (TBST), membranes were incubated with horse-radish peroxidase (HRP)-conjugated secondary antibodies diluted in TBST for 1 hour at room temperature with rocking. Donkey anti-rabbit IgG (Thermo Scientific) was used for anti-CD44 and donkey anti-goat IgG (Thermo Scientific) was used for anti-GAPDH. After secondary incubation, the membrane was rinsed and detection was performed using SuperSignal West Pico chemiluminescence substrate (Thermo Scientific). The membrane was exposed to x-ray film and developed, then film was digitally captured using ChemiDoc.

10. Hyaluronan detection

10.1. Hyaluronan ELISA

Conditioned media was collected from 3T3-L1 monolayers and centrifuged at 1,300 RPM for 10 minutes at 4°C to remove cellular debris. The supernatant was transferred to a new tube and stored at -80°C until analysis. Hyaluronan concentration was determined with the Hyaluronan DuoSet® with Substrate Reagent pack (R&D Systems. Minneapolis, MN) according to the manufacturer's instructions. Briefly, a 96-well flat bottom, high-binding, microplate (Costar, Corning, NY) was coated with diluted capture reagent, sealed, and incubated overnight at 4°C. They next day, the wells were washed 3 times with wash buffer (0.05% Tween 20 in PBS) before being blocked with blocking buffer (5% Tween 20/0.05% NaN_3 in PBS) for 1 hour at room temperature. Wells were washed 3 times in wash buffer, then standards and samples, diluted in reagent diluent (filtered 5% Tween 20 in PBS) if necessary, were added to wells then incubated for 2 hours at room temperature, sealed. Wash steps were repeated then detection reagent was added for 2 hours at room temperature, sealed, then washed again. The Streptavidin-HRP component was added to wells, the plate was sealed and incubated for 20 minutes at room temperature in the dark. One more series of washes was completed before the substrate solution was incubated in each well for 20 minutes at room temperature in the dark. Stop solution was added and then absorbance was read at 450 and 540 nm using a Multiskan Ascent plate reader (Thermo Scientific). Absorbances at 540 nm were subtracted from 450 nm readings to correct for optical imperfections in the plate. Standards were plotted using a best fit curve (5 or 6 order polynomial) and equation was used to calculate hyaluronan concentrations for samples.

10.2. Visualization of hyaluronan using HABP

3T3-L1 monolayers were plated in 4-chamber Falcon culture slides (Corning, Big Flats, NY) as described in section 1.3. Some cultures were treated with *Streptomyces* hyaluronidase as described in section 7.5. At time of testing, cultures were rinsed twice with PBS, then fixed with 3.7% paraformaldehyde for 5 minutes at 4°C. Cultures were then rinsed with 0.2 M glycine (Sigma) in PBS 3 times before being permeabilized with 0.5% Triton- X-100 (Sigma) for 10 minutes at room temperature. After rising 3 more times with 0.2 M glycine, the cultures were incubated with 4 µg/ml biotinylated hyaluronic acid binding protein-HABP (Calbiochem, EMD MilliPore, Billerica, MA) diluted in 1% BSA/PBS overnight at 4°C. The next day, cultures were carefully rinsed and incubated in Alexa-Fluor-488 conjugated with Streptavidin (green fluorescence; Jackson ImmunoResearch Labs, West Cove, PA) diluted in 1% BSA/PBS for 1 hour at room temperature. Cultures were rinsed, chambers removed, and cover slips mounted with DAPI containing mounting media, FluoroGel II (Electron Microscopy Services, Hatfield, PA). Monolayers were visualized with phase and fluorescent microscopy.

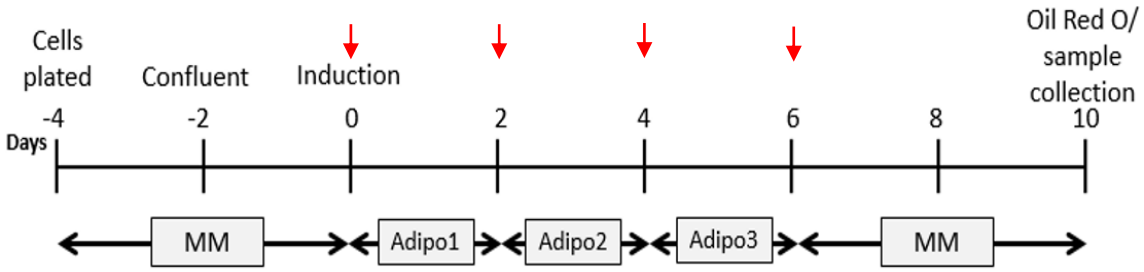
Cells plated
Confluent
Induction
Oil Red O/ sample collection
-4
-2
0
2
4
6
8
10
Days
MM
Adipo1
Adipo2
Adipo3
MM

Figure 4. Timeline for adipogenesis of 3T3-L1 cells. Cells plated on day -4, were maintained in DMEM+10% FBS (MM) until induction, at Day 0. Two days after reaching confluency (Day 0), cells were induced with 1uM Dex, 0.5 mM MIX, and 1.7 uM insulin in MM (Adipo1). On Day 2, cells were treated with MM+1.7 uM insulin (Adipo2). On Day 4, cells were treated with MM+0.43 uM insulin (Adipo3). On Day 6, media was changed back to MM for the remainder of culture. 3T3-L1 cells exhibit mesenchymal morphology at time of plating of 10^4 cells per cm^2 on Day -4. If any additional experimental treatments were administered, they were done so at each medium change indicated by the red arrows above the timeline.

.

CHAPTER 3: RESULTS

1. Detection of a side population of progenitor cells

1.1 Flow cytometry

Identification and isolation of side populations using flow cytometry to detect Hoechst 33342 dye efflux has been reported in many tissues such as muscle, liver, lung, skin, bone marrow, and cartilage [26, 215-219]. This method has also been used to detect a side population of progenitor cells within the widely used breast cancer cell line, MCF-7 [220]. We used the same MCF-7 cell line as a positive control to determine the conditions needed to detect a side population using flow cytometry. After staining MCF-7 cells with Hoechst 33342 and propidium iodide (PI) in the presence or absence of verapamil, the cells were analyzed with fluorescent microscopy. Verapamil, a calcium channel blocker traditionally administered to patients with cardiovascular issues such as coronary artery disease, arrhythmias, and hypertension [221], is also a P-glycoprotein inhibitor that blocks cells' ability to efflux Hoechst 33342 through action of the multi-drug resistance protein [222]. This serves as a control to ensure location of the side population is accurately determined. Even though verapamil treatment does have a slight negative effect on MCF-7 cell viability, which is shown by the increase in side scatter in Figure 5B and PI fluorescence in Figure 5D compared to untreated cells (Figure 1A and C) , viable, single cells were able to be gaited for Hoechst 33342 fluorescent analysis. Our method determined that 0.36% of MCF-7 cells consisted of the side population able to efflux Hoechst 33342 (control –verapamil treated) and this efflux ability was decreased by 86% with the treatment of verapamil (Figure 5, E & F).

This method was then used with primary cells isolated from bovine articular cartilage; a side population of 0.04, 0.18, and 0.24% in 3 separate experiments was found (Figure 6, A, C, & E). No side population was detected when cells were treated with verapamil (Figure 6, B, D, & F). With such a low number of cells comprising the progenitor side population, it was unlikely that differentiation experiments could be completed without population expansion. Expanding the cells was undesirable because bovine articular chondrocytes have been shown to dedifferentiate in culture with just a few passages [223]. This would make it difficult to determine if the cells that had been isolated were truly progenitor cells or simply dedifferentiated chondrocytes.

A previous study reported a higher number of progenitor cells in the more superficial articular cartilage zones when compared to deeper zones [28]. In an attempt to increase the percentage of the progenitor side population detected, cells were isolated from the superficial vs middle/deep layers of bovine articular cartilage (Figure 7A) and analyzed for Hoechst 33342 fluorescence separately. Isolated cells were stained with Hoechst 33342 and propidium iodide (PI) in the presence or absence of verapamil. The superficial layer of cartilage did have 3 times the percentage of progenitor side population detected at 0.06% (Figure 7B) compared to 0.02% for the middle/deep cartilage layer (Figure 7D). The verapamil treated cells had no detectable side population regardless of from where the cells were isolated (Figure 7C & E).

1.2 Adhesion to fibronectin to enrich progenitor cells

An alternative approach to enrich the progenitor side population, rather than clonal expansion, would be to select for the desired cell type. Identifying and isolating a progenitor side population

by differential adhesion to fibronectin was first achieved in epidermal cells [202]. This differential adhesion assay was later adopted in order to identify and isolate a progenitor sub-population from human articular cartilage [201]. We employed this method to enrich a progenitor side population from bovine articular cartilage. Petri dishes were coated with fibronectin and allowed to dry. Cells isolated from bovine articular cartilage were incubated on the fibronectin, unattached cells were rinsed away. The attached cells were termed Bovine Articular Stem Cells (BASC) while the cells that rinsed off were termed Bovine Articular Chondrocytes (BAC). At first, fibronectin was seeded onto the petri dishes in spots to ensure that the cells weren't just adhering to the dish non-discriminately. Figure 8A shows that cells adhered to the fibronectin spot and not to the uncoated dish. Based on previous reports, most of the cells that adhered to the fibronectin would constitute the progenitor side population (BASC) and would therefore be able to efflux Hoechst 33342 dye. Figure 8B shows that isn't the case. Regardless of whether the cells had 5 or 20 minutes exposure to Hoechst 33342 at 37 or 4°C, there was no obvious difference between BASC and BAC in Hoechst 33342 staining observed by fluorescent microscopy. However, a side population of acute myeloid leukemia cells was identified using this method [200]. In order to determine if any Hoechst 33342 efflux could be visualized via fluorescent microscopy, three cell lines that have shown differentiation capabilities were utilized. Both 3T3-L1 and C3H10T1/2 cells are mesenchymal in origin and MG-63 cells were derived from an osteosarcoma [71, 193, 224]. Figure 9 shows these three cells lines 1 and 3 hours after rinsing from Hoechst 33342 stain. At 3 hours, the cells attached and displayed their fibroblastic morphology. The 3T3-L1 cells had the most cells with little to no Hoechst 33342 staining, suggesting they might have the highest number of MDR/ABC transporters.

2. 3T3-L1 chondrogenic potential

3T3-L1 cells were derived from the NIH-3T3 mesenchymal fibroblastic cell line isolated from a mouse embryo because of their efficient adipogenic differentiation but they are usually referred to as "uni-potent" towards adipocytes [225]. We demonstrated that the 3T3-L1 cell line effluxes Hoechst 33342 more efficiently than the mesenchymal, multipotent progenitor cell line, C3H10T1/2 (Figure 9). Goodell *et al.* (1997) suggested that the degree of efflux activity seemed to correlate with the maturation state of cells, such that cells exhibiting the highest efflux activity are the most primitive or least restricted in terms of differentiation potential [226]. We wanted to test the multipotency of 3T3-L1 cells by testing their chondrogenic potential. Even though the parent NIH-3T3 cell line has been shown to undergo chondrogenesis, with low frequency, no work has been completed determining if the daughter 3T3-L1 cells are chondrogenic [227]. Micromass cultures and acidic alcian blue stain have been used successfully to study chondrogenesis since the mid-late 1970's [206]. In this study, 3T3-L1 cells displayed strong alcian blue staining after 11 days in micromass culture treated with chondrogenic medium (Figure 10A). The alcian blue stain was extracted with 4 M guanidine HCl and analyzed for absorbance which showed a statistically significant increase in the amount of alcian blue released from the treated 3T3-L1 micromass culture compared to the untreated control (Figure 10B). In addition, *Acan* mRNA expression was significantly increased compared to a non-treated micromass culture and 3T3-L1 cells in monolayer (Figure 10C). However, there was a significant reduction in *Vcan* and *Has2* mRNA expression in the chondrogenic treated micromass cultures compared to the untreated micromasses or the monolayer cultures (Figure 10D & E). Even though *Acan* expression increased by over 10-fold in chondrogenic micromass cultures, *Vcan* was still more abundant as demonstrated by the lower ΔCT values in Figure 10F.

3. Characterization of 3T3-L1 mesenchymal pericellular matrix

During mesodermal chondrogenic differentiation for limb bud development, dynamic changes to the pericellular matrix take place [153]. The pericellular matrix surrounding cells is resistant to staining techniques and is difficult to visualize. Over the past years, many labs have employed a particle exclusion assay to successfully visualize the pericellular matrix [153]. This method is based on small inert particles (fixed red blood cells) allowed to fall down around the cell and matrix leaving a halo or 'coat'. This coat is the pericellular matrix. First, we looked at the pericellular matrix of mesenchymal 3T3-L1 cells. The undifferentiated cells have a very characteristic mesenchymal morphology (Figure 11A). The particle exclusion assay reveals these cells to have a well-defined pericellular coat surrounding each cell (Figure 11B). After 1 hour treatment with exogenous aggrecan, the pericellular matrix appeared to swell and the visible coat became much larger (Figure 11C). When 3T3-L1 mesenchymal cells were exposed to *Streptomyces* hyaluronidase or HA_{oligos}, the pericellular matrix was nearly completely removed leaving the cells barely visible under the red blood cells (Figure 11D &E). The results from hyaluronidase treatment indicated that the pericellular matrix is dependent on hyaluronan while results from HA_{oligos} treatment suggest that the hyaluronan needs to be of high molecular weight to maintain the pericellular matrix. Additionally, displacement of pericellular coats by HA_{oligos} also indicated that the pericellular matrix is receptor–anchored and not covalently bound. However, if exogenous aggrecan were added to cells that have been pre-treated with HA_{oligos}, the pericellular matrix recovered and was not only visible, but of similar size to that of the untreated control (Figure 12C), suggesting mesenchymal 3T3-L1 cells can maintain a coat with newly synthesized hyaluronan that could be synthase bound or receptor bound hyaluronan-or both.

4. 3T3-L1 adipogenesis

4.1 Induction timeline and morphological changes

If maintained in culture medium with serum, 3T3-L1 cells will undergo adipogenesis in 2-4 weeks [228]. However, with adipogenic inducers, that timeline for adipogenesis is shortened to 7-10 days [229]. The general timeline used for the adipogenesis protocol is depicted in Figure 13A. The first day the cells were introduced to adipogenic inducers is termed Day 0. Four days before induction (Day -4), the cells were plated at a density of 10^4 cells per cm^2 on a culture dish in DMEM + 10% FBS-called Maintenance Media (MM). At this density, the cells became confluent in 2 days and entered a contact inhibitory phase. Two days post-confluency, Day 0, the cells were induced with the adipogenic medium Adipo 1 (1 µM Dexamethasone, 0.5 mM methylisobutylxanthine, and 1.7 µM insulin in MM). On Day 2, cells were treated with the full insulin dose in a medium called Adipo 2 (1.7 µM insulin in MM). On Day 4, cells were treated with a fourth of the original insulin dose with Adipo 3 (0.43 µM insulin in MM). Finally, on Day 6, the media was changed back to MM for the remainder of culture. If any experimental treatments were administered, they were done so at each medium change indicated by the red arrows above the timeline- on days 0, 2, 4, and 6 (Figure 4 in Methods). As 3T3-L1 cells undergo adipogenesis, drastic morphological changes were easily visible by phase contrast imaging. 3T3-L1 cells exhibited mesenchymal/fibroblastic morphology at time of plating (Figure 13B). By two days post-confluence, Day 0-the time of induction, the cells began to look a little less mesenchymal and started to round up like cobblestones (Figure 13C). By Day 4, four days post adipogenic induction, cells had more of a polygonal/cobblestone appearance and even a few cells were starting to contain visible lipid droplets (Figure 13D). Ten days post induction, the majority of cells were round and contained many lipid droplets made visible by staining with Oil Red O (Figure 13E).

3T3-L1 cells were used to confirm Hoechst 33342 efflux (Figure 9). 3T3-L1 cells were also planned to be an adipogenic control cell line to compare with the side population cells isolated from bovine articular cartilage. Therefore to serve as an adipogenic control, it was necessary to determine first if the differentiation assay could be scaled down to use a tenth of the cells usually required. This was a pre-requisite because of low cell numbers detected in the side population described in section 1.1. Figure 14 shows results from completing an adipogenic assay in a 48 and 96-well culture plate. 3T3-L1 cells adhered well and completed adipogenic differentiation in 48-well plates. While the 3T3-L1 monolayer was prone to detachment in the 96-well plate, there were enough cells still adhered to determine that 3T3-L1 cells can undergo adipogenesis on as little as a 0.32 cm^2 surface with an initial plating of 9,600 cells.

4.2. Markers for adipogenesis

One of the most commonly used markers for adipogenesis is positive Oil Red O staining. Oil Red O stains lipid droplets bright red and makes them easily visible by light microscopy. Mesenchymal 3T3-L1 cells had negligible Oil Red O staining (Figure 15A). After 3T3-L1 cells completed adipogenesis, the cells were round and contained many large lipid droplets that were highly stained (Figure 15B). Two other markers used for adipogenesis are the expression of fatty-acid binding protein-4 (*Fabp4*) and peroxisome-proliferator-activated receptor gamma (*Pparγ*) [230]. Messenger RNA for both these genes had similar expression patterns during adipogenesis but fold change was much greater for *Fabp4*. Expression from Day 0 to Day 2 remained constant but increased on Day 4. There was a 2-fold increase in *Pparγ* but nearly a 100-fold increase for *Fabp4* compared to Day 2 (Figure 15C & D). By Day 6, *Pparγ* increased another 3-fold and *Fabp4* increased another 50-fold compared to Day 4. Finally, on Day 10, expression of both makers

decreased. *Pparγ* showed about a 2-fold decrease while *Fabp4* showed approximately a 75-fold decrease when compared to Day 6.

4.3. Hyaluronan release and production

There are several media changes during 3T3-L1 adipogenic induction and it was observed that the medium became noticeably viscous around Day 4 or 6 when aspirating the medium with a Pasteur pipette connected to a vacuum. Long strings of medium were formed between the culture dish and the pipette tip (Figure 16A). If the change in viscosity had been the focus of this study, we could have quantified it with a viscometer (discussed more in Section 9). To determine if the increase in viscosity was due to an increase of hyaluronan, an ELISA was used to measure the hyaluronan concentration in the media collected prior to each media change (Figure 16B). The hyaluronan released into the media between days -4 and 0 (listed as Day 0) was the same concentration as the hyaluronan released between days 0 and 2 (listed as Day 2), both at around 2 µg/ml. There was a significant increase in hyaluronan detected in the medium that was released between days 2 and 4 (listed as Day 4) and again between days 4 and 6 (listed as Day 6), 5.8 and 7.8 µg/ml, respectively. Between days 6 and 10, hyaluronan detected in the medium had significantly decreased to 6.2 µg/ml. It is important to note that this last data point (listed as Day 10) was for 4 days of conditioning whereas the previous data points were for 2 days (except on day 0, which also had 4 days of conditioning). In order to determine that the ELISA used was specifically detecting hyaluronan, the Day 10 sample was treated with *Streptomyces* hyaluronidase because it specifically digests hyaluronan and not other glycosaminoglycans [231]. After analysis the digested sample produced a reading of 0.002 ng/ml, indicating that this ELISA was appropriate

for detecting and measuring hyaluronan in this conditioned medium and the results were not altered due to interfering components.

Three hyaluronan synthases have been identified in mammals, HAS1, HAS2, and HAS3 [232]. Total RNA was isolated and RT-PCR performed to determine which synthase was the major contributor to the hyaluronan detected in the conditioned media. On all days tested, -4, 0 and 10, *Has2* was found to have the highest level of mRNA expression as shown by the lowest ΔCT value when compared to *Has1* and *Has3* in Figure 16C. The ΔCT value was obtained by subtracting the *Has* CT (cycle threshold) value by the *Gapdh* CT value. This corrects for differences in sample metabolism. Day 0 saw the highest *Has2* and *Has3* expression while Days -4, and 10 were lower. *Has1* was only detected on Day -4 and was not detected (ND) on Day 0 or Day 10.

RT-PCR was also used to determine changes in *Has2* and *Has3* gene expression throughout adipogenesis (Figure 17). Both genes followed very similar expression patterns where expression initially decreased, then increased, then decreased again. There was a significant decrease in gene expression for both on Day 2 when compared to Day 0, and then both significantly increased on Day 4. Another decrease was observed for Day 6 and then again for Day 10. Expression levels for both *Has2* and *Has3* never rose above those detected for Day 0, which was set to 1.0.

4.4. Pericellular matrix of 3T3-L1 adipocytes

Western immunoblotting was used to determine changes in CD44 protein expression in 3T3-L1 cells on Days 0, 2, 4, 6, and 10 during adipogenesis (Figure 18A). Abundant CD44 protein was detected in cells that had not been treated with adipogenic inducers (Day 0) and two days post adipogenic induction (Day 2). There was a distinct reduction in CD44 protein detected on Day 4 and lower still on Day 6. By ten days post adipogenic detection (Day 10), CD44 was barely detected as faint band. GAPDH protein expression remained unchanged throughout adipogenesis.

RT-PCR was used to determine changes in mRNA expression of *Cd44* and *Vcan* genes, which are relevant to pericellular matrix production during adipogenesis of 3T3-L1 cells. Expression of *Cd44* mRNA showed an initial decrease in expression and then stayed essentially constant at more than 50% decrease through Day 10 (Figure 18B). However, *Vcan* expression increased slightly on Day 2 compared to Day 0 and then decreased significantly by Day 4. *Vcan* expression decreased a little more each day until it was about 90% lower than it started on Day 0 (Figure 18C). While there was an immediate reduction in *Cd44* message detected by RT-PCR two days after adipogenic induction, CD44 protein was present and detectable with immunoblotting until six days post adipogenic induction but was nearly undetectable after 10 days (Figure 18A).

Shown in Figure 11B, mesenchymal 3T3-L1 cells that had never been exposed to adipogenic inducers had a very prominent pericellular matrix. Even 3T3-L1 cells that had been exposed to adipogenic factors but retained their mesenchymal morphology had clearly visible coats (bottom micrographs in Figure 19A). However, once the 3T3-L1 cells differentiated into

adipocytes, this pericellular coat was lost (Figure 19A). Adipocytes appeared completely unable to form and retain a pericellular matrix. The 3T3-L1 adipocytes remained coatless even after the addition of exogenous aggrecan (Figure 19B), hyaluronan (Figure 19C), and the combination of exogenous aggrecan and hyaluronan (Figure 19D). It is important to note that the hyaluronan was incubated with the cells for 1 hour prior to the addition of aggrecan. This allowed time for exogenous hyaluronan to bind its receptor, CD44, before being decorated with the exogenous aggrecan. However, recall CD44 protein and mRNA expression decreased significantly during adipogenesis (Figure 18A and B). Only cells with mesenchymal morphology exhibited coats under these conditions.

4.5. Summary

In summary, a majority of 3T3-L1 cells successfully differentiated into adipocytes after adipogenic induction. This was demonstrated by intense Oil Red O staining of formed lipid droplets 10 days post induction and significant increases in *Fabp4* and *Pparγ* gene expression. Hyaluronan concentration significantly increased in culture medium during adipogenesis but expression of hyaluronan synthases, *Has2* and *Has3*, did not show a significant increase in expression. Expression of pericellular matrix components, *Cd44* and *Vcan*, both decreased during adipogenesis and adipocytes were unable to form or maintain a detectable pericellular coat.

5. Effects of 4-MU on 3T3-L1 adipogenesis

Our previous results showed that a large amount of hyaluronan was released from 3T3-L1 cells during adipogenesis. We wanted to determine the effects of inhibiting hyaluronan synthesis

on the ability of 3T3-L1 cells to adipogenically differentiate. 4-methylumbelleferone (4-MU) is a coumarin derivative that inhibits cellular production of hyaluronan by reducing UDP-GlcUA available inside the cell, which is a required precursor for hyaluronan synthesis [233-235]. 4-MU was added to the culture medium every time the medium was changed according to the timeline in Figure 13A.

5.1 Markers of adipocyte differentiation

4-MU significantly reduced the ability of 3T3-L1 cells to undergo adipogenesis. Figure 20A shows strong Oil Red O staining for the control sample and no visible staining for the 4-MU treated cultures. A higher magnification view of the two culture conditions in Figure 20B revealed that almost all cells in the control sample had large lipid droplets stained with Oil Red O. However, even though the 4-MU treated culture showed a confluent lawn of cells, only one cell had visible Oil Red O staining. When the Oil Red O stain was extracted from both samples and quantified, the absorbance readings showed that 4-MU treatment significantly reduced the amount Oil Red O stain retained by the cells (Figure 20C).

Phase contrast microscopy did not reveal any visible differences in morphology of the monolayers between control and 4-MU treated 3T3-L1 cultures for Day 2. A few round cells with lipid droplets were visible for the first time starting on Day 4 in the control cultures while 4-MU treated cells did not have visible lipid droplets until Day 6, but even then, the lipid droplets appeared smaller and fewer in number. On Day 10, the control cultures were largely composed of round adipocytes with many lipid droplets while the 4-MU treated cultures contained only a few adipocytes (Figure 21). Cells were counted from several micrographs (Table 2) and the

percentages of cells with mesenchymal or adipocyte morphology were graphed (Figure 22). After 4 days adipogenic induction, 2% of the entire control sample population had already accumulated lipid droplets while a scant few were counted for the 4-MU treated sample, 0.3%. Two days later, 50% of the entire control cell population had formed visible lipid droplets while the 4-MU treated sample contained 5%. By day 10, 80% of the total control cell population had visible lipid droplets while the 4-MU treated sample contained only 4%.

RT-PCR was used to determine gene expression of the adipogenic markers *Fabp4* and *Pparγ*. At all days tested, 2, 4, 6, and 10, *Fabp4* mRNA expression was significantly decreased in 4-MU cultures compared to controls (Figure 23A). The highest expression of *Fabp4* for the 4-MU treated group was a 30-fold increase observed on Day 6, when compared to Day 0. This was still significantly lower than the expression in the control cultures, which had an average of almost a 90-fold increase compared to Day 0. *Pparγ* expression was significantly decreased by 4-MU treatment on Days 2, 6, and 10 when compared to the untreated control cultures (Figure 23B). All 4-MU treated cultures had an average *Pparγ* expression below that of the Day 0 sample. The highest expression of *Pparγ* in control cultures was on Day 6 with an average of a 4-fold increase when compared to Day 0.

5.2 Hyaluronan release and production

An ELISA was used to determine if 4-MU treatment affected the amount of hyaluronan detected in conditioned media during 3T3-L1 adipogenesis. At each media change, the conditioned medium was collected, centrifuged to remove suspended cells, and then equal volumes were

analyzed via a commercially available hyaluronan ELISA. 3T3-L1 cells that were treated with 4-MU during adipogenesis had significantly reduced amounts of hyaluronan detected in the conditioned media for all days tested (Figure 24). The highest amount of hyaluronan quantified for the untreated control samples was 7.6 µg/ml on Day 6, while the highest amount detected for the 4-MU treated samples was less than half that at 2.3 µg/ml on Day 4.

RT-PCR was used to determine if the decrease in detected hyaluronan concentration in the culture medium for 4-MU treated 3T3-L1 cells was due to a change in hyaluronan synthase expression. While there was an initial decrease in *Has2* expression compared to the untreated control on Day 2, *Has2* expression was significantly increased in 4-MU treated samples compared to untreated for the rest of adipogenesis determined on Day 4, Day 6, and Day 10 (Figure 25A). However, all *Has2* expression levels for both control and 4-MU treated cultures were still less than what was detected on Day 0. *Has3* had very similar expression patterns except all 4-MU treated cultures had increased expression when compared to untreated control cultures on Days 2, 4, 6, and 10 (Figure 25B). Also, all *Has3* expression levels in all cultures were less than that seen on Day 0.

5.3. Pericellular matrix

A particle exclusion assay was used in order to determine if 4-MU treatment affects the ability of 3T3-L1 cells to form or maintain a pericellular matrix. Six or 10 days after adipogenic induction, with or without 4-MU treatment, 3T3-L1 cells were transferred to a new culture well and allowed to adhere overnight before undergoing a particle exclusion assay. Regardless of day tested, 3T3-L1 cells that had undergone adipogenic differentiation did not have a detectable

pericellular matrix while cells that remained mesenchymal had a clearly visible pericellular coat (Figure 26A & B). It should be noted that because so few 3T3-L1 cells undergo adipogenesis in the presence of 4-MU, no adipocytes were able to be tested with the particle exclusion assay. However, the mesenchymal cells that remained had visible coats at both 6 and 10 days (Figure 26C & D).

RT-PCR was used to determine changes in mRNA expression of pericellular matrix components, *Cd44* and *Vcan*. While *Cd44* expression was similar regardless of exposure to 4-MU on Day 2, for the remainder of the adipogenesis protocol, *Cd44* expression was significantly higher in 4-MU treated samples when compared to untreated control (Figure 27A). However, all *Cd44* expression levels were more than 50% lower than those seen on Day 0. Very similar expression patterns for *Vcan* were observed (Figure 27B). Expression levels for Day 2 were similar regardless of 4-MU exposure while for the remaining days analyzed, 4-MU treated samples had a significantly increased *Vcan* expression. Expression levels for Day 2 were similar to the level obtained for Day 0, regardless of exposure to 4-MU. All *Vcan* expression levels were lower than those observed on Day 0 for the remainder of adipogenesis.

5.4. Summary

Treatment with 4-MU decreased the ability of 3T3-L1 cells to undergo adipogenesis. This was demonstrated by an observed reduction in the number of cells containing lipid droplets in addition to significant decreases in adipogenic markers, Oil Red O stain and *Fabp4* and *Pparγ*

mRNA expression. Hyaluronan concentration was significantly decreased in the culture medium but hyaluronan synthases, *Has2* and *Has3*, were significantly increased in 4-MU treated cultures. 4-MU treatment did not affect the ability of mesenchymal 3T3-L1 cells to form a pericellular coat and adipocytes were still not able to synthesize a coat. Expression of pericellular related genes, *Cd44* and *Vcan* were upregulated in 4-MU treated cultures compared to the untreated control.

6. Isolation of proteoglycan from bovine articular cartilage

Aggrecan monomer is not always commercially available and even when it is, the product is of unknown purity and integrity. Our lab has found isolating aggrecan from bovine articular cartilage with a dissociative CsCl density gradient through ultra-centrifugation to be the most efficient at producing a consistent, quality product [177, 179]. This aggrecan isolation procedure is outlined in Figure 28A. Full thickness cartilage slices were harvested from the metacarpophalangeal joint of 18-24 month old steers and then flash frozen in liquid nitrogen before being pulverized into a powder. After extracting the cartilage components in 4 M guanidine HCl, the extract was centrifuged in a CsCl gradient at high speed to yield the D1 (bottom) fraction containing the desired proteoglycan monomer. This fraction was dialyzed to dilute the CsCl and any remaining guanidine. After lyophilization, the aggrecan preparation was tested for purity and quality by electrophoresis on a 1% agarose gel. Lanes 1-4 of Figure 28B demonstrated purity of the isolated aggrecan. Solubilized aggrecan is shown in lane 3, while a sample pre-treated with *Streptomyces* hyaluronidase is seen in lane 4. If the aggrecan product were contaminated with the hyaluronan of the neighboring fraction, the band in lane 4 would have shifted. Lane 2 contains commercial hyaluronan while lane 1 shows this hyaluronan treated with the same *Streptomyces*

hyaluronidase to ensure the enzyme and conditions were correct for digestion. Lanes 5-7 demonstrated the quality of the isolated aggrecan. Lane 5 contains the aggrecan monomer, commercial hyaluronan in lane 6, and aggrecan + hyaluronan in lane 7. When aggrecan and hyaluronan are combined, very large aggregates are produced that are not well resolved by electrophoresis. This proteoglycan aggregate is seen in the loading well of lane 7 indicating that the purified aggrecan retained the ability to bind hyaluronan. The isolated aggrecan was added to rat chondrosarcoma (RCS) cells to ensure it could bind endogenous, cellular hyaluronan and did not still contain any leftover deleterious agents. RCS cells were plated at subconfluent density and cultured for 48 hours. Using the particle exclusion assay, small pericellular matrices were observed surrounding the RCS cells (Figure 28C). However, following addition 2mg/ml of the isolated aggrecan to these RCS cultures for one hour, the sizes of the pericellular matrices were noticeably larger (Figure 28D). This demonstrated that the isolated aggrecan is capable of forming aggregates with endogenous hyaluronan.

7. Effects of exogenous aggrecan on 3T3-L1 adipogenesis

7.1. Markers of adipocyte differentiation

The addition of exogenous aggrecan significantly reduced the ability of 3T3-L1 cells to undergo adipogenesis. Figure 29A shows strong Oil Red O staining for the control cultures and much lighter staining for the aggrecan treated cultures. A higher magnification view of the two cultures in Figure 29B revealed that almost all cells in the control cultures had large lipid droplets

stained with Oil Red O. However, even though the aggrecan treated cultures appeared as a confluent lawn of cells, only a few cells had visible Oil Red O staining. When the Oil Red O stain was extracted from both samples and quantified, the absorbance readings showed that aggrecan addition during adipogenesis significantly reduced the amount of Oil Red O retained by the cells on Day 10 (Figure 29C).

Phase contrast microscopy did not reveal any visible differences in monolayers between control and aggrecan treated 3T3-L1 cultures for Day 2. A few round cells with lipid droplets were visible for the first time starting on Day 4 in the control cultures while aggrecan treated cultures did not contain cells with visible lipid droplets until Day 6. On Day 10, the control cultures were largely composed of round adipocytes with many lipid droplets while the aggrecan treated cultures had few visible adipocytes (Figure 30).

RT-PCR was used to determine gene expression of the adipogenic markers *Fabp4* and *Pparγ*. There were no significant differences in *Fabp4* expression observed between aggrecan treated and untreated control cultures for Days 2 and 10, however, *Fabp4* mRNA expression was significantly decreased in aggrecan treated samples on Days 4 and 6 compared to controls (Figure 31A). There was less than a 10-fold increase in *Fabp4* expression for both treated and untreated 3T3-L1 samples on Day 2. In Day 4 cultures, there was an ~150-fold increase in *Fabp4* expression in the controls while only a ~25-fold increase after aggrecan treatment when compared to Day 0. Although *Fabp4* expression for the aggrecan treated cultures was still ~25-fold increase on Day 6, expression for the controls climbed to a ~170-fold increase. Day 10 saw the largest increase in *Fabp4* expression for the aggrecan treated cultures at ~125-fold increase, but this was not

significantly different than the ~115-fold increase seen for the untreated control. *Pparγ* expression followed a very similar pattern to that of *Fabp4*. There were no significant differences in *Pparγ* expression observed between aggrecan treated and untreated control cultures for Days 2 and 10, however, *Pparγ* mRNA expression was significantly decreased in aggrecan treated cultures on Days 4 and 6 compared to control cultures (Figure 31B). There was less than a ~3-fold increase in *Pparγ* expression for both treated and untreated 3T3-L1 cultures on Day 2. Day 4 saw a little over a ~20-fold increase in expression for the control culture while the aggrecan treated culture was only a ~7-fold increase when compared to those from Day 0. While *Pparγ* expression for the aggrecan treated cultures dipped to a ~4-fold increase on Day 6, expression for the control remained significantly higher at a ~16-fold increase. Day 10 saw the largest increase in *Pparγ* expression for the aggrecan treated culture at a ~14-fold increase, but this was not significantly different than ~10-fold increase seen for the untreated 3T3-L1 culture.

7.2. Pericellular matrix

RT-PCR was used to determine changes in mRNA expression of pericellular matrix components, *Has2*, *Has*3, *Vcan*, and *Cd44*. The only day *Has2* expression was lower in the aggrecan treated cultures than the untreated controls was on Day 2 (Figure 32A). For the remaining days tested, 4, 6, and 10, *Has2* expression in the aggrecan treated cultures was significantly higher than the untreated controls. While *Has2* expression levels in the untreated controls never rose above those observed on Day 0, which was set equal to 1.0, *Has2* expression on Days 4, 6, and 10 ranged between 1.4 and 2-fold higher for the aggrecan treated cultures. Expression patterns for *Has3* were similar to those of *Has2*. The only day *Has3* expression was lower in aggrecan treated cultures than the untreated controls as on Day 2 (Figure 32B). For the remaining days tested, 4, 6,

and 10, *Has3* expression levels in the aggrecan treated samples were higher than the untreated control but only significantly higher on Day 6. While *Has3* expression levels in the untreated controls never rose above 1.5-fold higher than observed on Day 0, the largest *Has3* mRNA increase was for the aggrecan treated cultures on Day 6 at a 3-fold increase.

There were no statistically significant differences observed in *Cd44* mRNA expression levels between 3T3-L1 cells undergoing adipogenesis with or without exposure to exogenous aggrecan (Figure 33A). Expression for Day 2 was similar to Day 0 which was set equal to 1.0. All remaining days tested, 4, 6, and 10 demonstrated lower levels of expression with the lowest observed on Day 6 at 0.75-fold less than that of Day 0. Unlike *Cd44* expression, aggrecan exposure did have a significant impact on *Vcan* mRNA levels. For all days tested, *Vcan* expression was significantly higher in aggrecan treated 3T3-L1 cultures than the untreated controls for the same day (Figure 33B). The highest *Vcan* expression seen for the aggrecan treated cultures was on Day 2, which was a 15-fold increase compared to 3-fold increase for the untreated controls over Day 0. The highest expression for the untreated controls was observed on Day 4, a 7-fold increase, while the aggrecan treated 3T3-L1 sample was significantly higher at a 10-fold increase as compared to Day 0.

7.3. Partial recovery of adipogenesis

The previous sections demonstrated that exposure to exogenous bovine aggrecan inhibited adipogenesis of 3T3-L1 cells. Because there were no significant differences in adipogenic markers,

Fabp4 and *Pparγ*, on Day 10, that may suggest the 3T3-L1 cells are able to overcome the inhibitory effects of aggrecan if allowed to differentiate a little longer without aggrecan. To determine if adipogenesis of 3T3-L1 cells could recover, cells were treated with exogenous aggrecan in induction media for 6 days or 10 days, then fresh MM was added excluding the aggrecan. Figures 34 and 35 depict micrographs of 3T3-L1 monolayers after fixation and Oil Red O staining at 400 and 600x final magnification, respectively. Only samples for untreated control and aggrecan treated are present for Day 6 because this was the first day aggrecan was excluded from the culture medium. The control cultures contained many more cells with visibly stained lipid droplets than the aggrecan treated cultures. Day 10 shows similar results to Day 6, the control sample had many more stained cells than did the aggrecan treated sample. 3T3-L1 cells that were exposed to aggrecan until Day 6 of the adipogenesis protocol but switched to MM from Day 6 to Day 10 are shown under "+/- Aggrecan" for Day 10. The absence of aggrecan for the remaining 4 days of the adipogenesis protocol appeared to result in a slight increase in the number of adipocytes compared to the cultures that contained aggrecan for the entire adipogenesis protocol (+Aggrecan). The Day 14 and 18 images depict control 3T3-L1 cultures that completed adipogenesis untreated and were maintained in MM for 4 and 8 additional days, cultures that were treated with aggrecan during adipogenesis and with aggrecan added to the MM for 4 and 8 extra days, and 3T3-L1 cultures that were treated with aggrecan during adipogenesis but then not exposed to aggrecan for the 4 and 8 extra days while in MM (+/-Aggrecan). Cultures that were treated with exogenous aggrecan for the entire culture period had visibly fewer stained adipocytes than did the untreated control cultures for both Days 14 and 18. Additionally, cultures that had aggrecan removed from culture on Day 10 (+/-Aggrecan), appeared to have slightly more stained adipocytes than the cultures that were exposed with exogenous aggrecan for the entire experiment. However, the +/- Aggrecan cultures

had noticeably fewer adipocytes than did the untreated control cultures. Adipocytes that were cultured for 14 and 18 days in the control conditions appeared to have larger lipid droplets than the cells of all the other cultures (Figure 34).

As an indirect way to quantify the amount of adipogenesis that occurred in 3T3-L1 cultures treated with and without exogenous aggrecan, Oil Red O stain was ethanol extracted and absorbance was obtained (Figure 36). 3T3-L1 cultures treated with aggrecan to Day 6 had less Oil Red O staining than untreated controls. This observation was made for all days tested. There was an increase in Oil Red O staining for both aggrecan treated and untreated cultures on Day 10 compared to Day 6. Cultures that were treated with aggrecan for 6 or 10 days of adipogenesis and then not for the remainder of the experiment had a statistically significant increase in Oil Red O staining when compared to cultures treated with aggrecan for the entire duration of adipogenesis. Although this trend was observed for all days tested, the amount of staining for these cultures never increased to what was observed in the untreated control cultures.

7.4. Summary

Treatment with exogenous bovine aggrecan decreased the ability of 3T3-L1 cells to undergo adipogenesis. This was demonstrated by an observed reduction in the number of cells containing lipid droplets in addition to significant decreases in adipogenic markers, Oil Red O staining and *Fabp4* and *Pparγ* mRNA expression. Hyaluronan concentration could not be determined in aggrecan treated samples because of interference with hyaluronan detection.

However, hyaluronan synthases, *Has2* and *Has3*, were significantly increased in aggrecan treated cultures. Expression of pericellular related gene, *Cd44*, was not significantly affected by aggrecan treatment but *Vcan* was significantly upregulated compared to the untreated control. When aggrecan was removed from previously treated samples, 3T3-L1 cells were able to partially recover their adipogenic capabilities when culture periods were extended.

8. Visualization of hyaluronan internalization

To determine if hyaluronan was internalized by the 3T3-L1 cells during adipogenic differentiation, the cells were fixed, permeabilized, and incubated with a commercially available biotinylated hyaluronan binding protein (bHABP) followed by avidin conjugated to a fluorophore to visualize hyaluronan (-SH). Some cells were pre-treated with *Streptomyces* hyaluronidase (+SH) to remove extracellular hyaluronan so only intracellular hyaluronan would be visible. Figure 37 depicts fluorescent micrographs of 3T3-L1 cells during adipogenesis probed with bHABP for hyaluronan (green) and with DAPI for nuclear staining (blue). Mesenchymal 3T3-L1 cells (-SH) had intense fluorescence for hyaluronan but that was reduced for the +SH treated cells indicating most of the hyaluronan is located externally. Confluent 3T3-L1 cells lost intensity of external hyaluronan fluorescence on Day 0, but regained it by Day 2. SH treatment revealed that there is little internal hyaluronan until cells contained lipid droplets (from day 4 to 10) which then appeared to be outlined by the hyaluronan. Figure 38 contains fluorescent micrographs of 3T3-L1 cells treated with exogenous bovine aggrecan throughout adipogenesis. These cells were also probed with bHABP and DAPI and show similar results to those in Figure 37 in that 3T3-L1 cells did not exhibit intense internal hyaluronan fluorescence until differentiation into adipocytes.

9. Limitations of study

The low recovery of side population cells from bovine articular cartilage limited the proposed studies using these cells. Nonetheless, this study achieved its aim to gain insight into how hyaluronan and its associated components participate in directing adipogenesis of 3T3-L1 cells but contained some limitations worth mentioning. First, it is important to emphasize that any RNA or protein samples obtained from cell cultures at different stages during adipogenesis contained cells at various stages of differentiation. In some experiments, such as the particle exclusion assay, this mixed population was beneficial because there was essentially a control (undifferentiated mesenchymal) population of cells in the same well as differentiating cells. However, RNA collected from cells during adipogenic differentiation consisted of RNA isolated from undifferentiated mesenchymal cells as well as fully differentiated adipocytes and the stages in between. From these data, it is unclear what percentage of cells had altered gene expression and we can only conclude that the average gene expression for the whole cell population changed. This resulted in increased variability from experiment to experiment and could have interfered with the statistical analysis. Nonetheless, statistical significance was shown for many data points and supports the trends of differentiation revealed in this study.

The shift in focus of this study was prompted by the observation that culture medium of differentiating 3T3-L1 cells was more viscous than that of mesenchymal 3T3-L1 cells. At no point was the actual viscosity measured and observations were simply made while aspirating the medium. This observation could have been easily quantified with an Ubbelohde viscometer, mass spectrometry, or size exclusion chromatography. Media samples were collected and stored for all

time points tested so the viscosity could be analyzed for a future study that has more emphasis on comparing viscosity at various time points during adipogenesis.

Lastly, a lot of trust was placed into ZenBio, Inc. to provide a pure culture of 3T3-L1 cells as we did not authenticate their identity or purity. The biggest concern for contamination lies with our novel finding that 3T3-L1 cells have chondrogenic potential. The 3T3-L1 cell line was derived from the parental NIH-3T3 cell line which is capable of undergoing chondrogenic differentiation [236]. Studies using chondrogenic media and micromass cultures of mesenchymal cells require a high cell number density for cell-cell interactions to generate aggrecan-positive cartilage nodules. This study used the same preparation of 3T3-L1 cells for both chondrogenic and adipogenic differentiation. The parental NIH-3T3 does not undergo efficient adipogenic differentiation under the same conditions as 3T3-L1 cells [237] and since this study observed consistently efficient adipogenesis with recommended 3T3-L1 adipogenesis conditions, it is unlikely there is significant, if any, NIH-3T3 contamination.

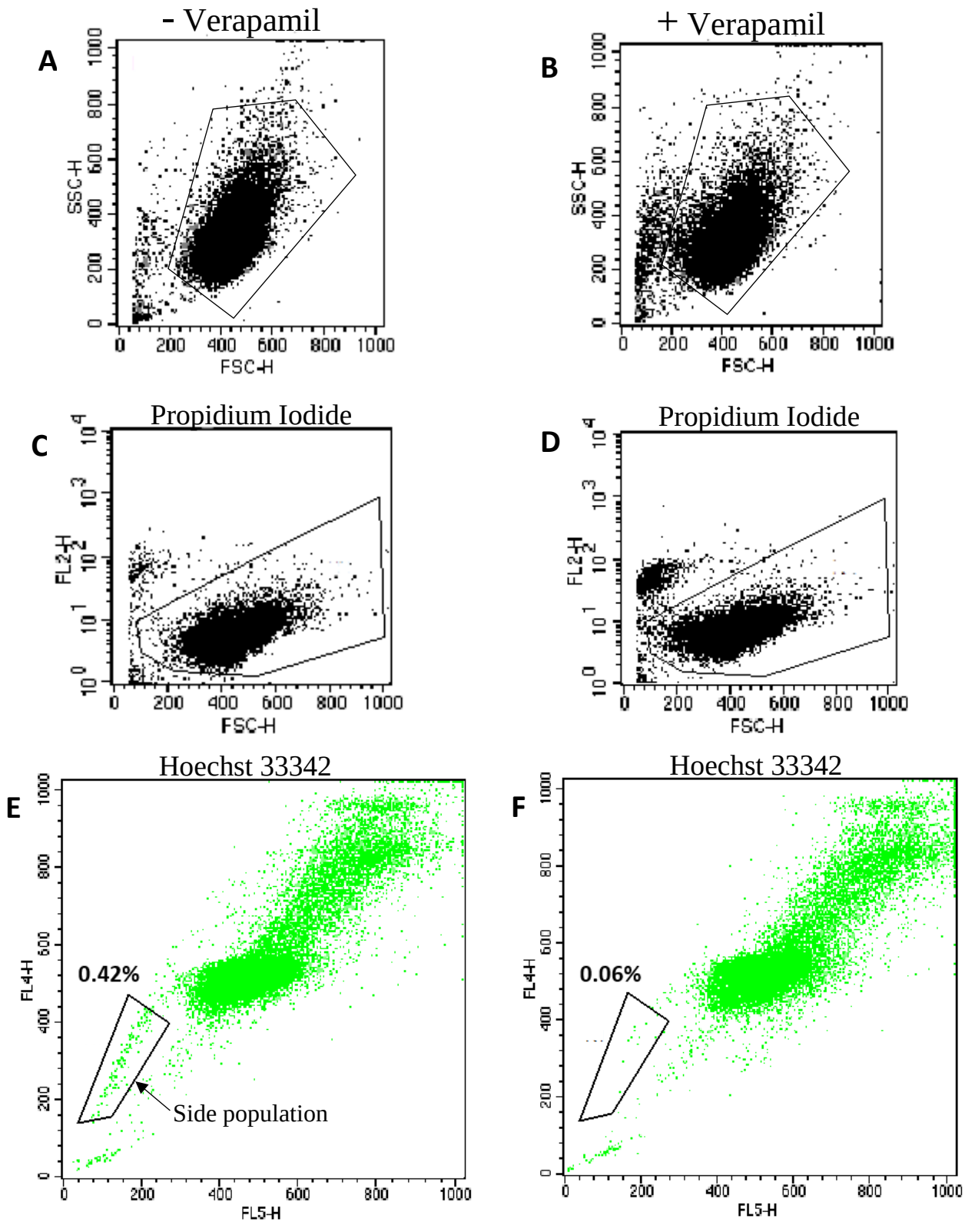
- Verapamil
A
SSC-H
FSC-H
+ Verapamil
B
SSC-H
FSC-H
Propidium Iodide
C
FL2-H
FSC-H
Propidium Iodide
D
FL2-H
FSC-H
Hoechst 33342
E
0.42%
FL4-H
FL5-H
Side population
Hoechst 33342
F
0.06%
FL4-H
FL5-H

Figure 5. Verification of side population detection method using flow cytometry.

MCF-7 cells were stained with 10 μg/ml Hoechst 33342 and 2 μg/ml propidium iodide (PI) after treatment with (B, D, F) and without (A, C, E) 50 μM verapamil and then analyzed via flow cytometry to determine the presence of a side population. Cell singlets versus doublets were determined using FSC-A (forward scatter)/SSC-A (side scatter) analysis. Cell doublets were excluded and only cell singlets were gated (inside polygons) for analysis (A+B). Live versus dead cells were determined using PI fluorescence (FL2-H) plotted against forward scatter. Only live cells were gated (inside polygon) and analyzed (C+D). Single, live cells were analyzed for Hoechst 33342 fluorescence using blue (FL4-H) and red (FL5-H) channels. Dots enclosed in polygons represent the side population of MCF-7 cells with the percentage of side population out of total cells is listed (E+F).

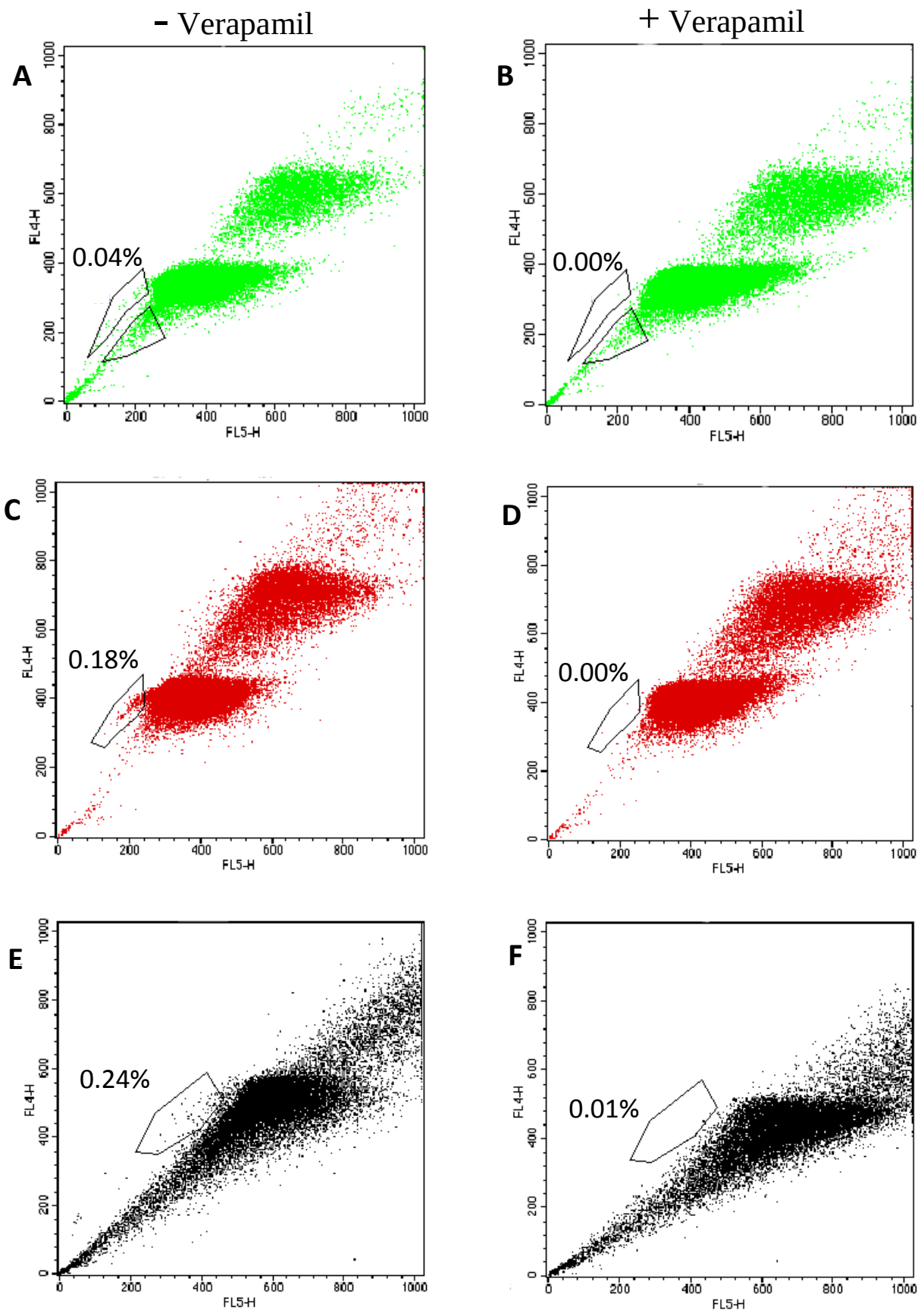
- Verapamil
+ Verapamil
A
B
C
D
E
F
0.04%
0.00%
0.18%
0.00%
0.24%
0.01%
FL4-H
FL5-H
0
200
400
600
800
1000

Figure 6. Detection of side population in cells isolated from bovine articular cartilage. Primary cells, isolated from articular cartilage of bovine metacarpophalangeal joints, were stained with 10 μg/ml Hoechst 33342 and 2 μg/ml propidium iodide (PI) with (B, D, F) and without (A, C, E) 50 μM verapamil treatment and then analyzed via flow cytometry to detect a side population. Single, live cells were determined using forward vs. side scatter and PI staining and then analyzed for Hoechst 33342 fluorescence using blue (FL4-H) and red (FL5-H) channels. Percentage of side population is listed for each experimental set. Three separate experiments are shown.

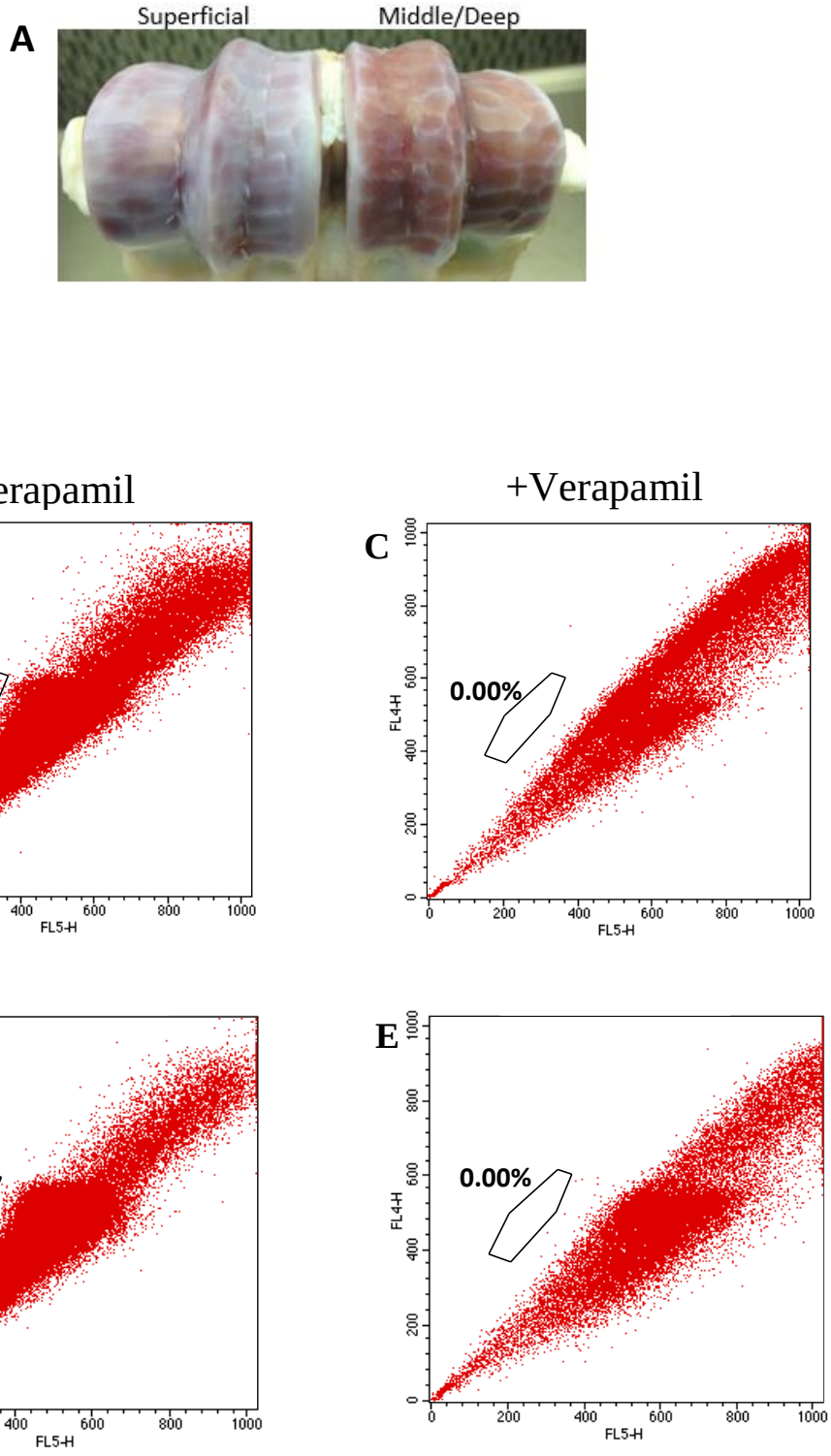
A
Superficial
Middle/Deep
-Verapamil
+Verapamil
B
C
D
E
Superficial
Middle/Deep
0.06%
0.00%
0.02%
0.00%
FL4-H
FL5-H
0
200
400
600
800
1000

Figure 7. Detection of side population in cells isolated from superficial and middle/deep layers of bovine articular cartilage. Thin, superficial slices of cartilage tissue were harvested from the upper condyles of bovine metacarpophalangeal joints leaving both middle and deep cartilage layers behind. An additional layer was harvested as the middle/deep cartilage layer (A). Primary cells were isolated from these separate superficial and middle/deep layers and stained with 10 μg/ml Hoechst 33342 and 2 μg/ml propidium iodide (PI) with (C & E) and without (B & D) 50 μM Verapamil treatment and then analyzed via flow cytometry to detect a side population. Single, live cells were determined using forward vs. side scatter and PI staining and then analyzed for Hoechst 33342 fluorescence using blue (FL4-H) and red (FL5-H) channels. Percentage of side population from the total cell population is listed for each experimental above polygon.

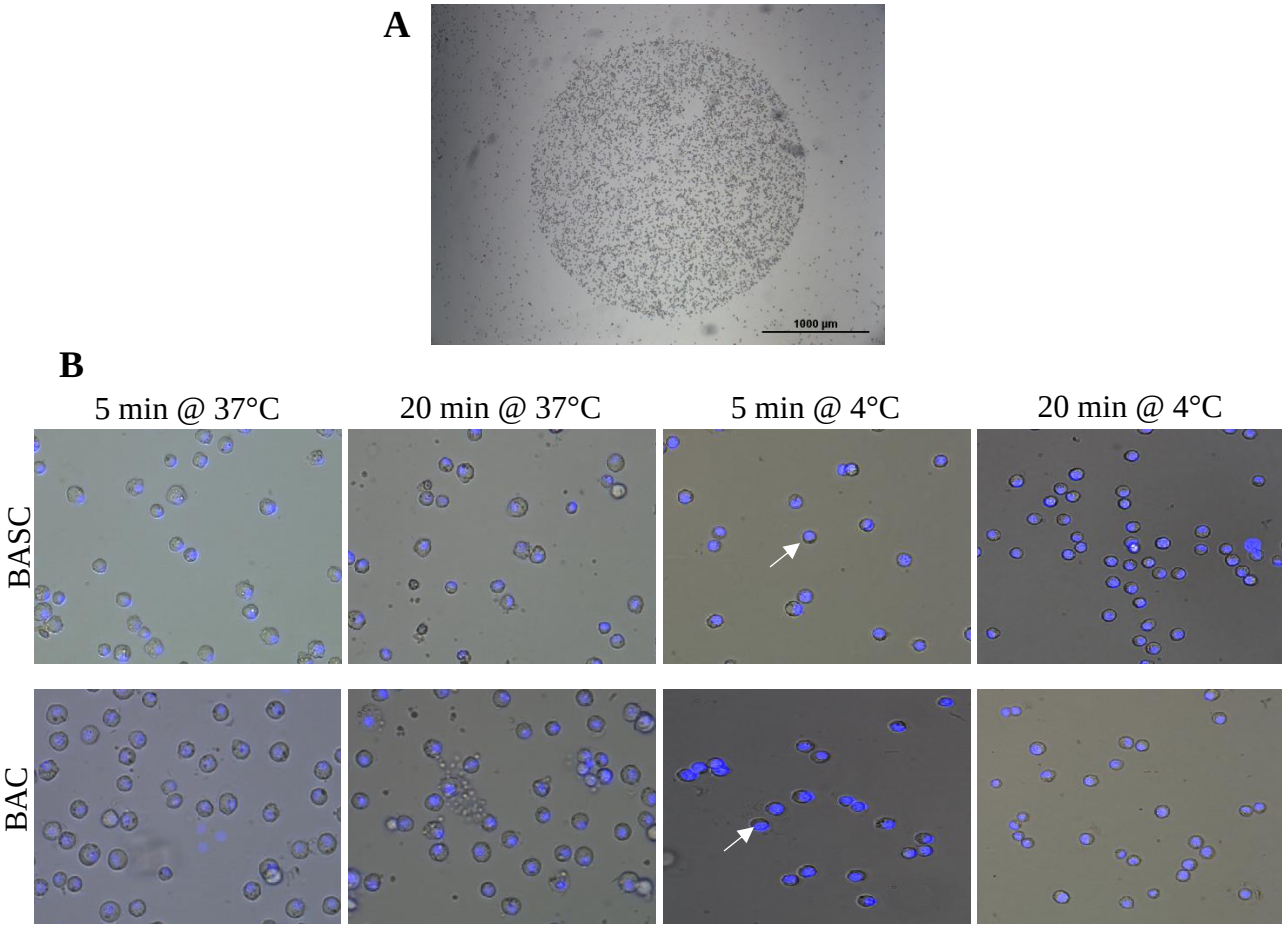
A
1000 µm
B
5 min @ 37°C
20 min @ 37°C
5 min @ 4°C
20 min @ 4°C
BASC
BAC

Figure 8. Isolation of side population using fibronectin adhesion. Primary cells isolated from bovine articular cartilage were allowed to adhere to fibronectin spots coated onto sterile petri dishes for 20 minutes at 37°C then rinsed. One spot is shown in panel A (Bar = 1000 μm). Cells that were able to adhere to fibronectin are termed Bovine Articular Stem Cells (BASC) and comprise the side population. Cells that did not adhere where collected and termed Bovine Articular Chondrocytes (BAC). Both populations were incubated with 10 μg/ml Hoescht 33342 for 5 or 20 minutes at 4 or 37°C, rinsed, and then microscopically observed for Hoechst fluorescence (B). White arrows indicate representative fluorescing cells.

A.

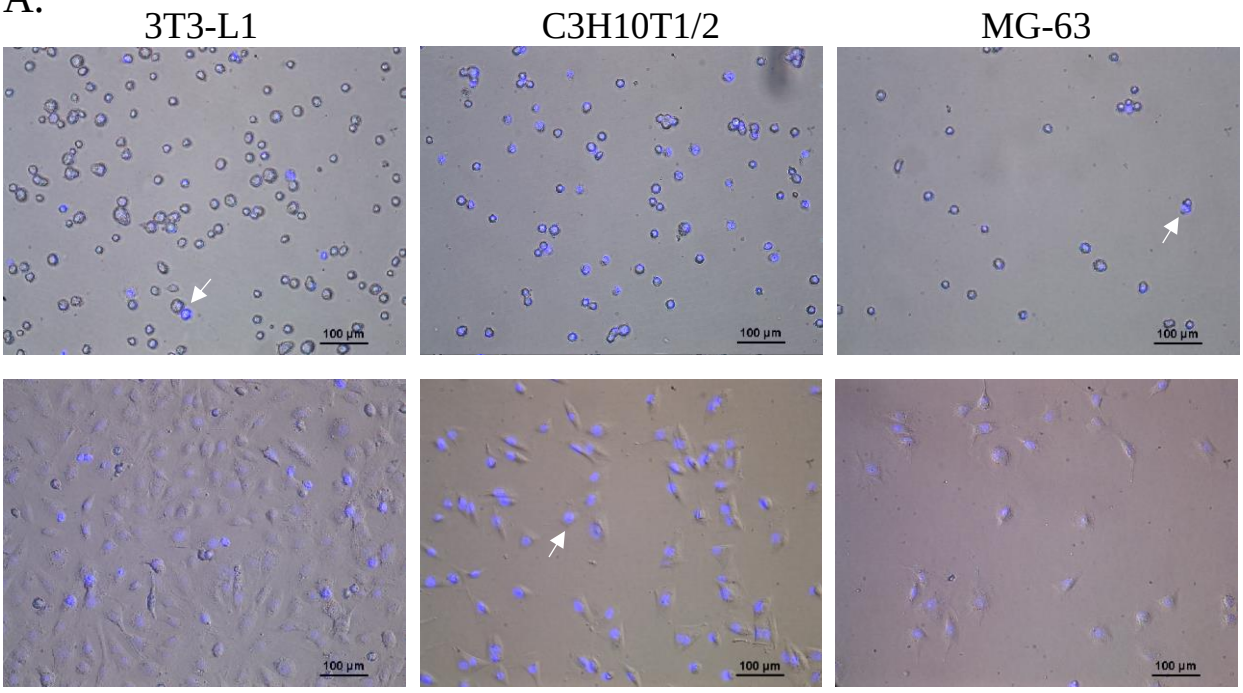

B.

	Total cells	No Efflux
3T3-L1	545	54
C3H10T1/2	257	254
MG-63	81	60

C.

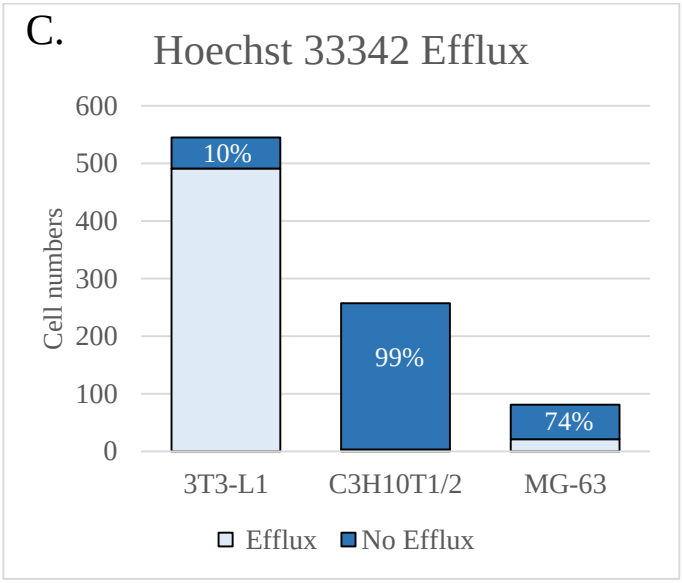

Figure 9. Determination of Hoechst 33342 efflux from various cell lines. 3T3-L1, C3H10T1/2, and MG-63 cells were incubated with 10 μm/ml Hoechst 33342 for 5 minutes at 37°C. After centrifugation and re-suspension, the cells were plated in culture dishes and incubated at 37°C. Hoechst 33342 efflux was checked by microscopic observation at 1 (top row) and 3 hours (bottom row). White arrows indicate representative fluorescing cells (A). Two micrographs of 1 hour incubation and 1 micrograph of 3 hour incubation were used to count cells for each cell type and summed in the chart depicted in panel B. Cells that did not efflux Hoechst 33342 are represented by dark blue and cells that did efflux Hoechst 33342 are represented by light blue in the bar graph shown in C. The percentage of cells that had not effluxed Hoechst 33342 stain (blue cells) compared to total cells are listed in white.

A

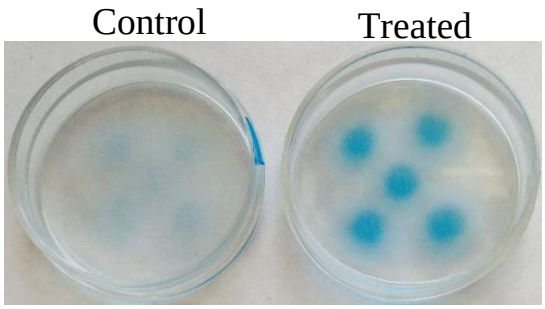

B

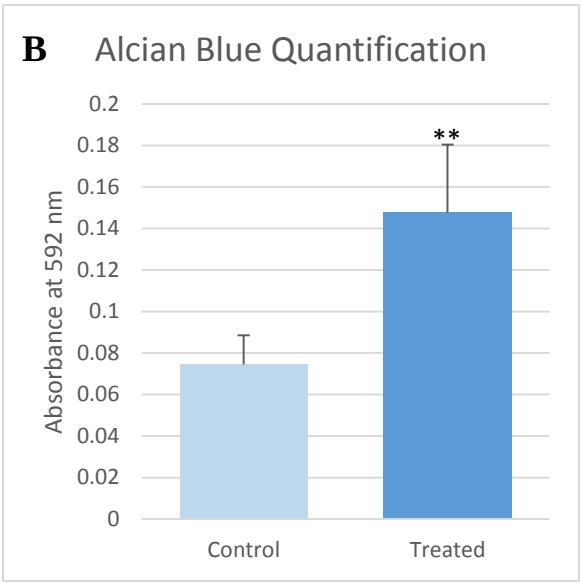

C

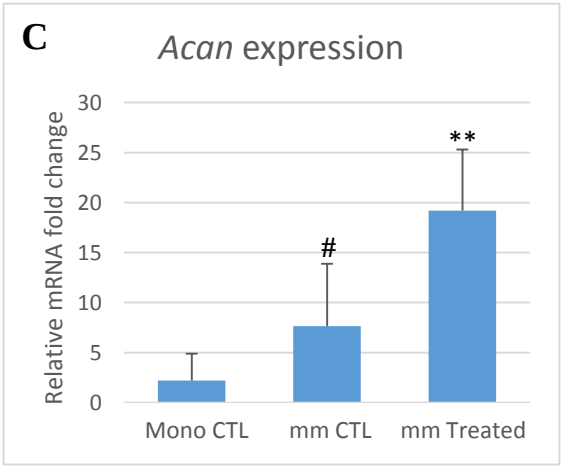

D

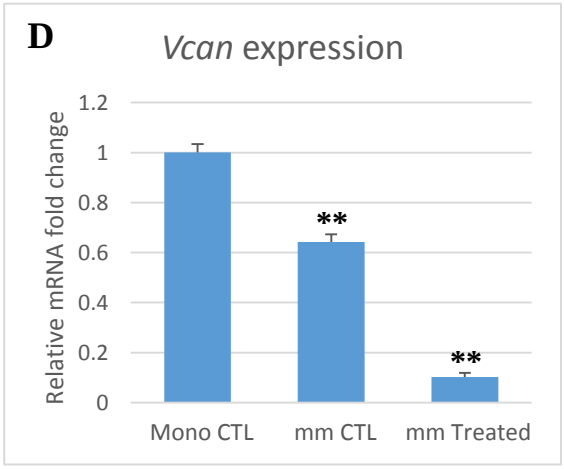

E

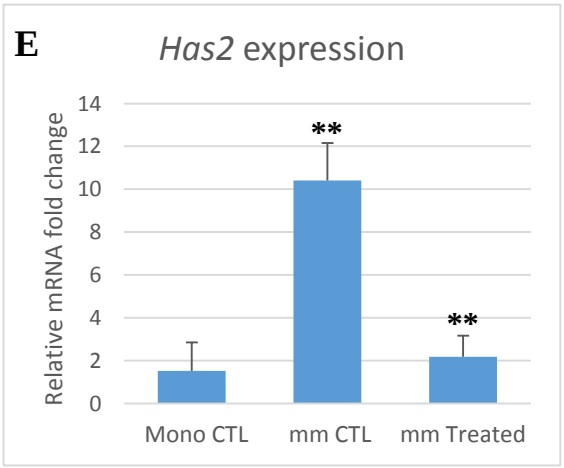

F

	ΔCT	
	Acan	*Vcan*
Mono CTL	17.61	4.19
mm CTL	15.02	4.83
mm Treated	13.40	7.48

Figure 10. Chondrogenic potential of 3T3-L1 cells. Micromass cultures of 3T3-L1 cells were incubated with a without a chondrogenic medium for 10 days and then stained with Alcian blue (A). Alcian blue stain was extracted from micromass cultures with overnight incubation of 4 M gaunidine HCl and absorbance was obtained at a 592 nm wavelength (B). Bars in B represent the mean $\pm$ standard deviation from 3 independent experiments analyzed in duplicate. Total RNA was extracted from micromass cultures after 10 days incubation with (mm treated) and without (mm CTL) a chondrogenic medium. The relative fold change of *Acan* (C), *Vcan* (D), and *Has2* (E) mRNA were quantified using the $\Delta\Delta$CT method using a 3T3-L1 monoculture as the control (Mono CTL) and normalizing with *Gapdh* mRNA expression. Bars in C, D, and E represent the mean $\pm$ standard deviation from 2 independent experiments analyzed in duplicate. The relative detection of *Acan* and *Vcan* mRNA are represented as mean ΔCT values in panel F. ΔCT values equal the gene of interest CT value – reference gene (*Gapdh*) CT value which compensates for differences in cell sample metabolisms. Values are inversely proportional to relative amount of mRNA (smaller numbers mean larger amounts of mRNA). #: p-value < 0.1, **: p-value < 0.01

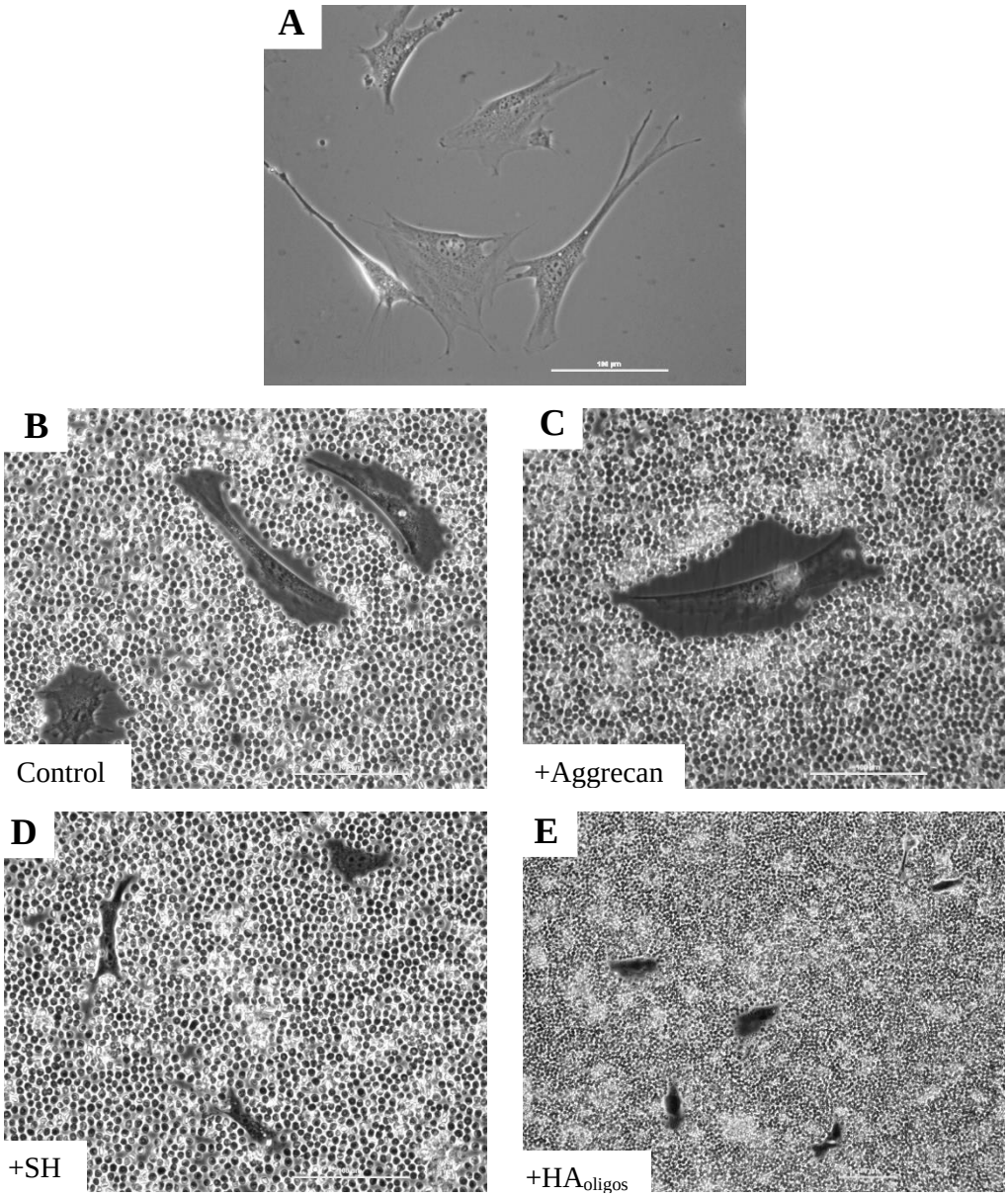
A
B
Control
C
+Aggrecan
D
+SH
E
+HA$_{oligos}$

Figure 11. Effects of exogenous aggrecan, *Streptomyces* hyaluronidase and HA_{oligos} on pericellular matrices of mesenchymal 3T3-L1 cells. The pericellular matrix (PCM) assembled by cells is composed largely of water and difficult to visualize with traditional staining methods. Adding small inert particles, like formalin fixed red blood cells (RBC) that settle down around the living cell and are excluded from its matrix creates a halo. This halo represents the PCM or 'coat' of each cell. Mesenchymal 3T3-L1 cells appear elongated in shape (A) and have easily detected PCMs (B) that are increased in size with the addition of exogenous aggrecan (C). These coats are no longer detected when 3T3-L1 cells are treated with 20 U/ml *Streptomyces* hyaluronidase (SH) (D) or 200 μg/ml HA_{oligos} (E). Panels depict representative cells, Bars = 100 μm, original magnification, 400x.

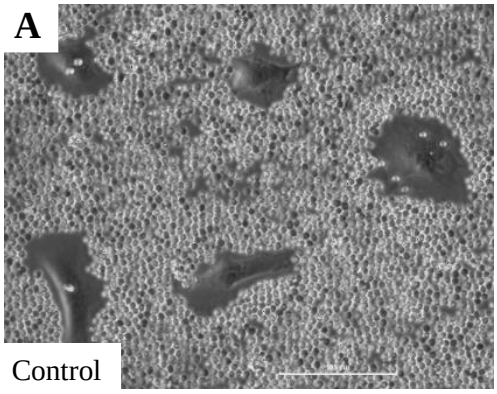
A
Control

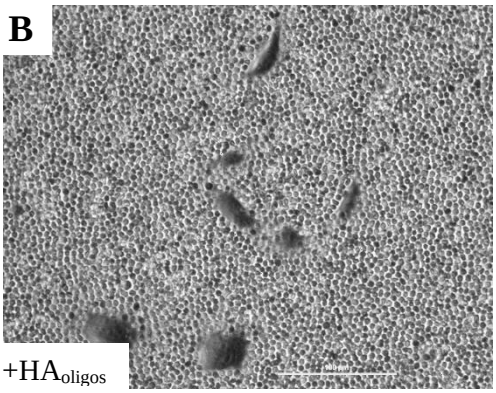
B
+HA$_{oligos}$

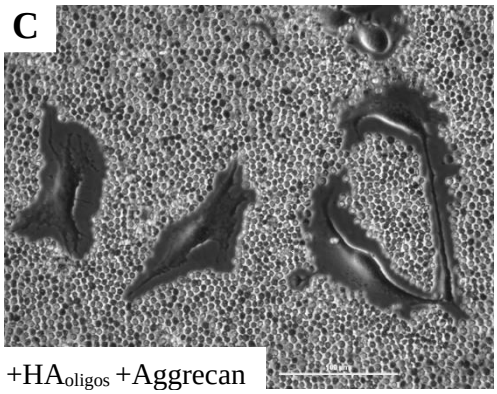
C
+HA$_{oligos}$ +Aggrecan

Figure 12. Effects of adding exogenous aggrecan after HA_{oligos} treatment on pericellular matrices (PCMs) of mesenchymal 3T3-L1 cells. Control 3T3-L1 cells have detectible PCMs (A) that are decreased in size after treatment with 200 μg/ml HA_{oligos} for 90 minutes (B). However, the PCM is recovered after treatment with 2 mg/ml exogenous aggrecan treatment for 1 hour in fresh medium excluding HA_{oligos}. Panels depict representative cells, Bars = 100 μm.

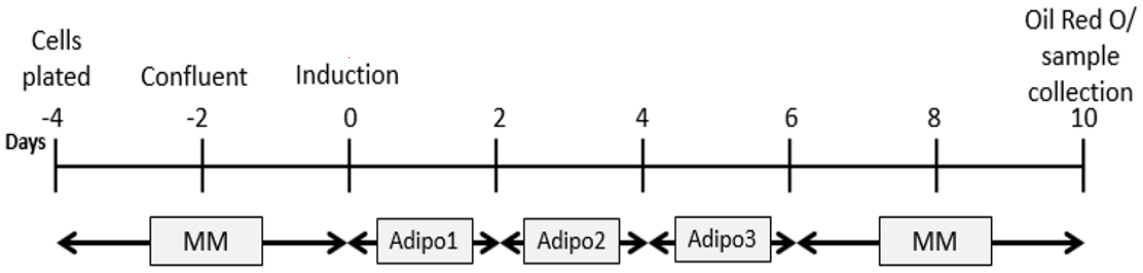
Cells plated
Confluent
Induction
Oil Red O/ sample collection
Days
-4
-2
0
2
4
6
8
10
MM
Adipo1
Adipo2
Adipo3
MM

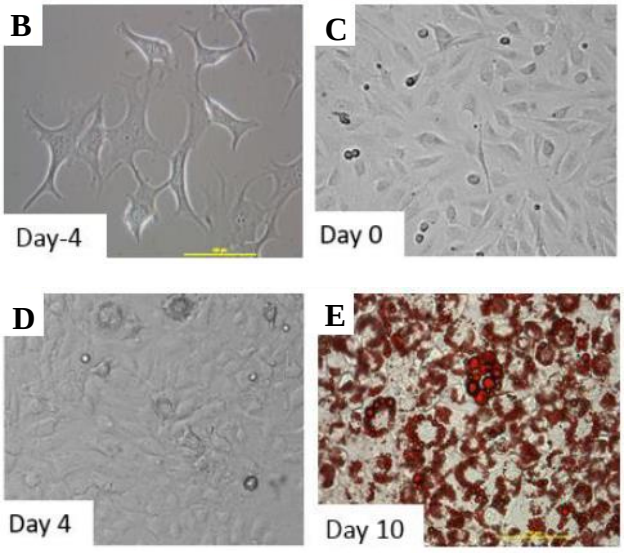
B
Day-4
C
Day 0
D
Day 4
E
Day 10

Figure 13. Adipogenesis of 3T3-L1 cells. As 3T3-L1 cells undergo adipogenesis, drastic morphological changes are easily visible by phase contrast imaging. The timeline for the adipogenesis protocol is outlined in A. Cells are plated on day -4, then maintained in DMEM+10% FBS (MM) until induction, at Day 0. Two days after reaching confluency (Day 0), cells were induced with 1uM Dex, 0.5 mM MIX, and 1.7 uM insulin in MM (Adipo1). On Day 2, cells were treated with MM+1.7 uM insulin (Adipo2). On Day 4, cells were treated with MM+0.43 uM insulin (Adipo3). On Day 6, media was changed back to MM for the remainder of culture. If any additional experimental treatments were administered, they were done so at each medium change indicated by the red arrows above the timeline. 3T3-L1 cells exhibit mesenchymal morphology at time of plating of 10^4 cells per cm^2 on Day -4 (B). Two days post-confluence, cells begin to have a cobblestone appearance (C). Four days post adipogenic induction, lipid droplets begin to form (D). Ten days post induction, the majority of cells are round and contain many lipid droplets made visible by staining with Oil Red O (E).

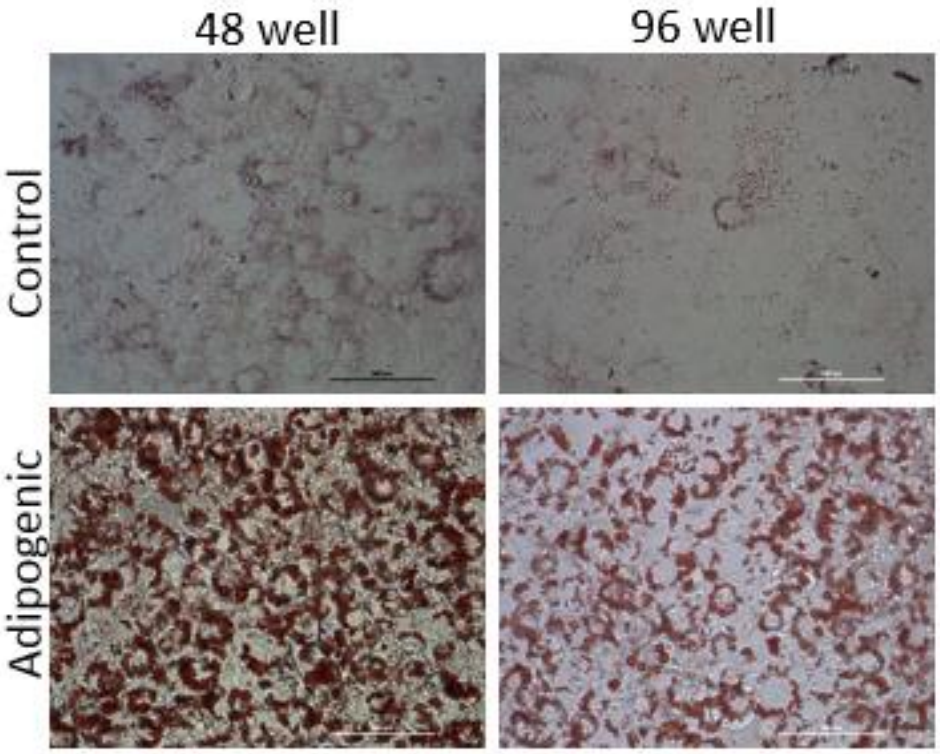
48 well
96 well
Control
Adipogenic

Figure 14. Miniaturization of adipogenic assay. 3T3-L1 cells were plated at 10^4 cells per cm^2 in 48 or 96-well culture plates and grown with (Adipogenic) and without (Control) adipogenic inducers. Ten days after induction, following the scheme in 9A, cell monolayers were stained with Oil Red O to visualize formation of lipid droplets.

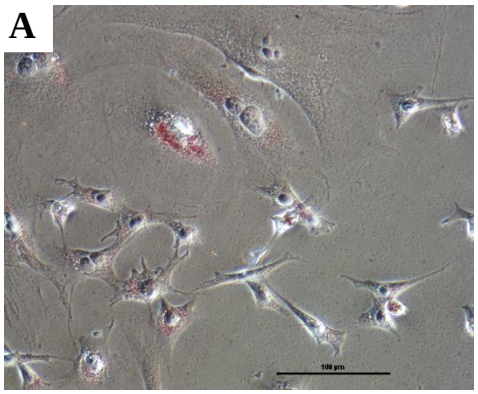
A

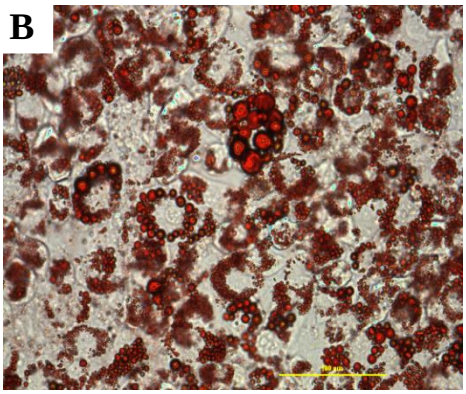
B

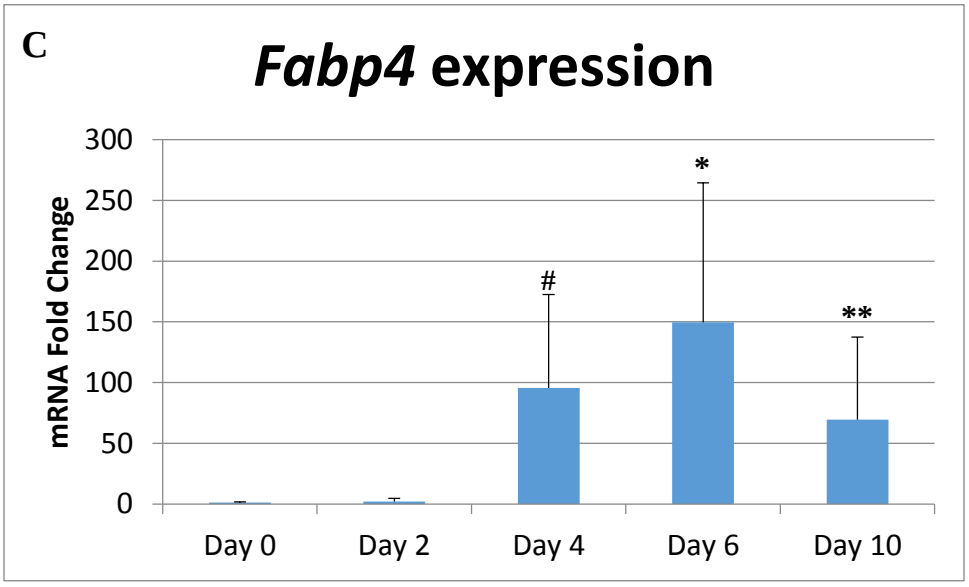
C
Fabp4 expression
mRNA Fold Change
300
250
200
150
100
50
0
#
*
**
Day 0
Day 2
Day 4
Day 6
Day 10

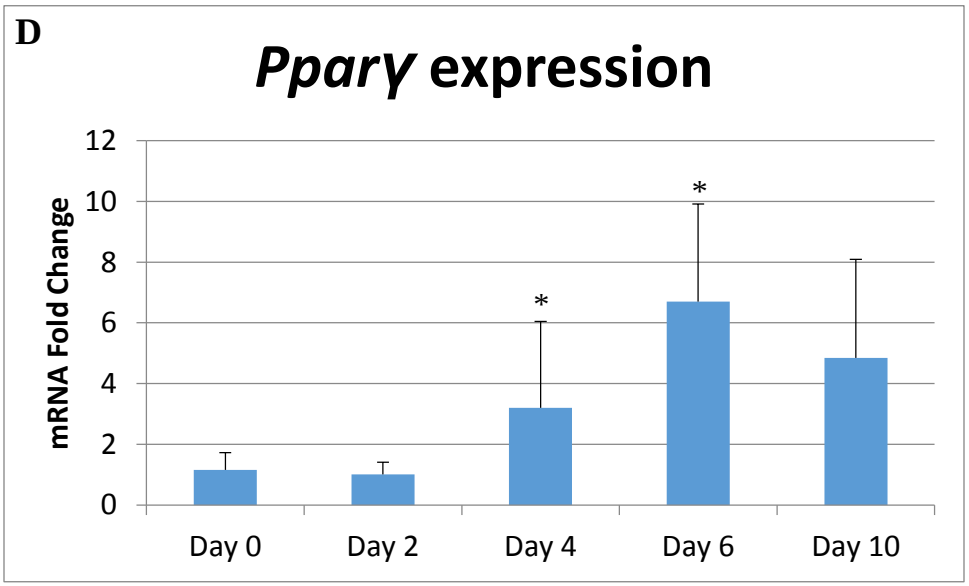
D
Pparγ expression
mRNA Fold Change
12
10
8
6
4
2
0
*
*
Day 0
Day 2
Day 4
Day 6
Day 10

Figure 15. Adipogenesis of 3T3-L1 cells is verified with Oil Red O stain and increases in *Fabp4* and *Pparγ* mRNA expression. The most identifying characteristic of adipocytes is the collection of large lipid droplets made visible with Oil Red O. Mesenchymal 3T3-L1 cells do not display any Oil Red O staining (A) while 3T3-L1 adipocytes have many lipid droplets made observable with Oil Red O stain (B). Total RNA was isolated from 3T3-L1 cells 0, 2, 4, 6, and 10 days after induction with adipogenic media. The relative fold change of *Fabp4* (C) and *Pparγ* (D) mRNA was quantified using the ΔΔCT method using Day 0 as the control and normalizing with *Gapdh* mRNA expression. Bars represent the mean $\pm$ standard deviation from 7 experiments analyzed in duplicate. *: p-value < 0.05, **: p-value < 0.01

A

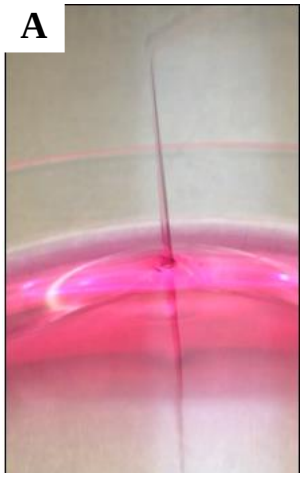

B

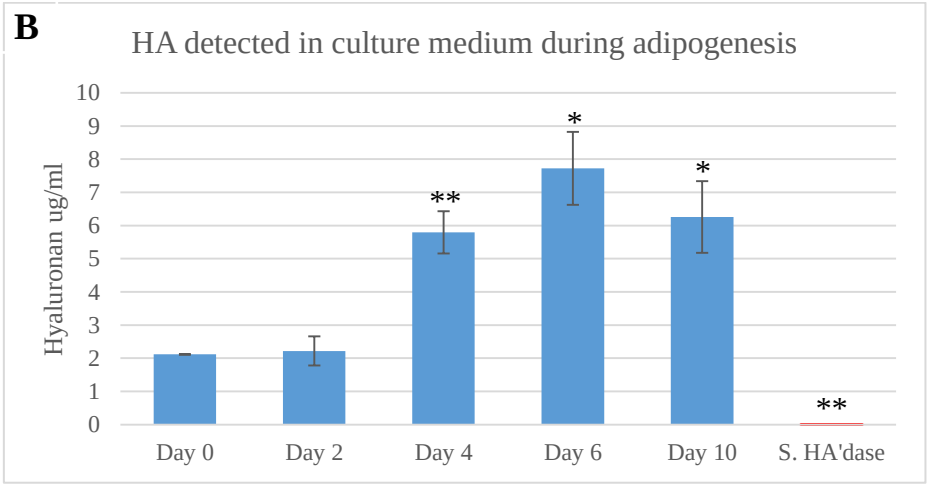

C

	Day -4	Day 0	Day 10
Has2	9.4 + 0.3	6.9 + 0.4	9.4 + 0.9
Has3	16.7 + 0.6	14.0 + 0.4	16.6 + 0.9
Has1	19.7 + 0.6	ND	ND

D

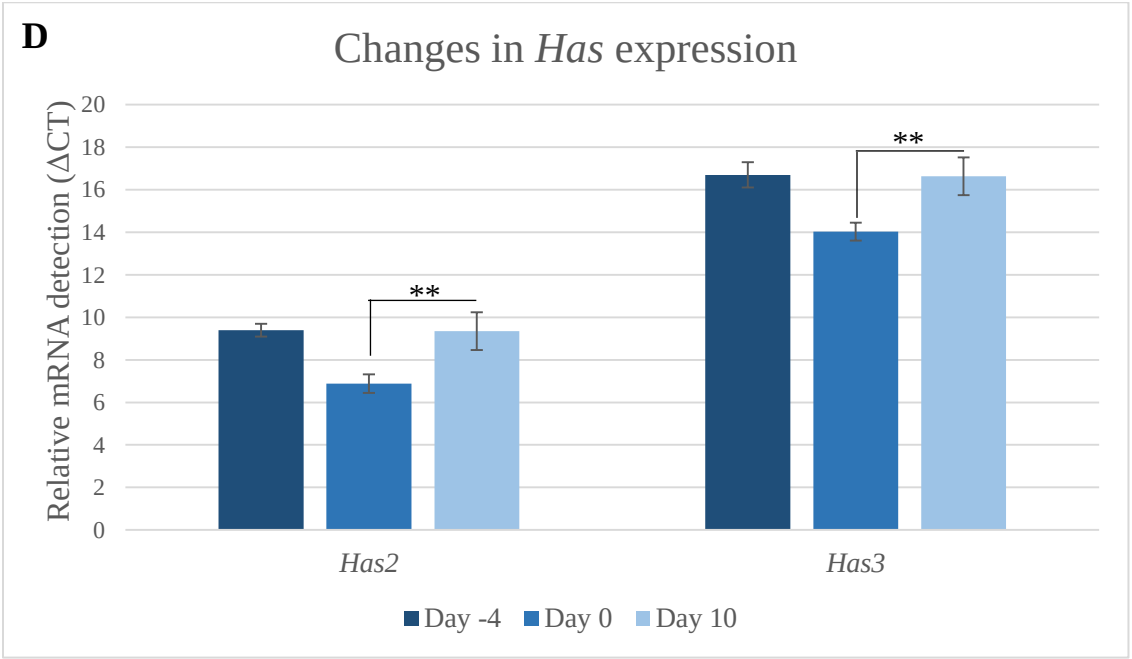

Figure 16. Changes in hyaluronan production and release during 3T3-L1 adipogenesis. During adipogenesis of 3T3-L1 cells, conditioned medium becomes noticeably viscous by Day 6. This is demonstrated in panel A by the tension string created when the medium is aspirated with a Pasteur pipette. Media collected from 3T3-L1 cells during adipogenesis on Days 0, 2, 4, 6 and 10 were analyzed for hyaluronan (HA) concentration using a commercially available HA ELISA kit. To ensure the specificity of HA detection, the Day 10 sample was treated with 20 U/ml *Streptomyces* hyaluronidase and analyzed for HA content which is represented by the red bar. Bars represent the average $\pm$ standard deviation (B). Total RNA was isolated from 3T3-L1 cells at time of plating, Day -4, the day on induction, Day 0, and 10 days after induction with adipogenic media, Day 10. The relative detection of *Has2*, *Has3* and *Has1* mRNA levels are represented as ΔCT values $\pm$ standard deviation. ΔCT values equal the gene of interest CT value – reference gene (*Gapdh*) CT value. Values are inversely proportional to relative amount of *Has* (smaller numbers mean larger amounts of *Has* mRNA; C). Values listed for *Has2* and *Has3* in panel C are graphed in panel D. ND=not detected *: p-value <0.05 **: p-value <0.01

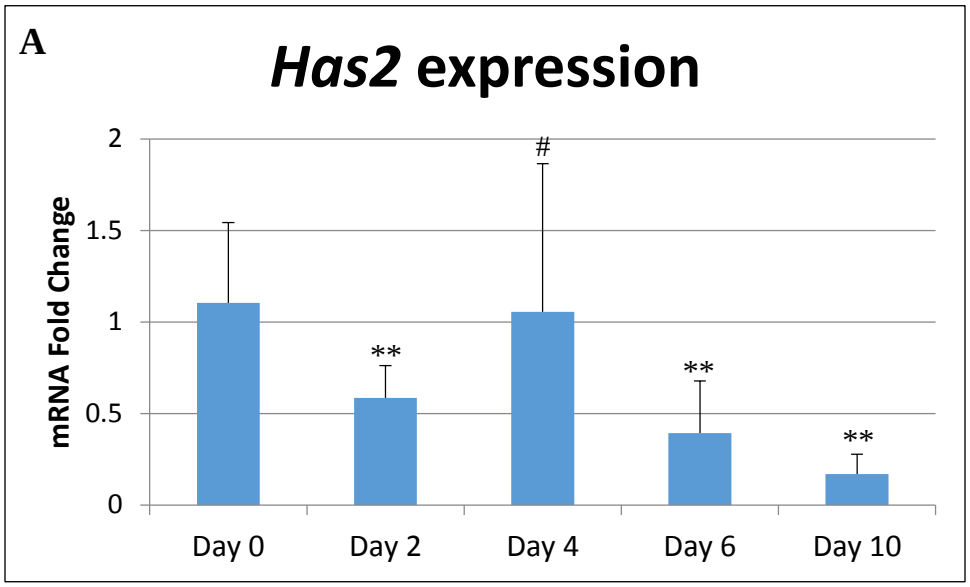
A
Has2 expression
mRNA Fold Change
2
1.5
1
0.5
0
#
**
**
**
Day 0
Day 2
Day 4
Day 6
Day 10

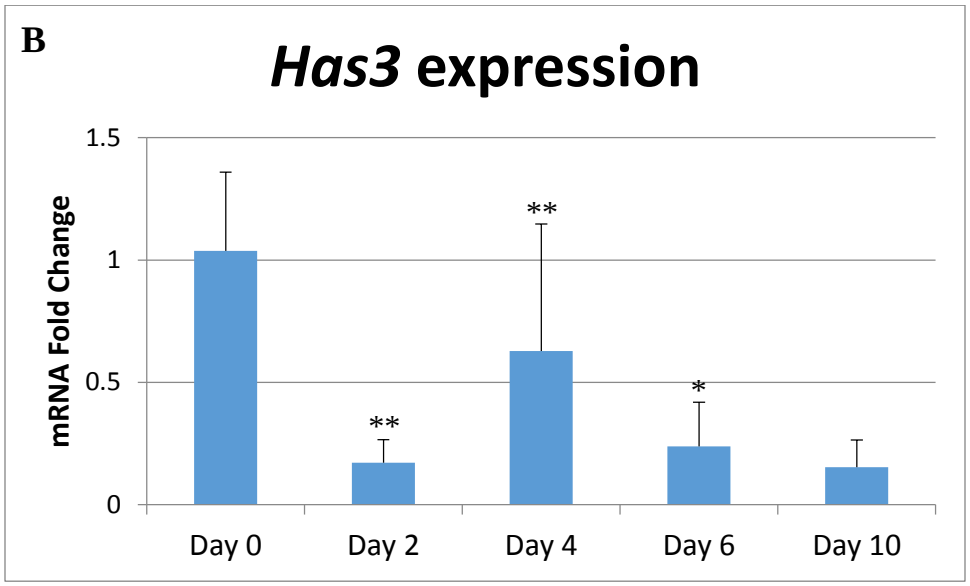
B
Has3 expression
mRNA Fold Change
1.5
1
0.5
0
**
**
*
Day 0
Day 2
Day 4
Day 6
Day 10

Figure 17. Analysis of *Has2* and *Has3* expression during 3T3-L1 adipogenesis. Total RNA was isolated from 3T3-L1 cells 0, 2, 4, 6, and 10 days after induction with adipogenic media. The relative fold change of *Has2* (A) and *Has3* (B) mRNA was quantified using the ΔΔCT method using Day 0 as the control and normalizing with *Gapdh* mRNA expression. Bars represent the mean $\pm$ standard deviation from 5 experiments analyzed in duplicate.

#: p-value < 0.10, *: p-value < 0.05, **: p-value < 0.01

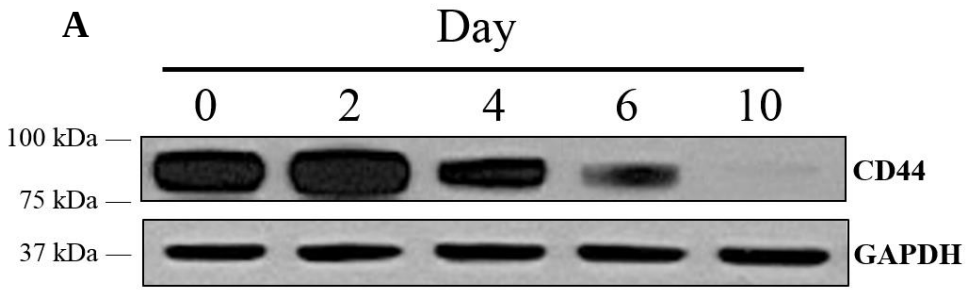
A
Day
0
2
4
6
10
100 kDa
75 kDa
37 kDa
CD44
GAPDH

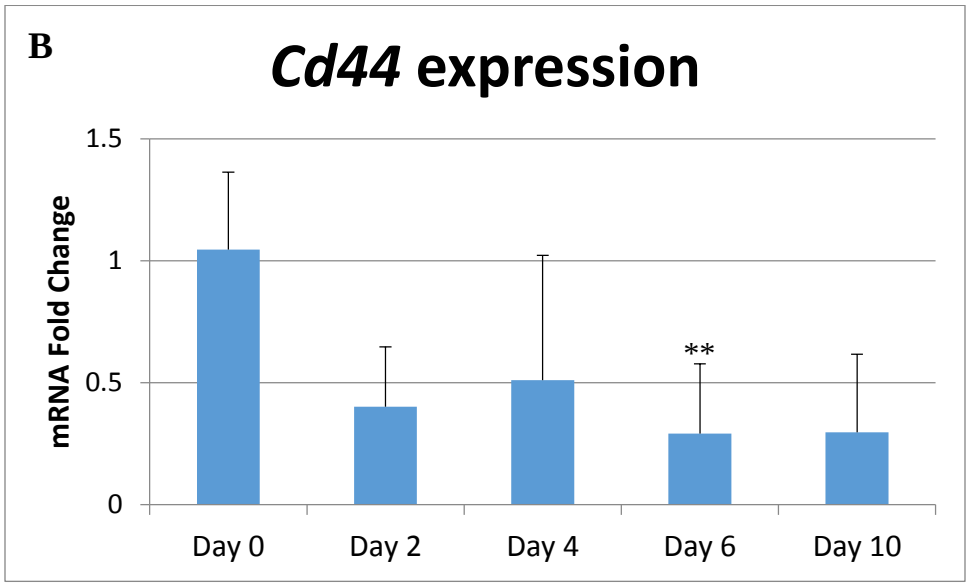
B
Cd44 expression
mRNA Fold Change
1.5
1
0.5
0
**
Day 0
Day 2
Day 4
Day 6
Day 10

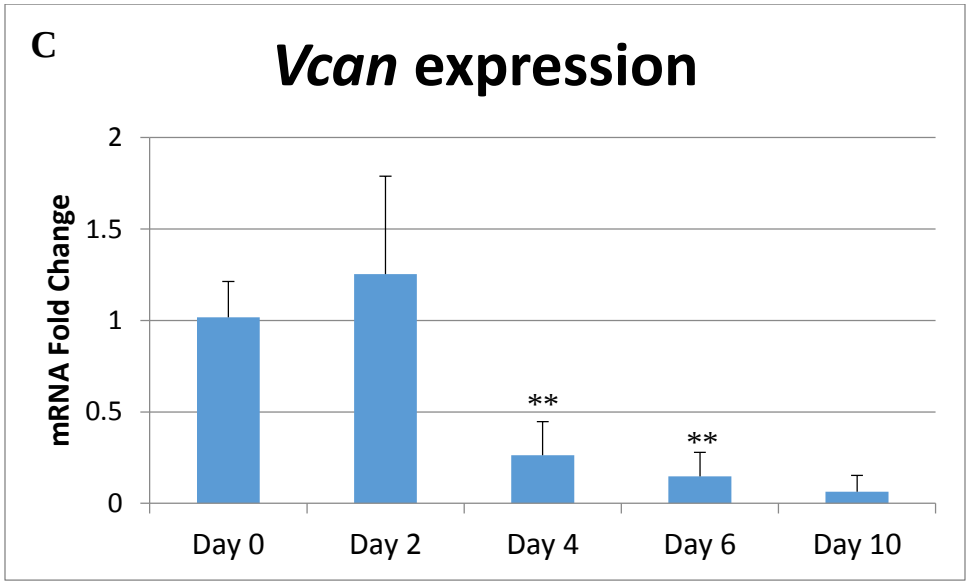
C
Vcan expression
mRNA Fold Change
2
1.5
1
0.5
0
**
**
Day 0
Day 2
Day 4
Day 6
Day 10

Figure 18. Analysis of *Cd44* and *Vcan* expression during 3T3-L1 adipogenesis. Total protein and RNA was isolated from 3T3-L1 cells 0, 2, 4, 6, and 10 days after induction with adipogenic media. Protein expression of CD44 and GAPDH (as loading control) were determined by Western blotting with bands present at approximately 85 kDa for CD44 and 37 kDa for GAPDH (A). The relative fold change of *Cd44* (B) and *Vcan* (C) mRNA was quantified using the ΔΔCT method using Day 0 as the control and normalizing with *Gapdh* mRNA expression. Bars represent the mean $\pm$ standard deviation from 5 experiments analyzed in duplicate. **: p-value < 0.01

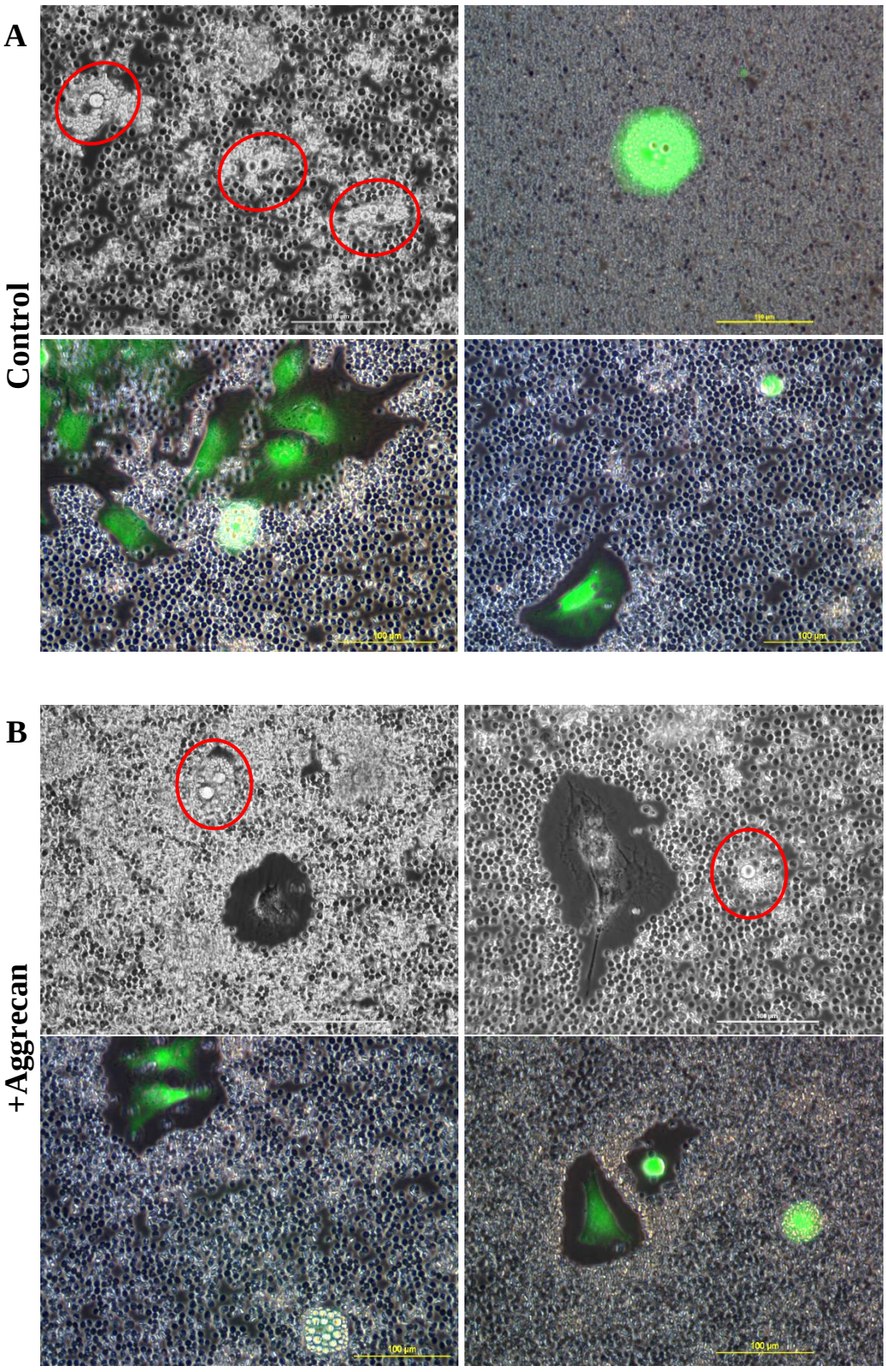
A
Control
B
+Aggrecan

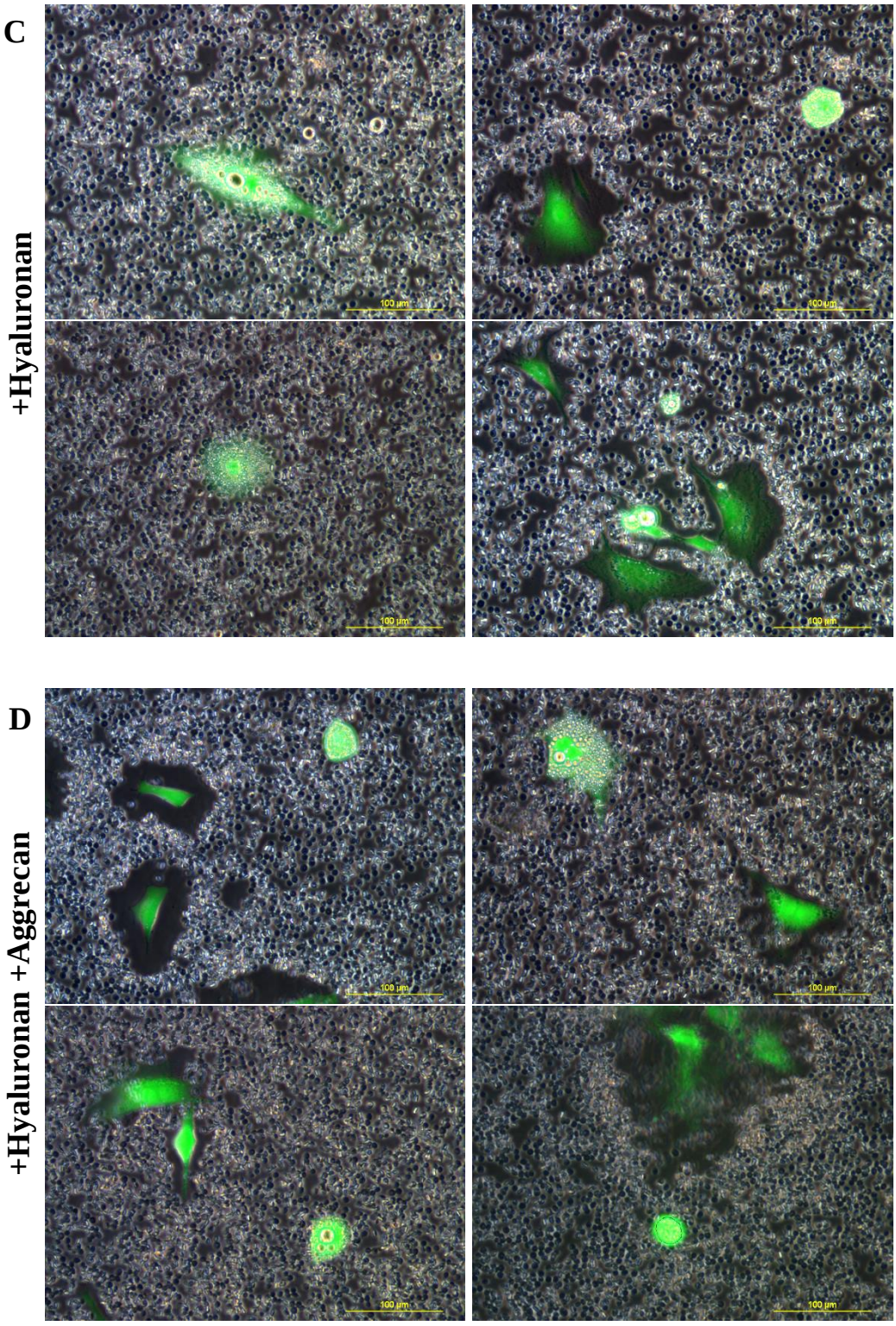
C
+Hyaluronan
D
+Hyaluronan +Aggrecan

Figure 19. 3T3-L1 adipocytes do not have a detectable pericellular matrix. Ten days after adipogenic induction, 3T3-L1 cells were re-plated at a lower density and submitted to a particle exclusion assay the next day. Cells that had undergone adipogenesis, as noted by their round shape and presence of lipid droplets (circled in red if not stained green), did not have any visible pericellular matrix (PCM) while cells that remained mesenchymal had clearly visible PCMs (A). The addition of 2 mg/ml exogenous aggrecan for 1 hour (B), 100 μg/ml hyaluronan (C), or hyaluronan + aggrecan (D) had no effect on the ability of 3T3-L1 adipocytes to assemble a PCM but enlarged the PCM of mesenchymal 3T3-L1 cells. Four different representative images are shown for each treatment group. For some samples, 1 μM Calcein AM fluorescence (green) was used to increase and confirm cell visibility. Scale bar = 100 μm

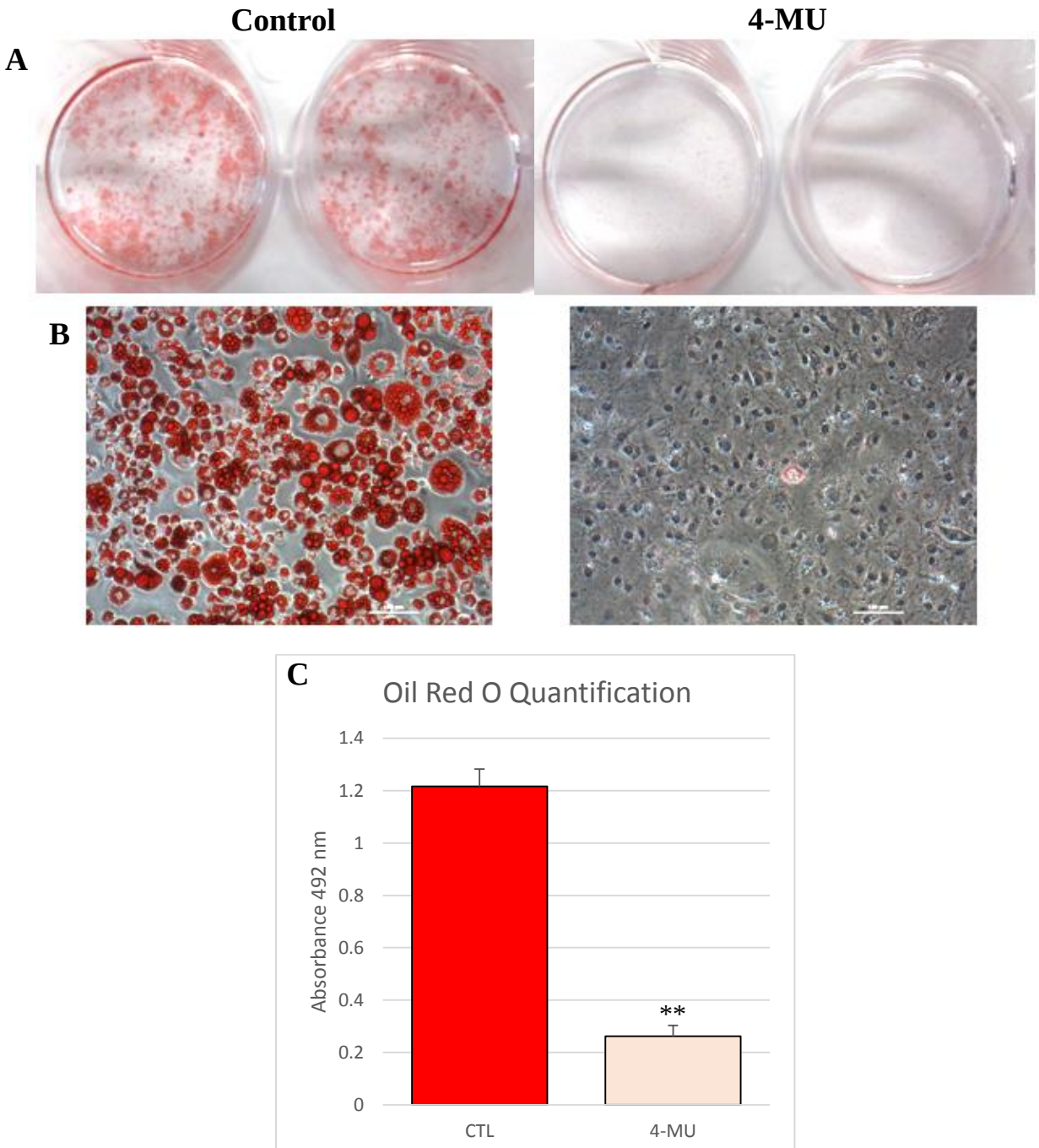
Control
4-MU
A
B
C
Oil Red O Quantification
Absorbance 492 nm
1.4
1.2
1
0.8
0.6
0.4
0.2
0
**
CTL
4-MU

Figure 20. Effects of 4-methylumbelliferone (4-MU) treatment on lipid droplet formation in adipogenically induced 3T3-L1 cells. Culture dishes with 3T3-L1 cells were stained with Oil Red O 10 days post adipogenic induction with and without 200 uM 4-MU treatment according to the red arrows in 9A. Representative wells are depicted in panel A. Representative micrographs of cells from culture dishes from panel A are shown in panel B. After Oil Red O stain was extracted from the cell monolayers with 100% ethanol, the absorbance was measured at wavelength of 492 nm (C). Bars represent the average absorbance $\pm$ standard deviation for 3 independent experiments analyzed in duplicate. ** = p-value <0.01

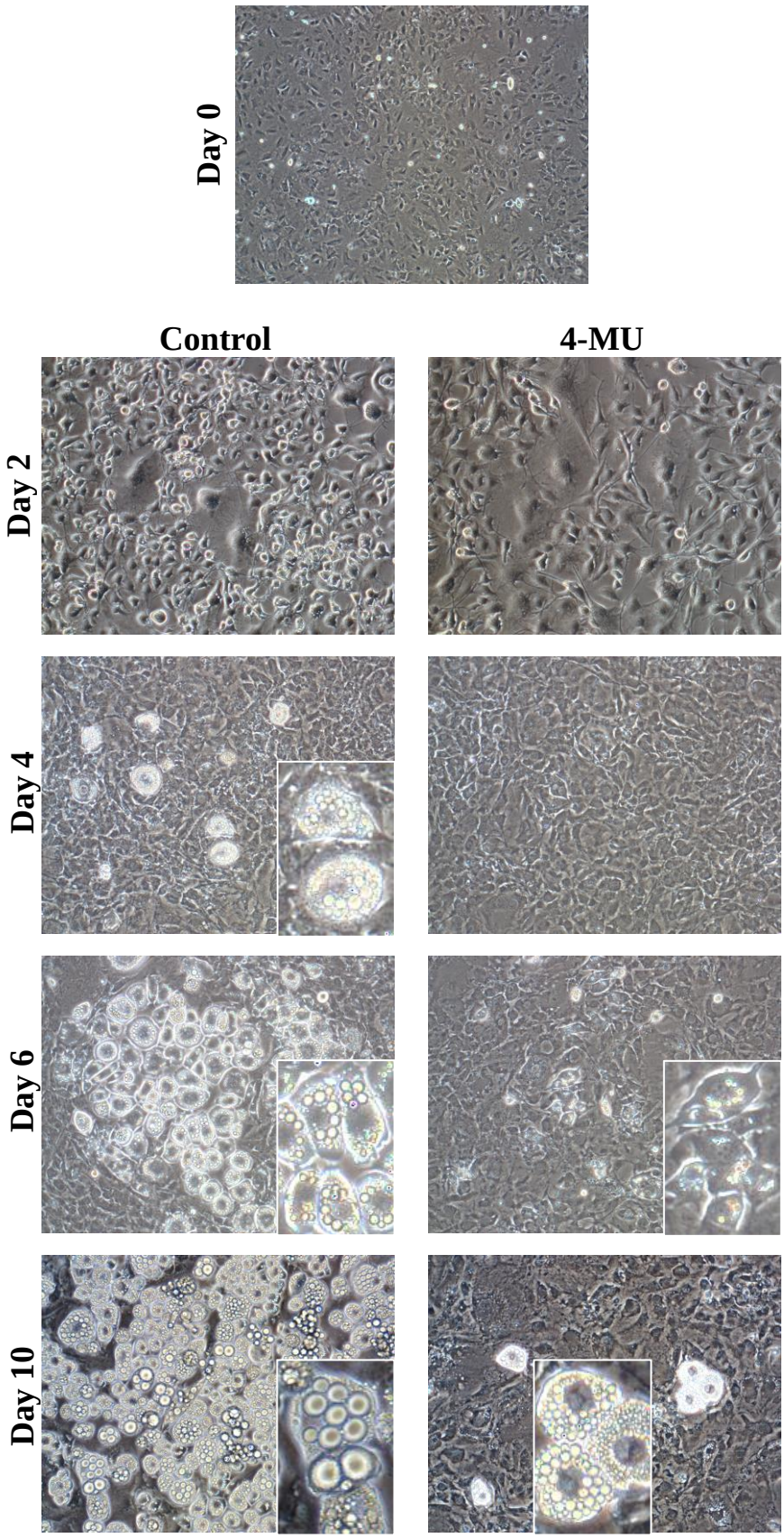
Day 0
Control
4-MU
Day 2
Day 4
Day 6
Day 10

Figure 21. 3T3-L1 cells treated with 4-methylumbelliferone (4-MU) during adipogenesis. Representative phase contrast micrographs show 3T3-L1 monolayers 0, 2, 4, 6, and 10 days after induction with adipogenic media with and without treatment of 200 μM 4-MU as shown in (Figure 4).

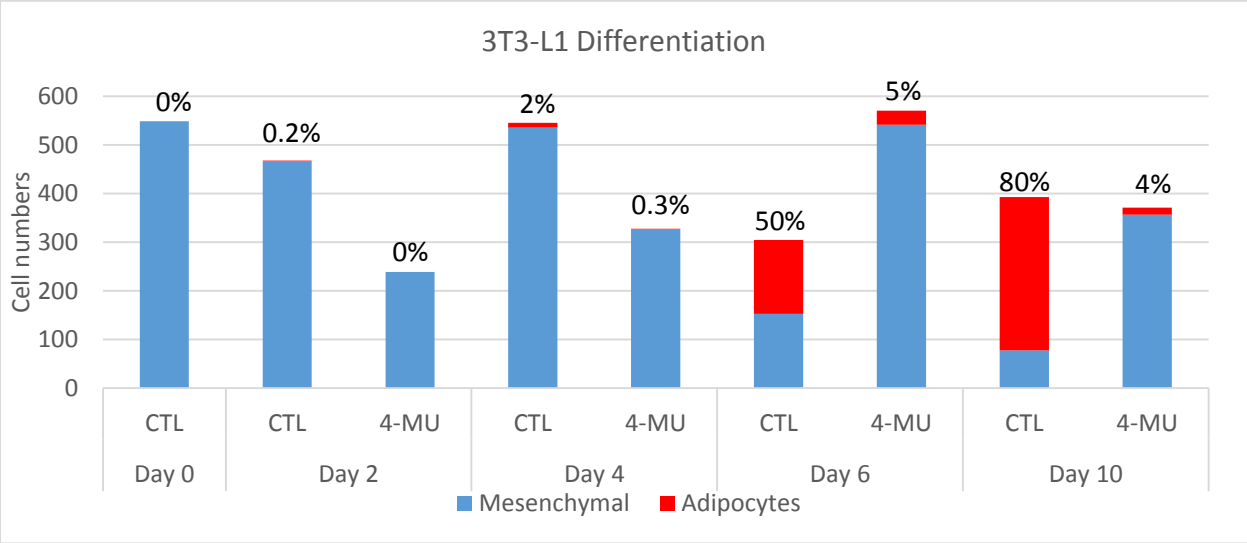

Table 2	Day 0	Day 2	Day 4	Day 6	Day 10
Control	549 (0)	467 (1)	536 (10)	153 (152)	78 (315)
4-MU		239 (0)	327 (1)	542 (29)	357 (14)

Figure 22. Effects of 4-methylumbelliferone (4-MU) treatment on mesenchymal versus adipocyte 3T3-L1 cell number. Mesenchymal 3T3-L1 cells and 3T3-L1 adipocytes were counted from micrographs 0, 2, 4, 6, and 10 days after adipogenic induction. Mesenchymal cells are represented by blue portion while adipocytes are represented by red portion of each bar. The percentage of adipocytes of the total cells counted is shown at the top of each bar for that sample.

Table 2. Number of mesenchymal versus adipocyte 3T3-L1 cells with and without 4-methylumbelliferone (4-MU) treatment. Mesenchymal 3T3-L1 cells and 3T3-L1 adipocytes were counted from micrographs 0, 2, 4, 6, and 10 days after adipogenic induction. This table shows total cell counts for each sample represented as mesenchymal cells versus (adipocytes).

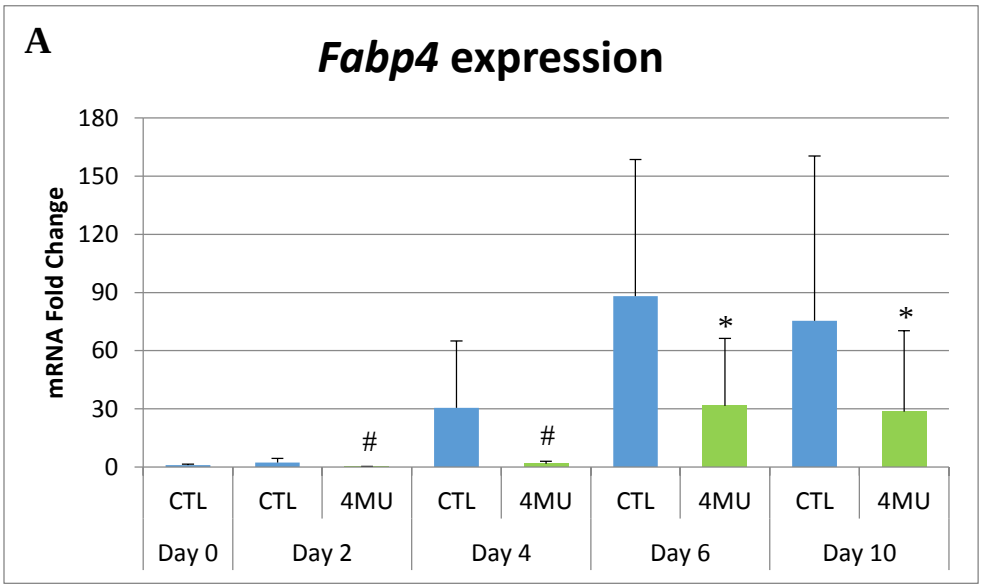
A
Fabp4 expression
mRNA Fold Change
180
150
120
90
60
30
0
#
#
*
*
CTL
CTL
4MU
CTL
4MU
CTL
4MU
CTL
4MU
Day 0
Day 2
Day 4
Day 6
Day 10

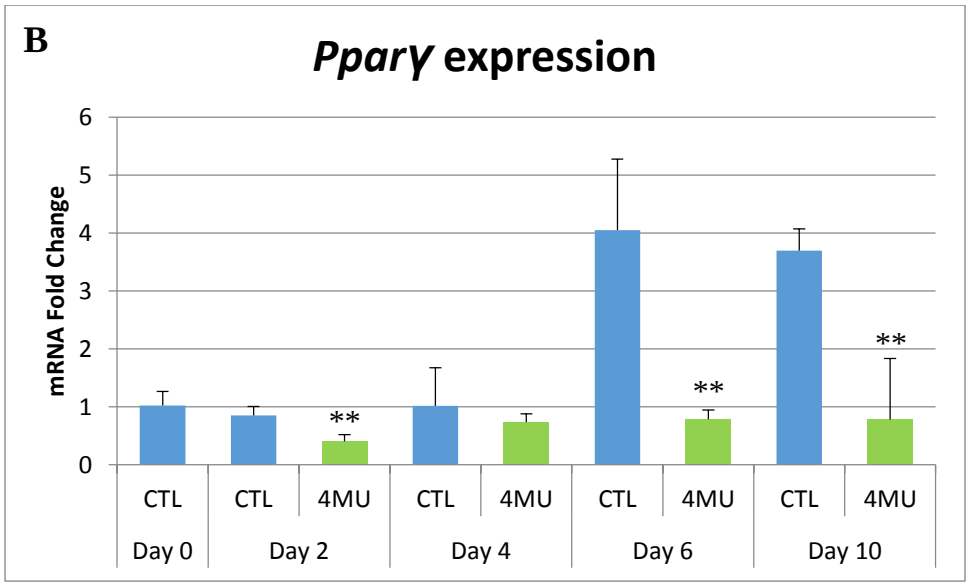
B
PparγExpression
mRNA Fold Change
6
5
4
3
2
1
0
**
**
**
CTL
CTL
4MU
CTL
4MU
CTL
4MU
CTL
4MU
Day 0
Day 2
Day 4
Day 6
Day 10

Figure 23. Effects on *Fabp4* and *Pparγ* expression during 3T3-L1 adipogenesis with and without 4-MU treatment. Total RNA was isolated from 3T3-L1 cells 0, 2, 4, 6, and 10 days after induction with adipogenic media with and without 200 μM 4-MU as shown in Figure 4. The relative fold change of *Fabp4* (A) and *Pparγ* (B) mRNA was quantified using the ΔΔCT method using Day 0 as the control and normalizing with *Gapdh* mRNA expression. Bars represent the mean ± standard deviation from 3 experiments analyzed in duplicate.

#: p-value < 0.10, *: p-value < 0.05, **: p-value < 0.01

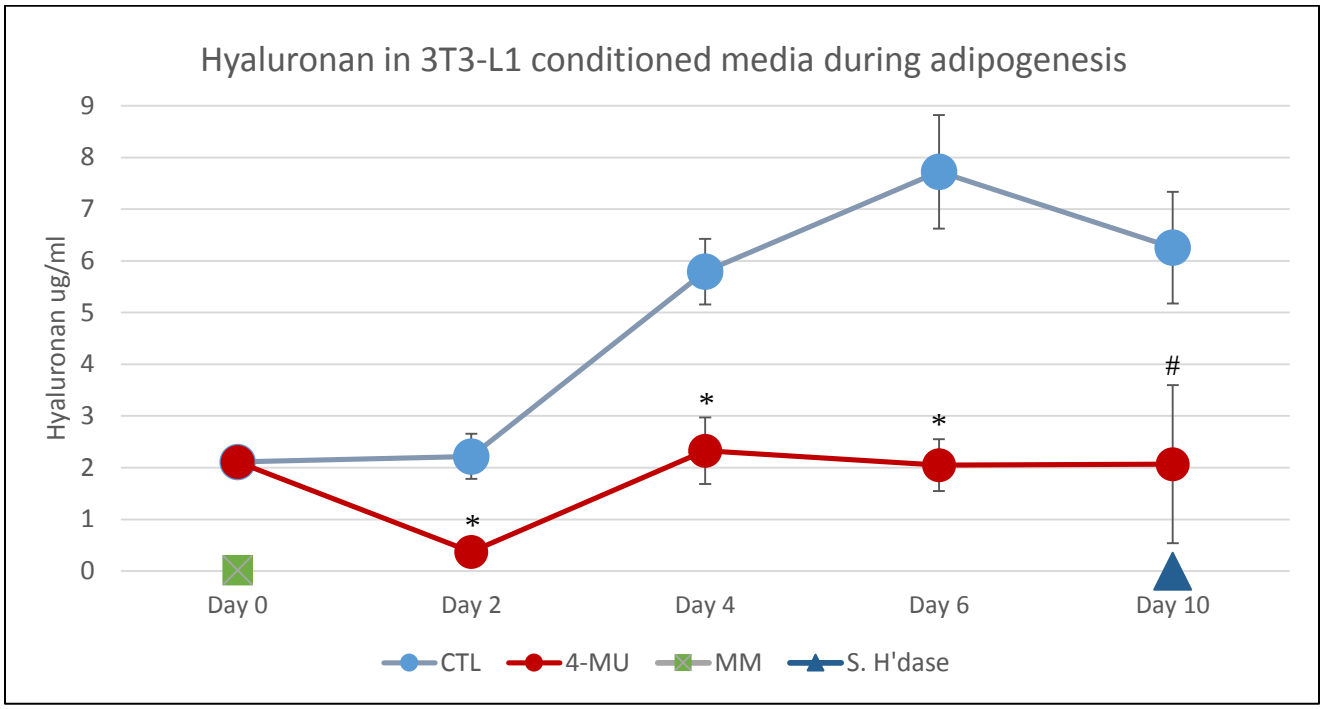
Hyaluronan in 3T3-L1 conditioned media during adipogenesis
Hyaluronan ug/ml
9
8
7
6
5
4
3
2
1
0
Day 0
Day 2
Day 4
Day 6
Day 10
*
*
*
#
CTL
4-MU
MM
S. H'dase

Figure 24. **Effects of 4-MU treatment on HA in 3T3-L1 conditioned media during adipogenesis**. Media collected from 3T3-L1 cells during adipogenesis without treatment (CTL-blue line) or with 200 μM 4-MU (4-MU-red line) on Days 0, 2, 4, 6 and 10 were analyzed for HA concentration using a commercially available HA ELISA kit. The maintenance medium (MM) was analyzed to determine if it contributed to calculated HA concentrations (represented by a green square at Day 0). To ensure the specificity of HA detection, the Day 10 sample was treated with 20 U/ml *S. hyaluronidase* and analyzed for HA content (represented by the blue triangle at Day 10). Points represent the average $\pm$ standard deviation of 2 independent experiments run in duplicate. #: p-value < 0.10, *: p-value < 0.05

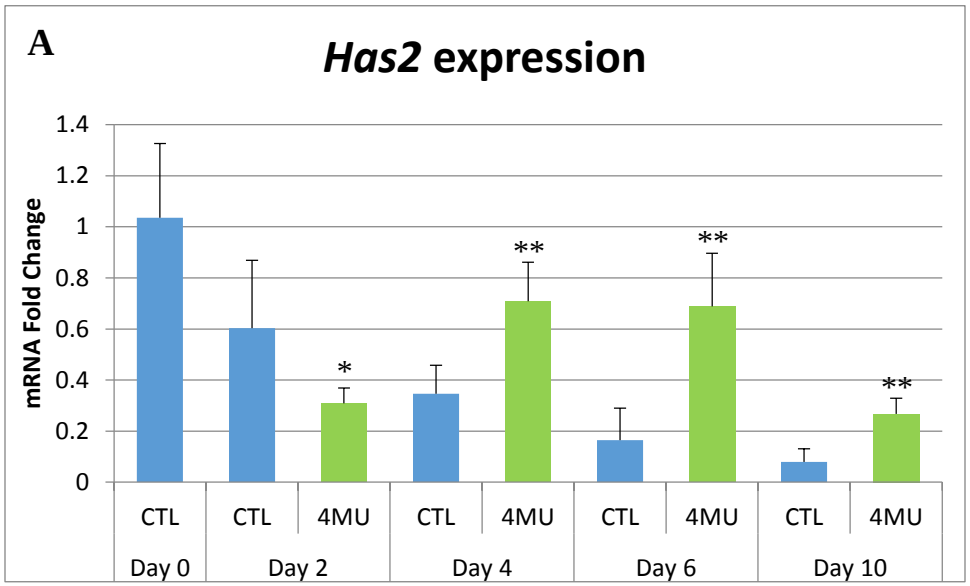
A
Has2 expression
mRNA Fold Change
1.4
1.2
1
0.8
0.6
0.4
0.2
0
*
**
**
**
CTL
CTL
4MU
CTL
4MU
CTL
4MU
CTL
4MU
Day 0
Day 2
Day 4
Day 6
Day 10

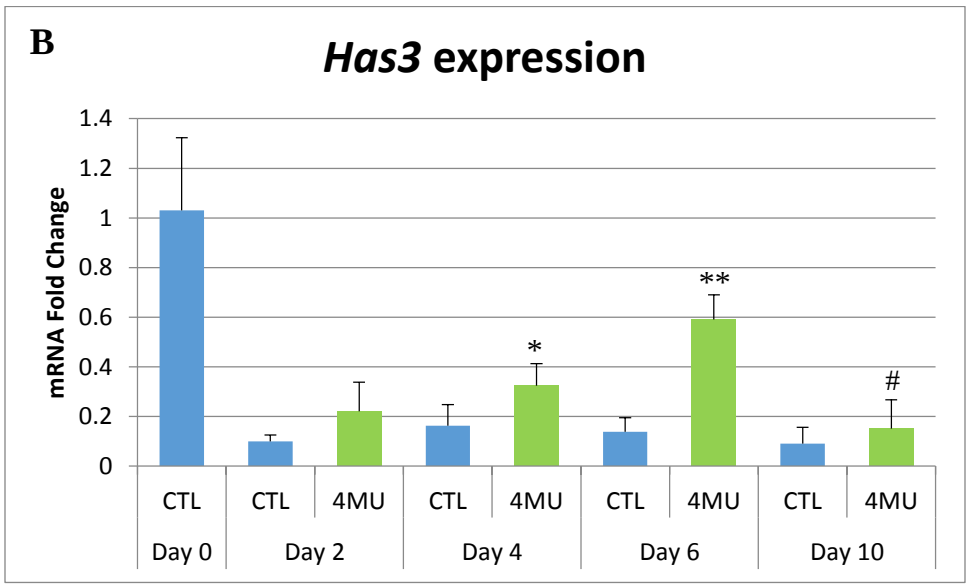
B
Has3 expression
mRNA Fold Change
1.4
1.2
1
0.8
0.6
0.4
0.2
0
*
**
#
CTL
CTL
4MU
CTL
4MU
CTL
4MU
CTL
4MU
Day 0
Day 2
Day 4
Day 6
Day 10

Figure 25. Effects on *Has2* and *Has3* expression during 3T3-L1 adipogenesis with and without 4-MU treatment. Total RNA was isolated from 3T3-L1 cells 0, 2, 4, 6, and 10 days after induction with adipogenic media with and without 200 μM 4-MU as shown in Figure 4. The relative fold change of *Has2* (A) and *Has3* (B) mRNA was quantified using the ΔΔCT method using Day 0 as the control and normalizing with *Gapdh* mRNA expression. Bars represent the mean ± standard deviation from 3 independent experiments analyzed in duplicate.

#: p-value < 0.10, *: p-value < 0.05, **: p-value < 0.01

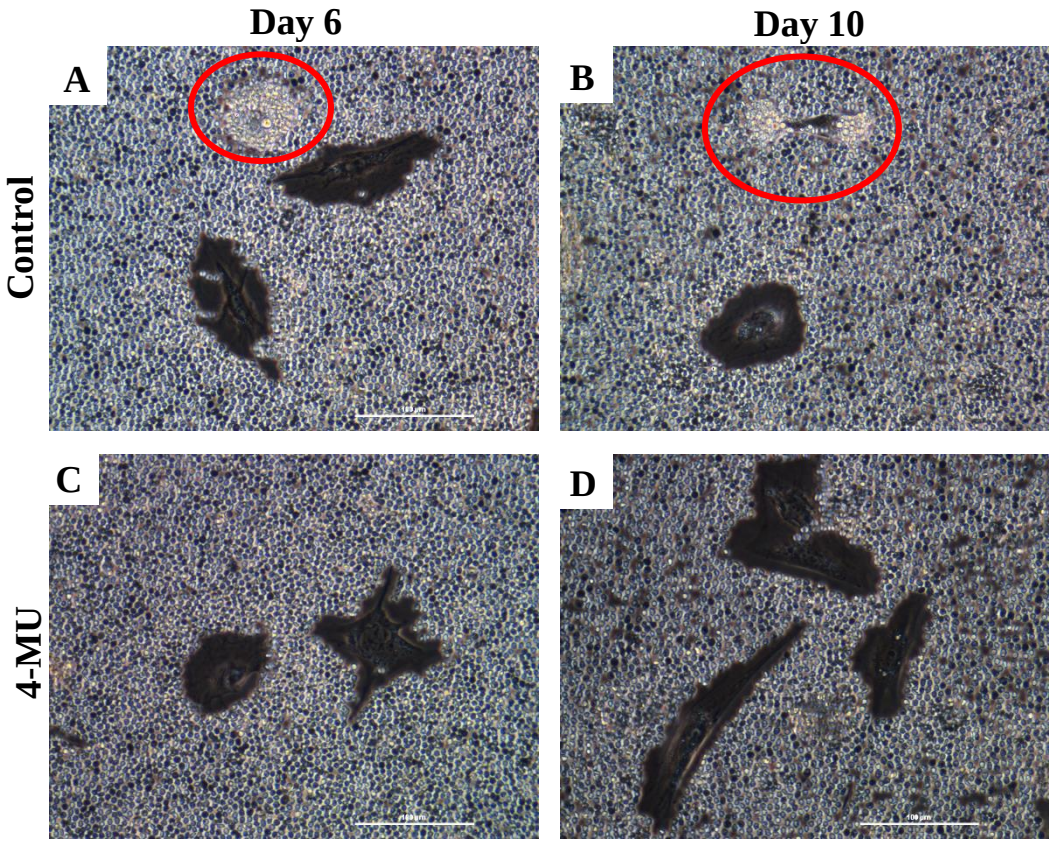
Day 6
Day 10
A
B
Control
C
D
4-MU

Figure 26. Effects of 4-MU treatment on 3T3-L1 pericellular matrix. 3T3-L1 cells were induced to undergo adipogenesis without or with the addition of 200 μM 4-MU as shown in Figure 4. The pericellular matrix (PCM) was revealed by a particle exclusion assay. 3T3-L1 cells induced without 4-MU treatment are shown at Day 6 (A) and Day 10 (B) and cells induced with 4-MU treatment are shown also for Day (6) and Day 10 (D). Because few 3T3-L1 cells treated with 4-MU undergo adipogenesis, no adipocytes were found in plated samples to analyze during particle exclusion assay. Only cells with mesenchymal morphology and a PCM were observed. Adipocytes are circled in red, in control cultures

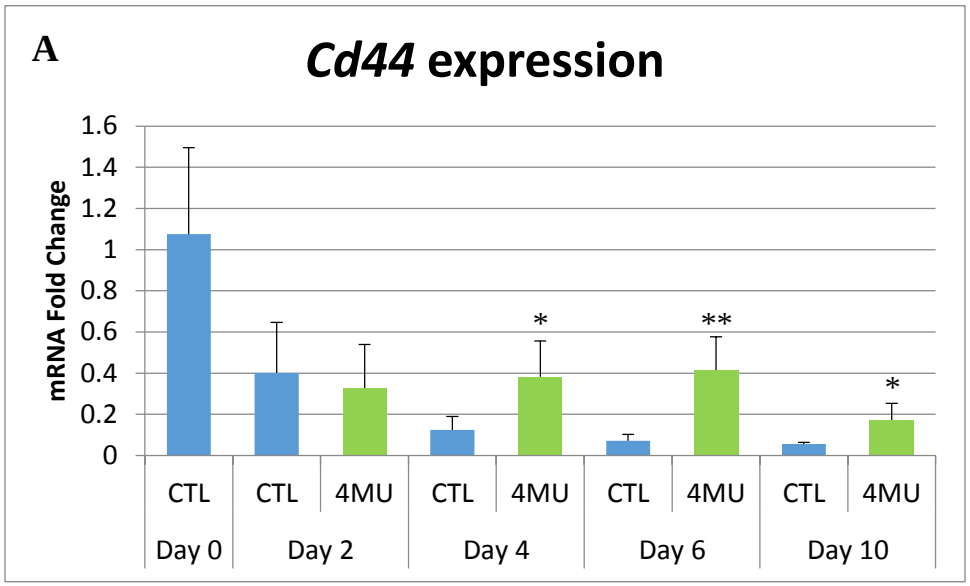
A
Cd44 expression
mRNA Fold Change
1.6
1.4
1.2
1
0.8
0.6
0.4
0.2
0
*
**
*
CTL
CTL
4MU
CTL
4MU
CTL
4MU
CTL
4MU
Day 0
Day 2
Day 4
Day 6
Day 10

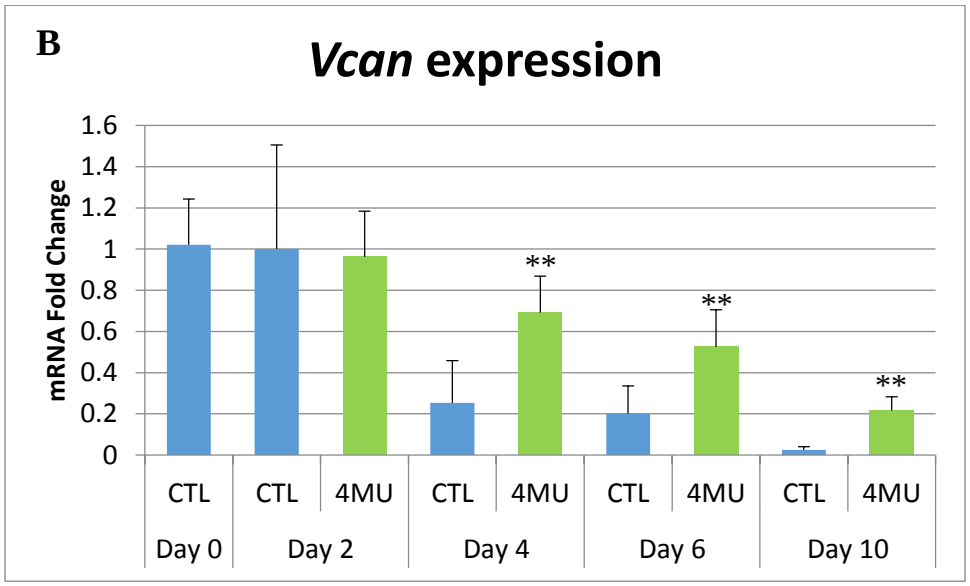
B
Vcan expression
mRNA Fold Change
1.6
1.4
1.2
1
0.8
0.6
0.4
0.2
0
**
**
**
CTL
CTL
4MU
CTL
4MU
CTL
4MU
CTL
4MU
Day 0
Day 2
Day 4
Day 6
Day 10

Figure 27. Effects on *Cd44* and *Vcan* expression during 3T3-L1 adipogenesis with and without 4-MU treatment. Total RNA was isolated from 3T3-L1 cells 0, 2, 4, 6, and 10 days after induction with adipogenic media with and without 200 μM 4-MU as shown in Figure 4. The relative fold change of *Cd44* (A) and *Vcan* (B) mRNA was quantified using the ΔΔCT method using Day 0 as the control and normalizing with *Gapdh* mRNA expression. Bars represent the mean ± standard deviation from 3 independent experiments analyzed in duplicate. *: p-value < 0.05, **: p-value < 0.01

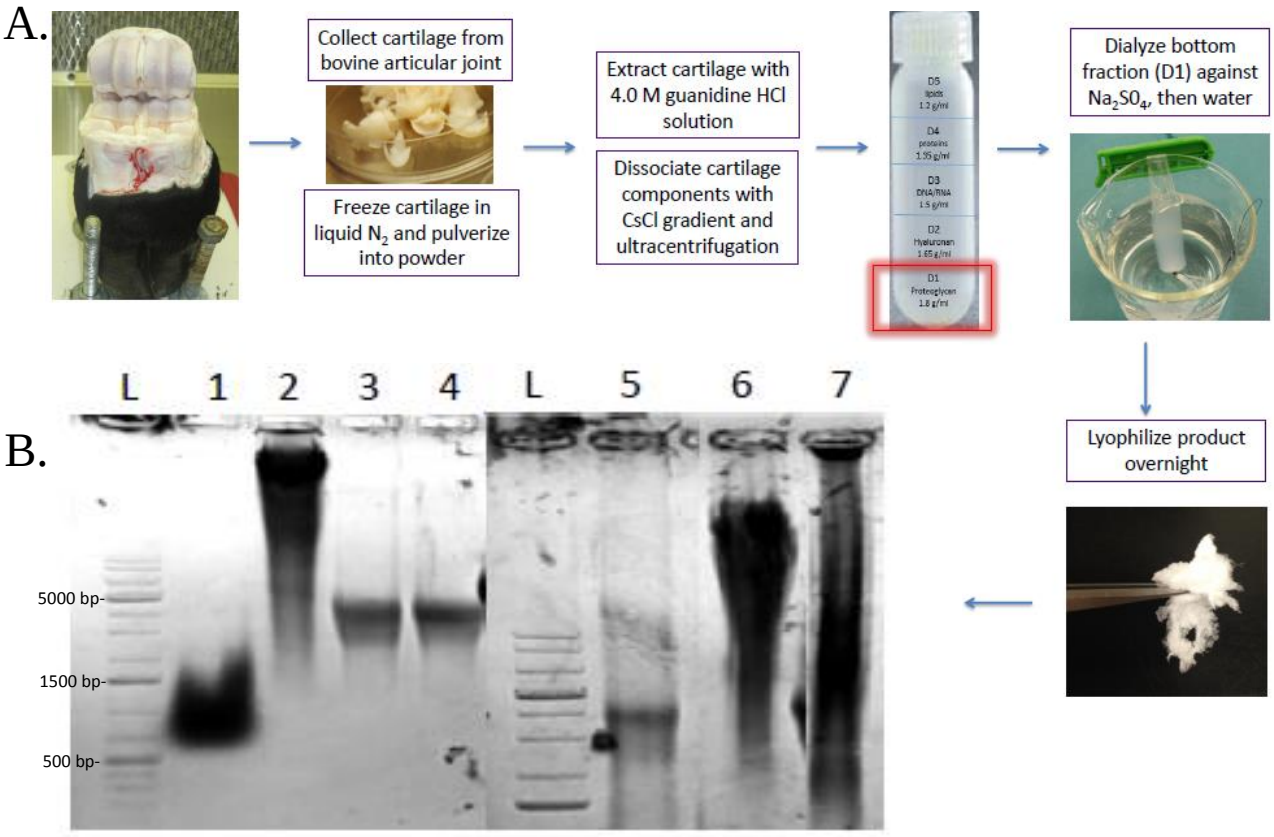
A.
Collect cartilage from bovine articular joint
Freeze cartilage in liquid N_2 and pulverize into powder
Extract cartilage with 4.0 M guanidine HCl solution
Dissociate cartilage components with CsCl gradient and ultracentrifugation
D5 lipids 1.2 g/ml
D4 proteins 1.55 g/ml
D3 DNA/RNA 1.5 g/ml
D2 Hyaluronan 1.65 g/ml
D1 Proteoglycan 1.8 g/ml
Dialyze bottom fraction (D1) against Na_2SO_4, then water
Lyophilize product overnight
B.
L 1 2 3 4 L 5 6 7
5000 bp-
1500 bp-
500 bp-

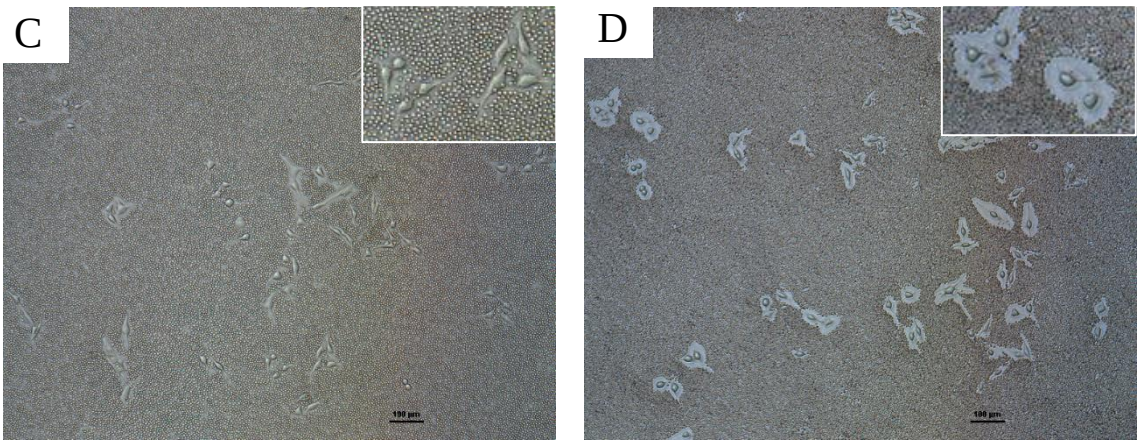
C
D

Figure 28. Isolation of aggrecan from bovine articular cartilage. Panel A depicts a flow chart for aggrecan isolation from bovine articular cartilage. First, full thickness slices are removed from the metacarpophalangeal joint of 18-24 month old steers. The slices are flash frozen in liquid nitrogen and ground into a powder. 4M guanidine HCl is used to dissociate individual cartilage components that were then separated by density with ultracentrifugation in cesium chloride. The densest fraction (D1) containing the aggrecan was dialyzed to remove guanidine and cesium chloride before lyophilization. The product was reconstituted in water and run on a 1% agarose gel (lanes 3 and 5). One sample was pre-treated with *Streptomyces* hyaluronidase for 3 hours prior to loading gel (lane 4). Another sample was combined with hyaluronan for 1 hour prior to loading (7). Hyaluronan alone was run on lanes 2 and 6 and was treated with *Streptomyces* hyaluronidase for one hour prior to loading on lane 1. DNA ladders are marked as L. Rat chondrosarcoma cells were cultured for 48 hours. One culture was pre-treated with 2 mg/ml of the isolated aggrecan for 1 hour. The pericellular matrix of cells both untreated (C) and pre-treated (D) cultures was observed by phase contrast microscopy. Bar = 100 μm

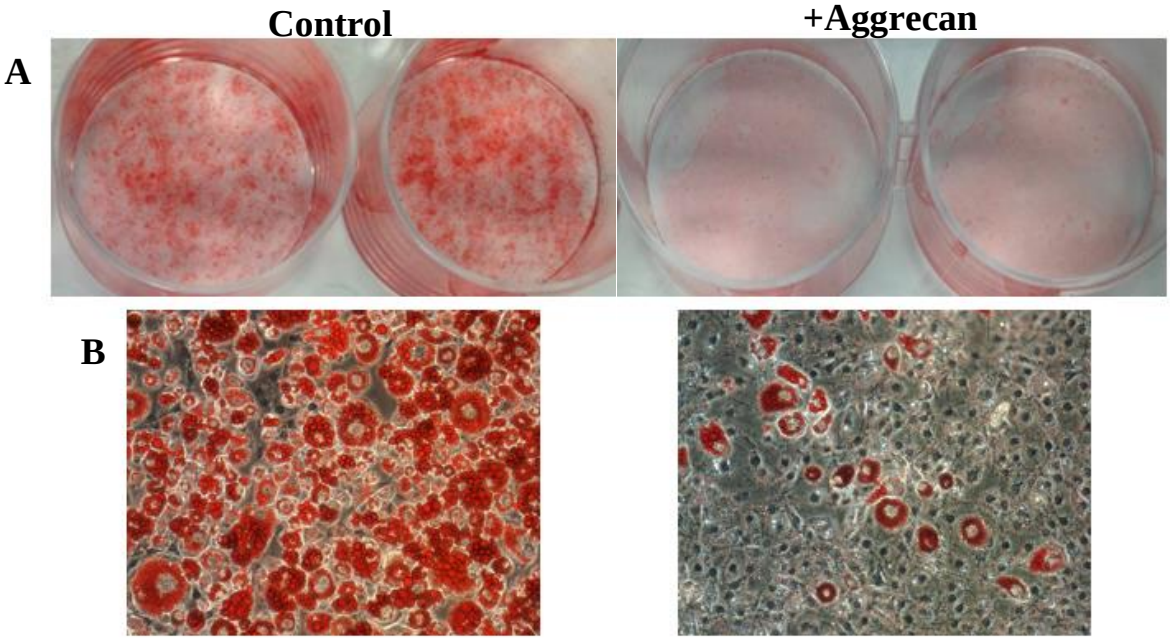
A
Control
+Aggrecan
B

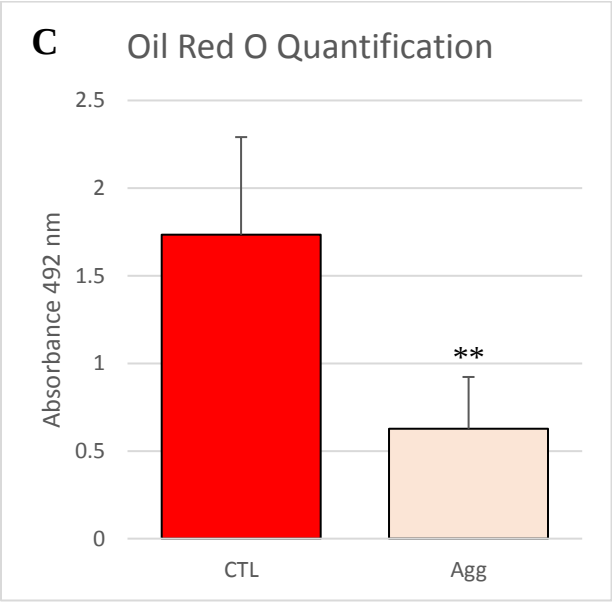
C
Oil Red O Quantification
Absorbance 492 nm
2.5
2
1.5
1
0.5
0
**
CTL
Agg

Figure 29. Effects of exogenous aggrecan treatment on lipid droplet formation in adipogenically induced 3T3-L1 cells. Culture dishes with 3T3-L1 cells were stained with Oil Red O 10 days post adipogenic induction with and without 2 mg/ml exogenous aggrecan added at the time points indicated in Figure 9A. Representative wells are depicted in panel A. Representative micrographs of cells from the culture dishes in panel A are shown in panel B. The Oil Red O stain was extracted from the cell monolayers with 100% ethanol and absorbance was measured at 492 nm (C). Bars represent the average absorbance $\pm$ standard deviation for 3 experiments run in duplicate. **: p-value <0.01

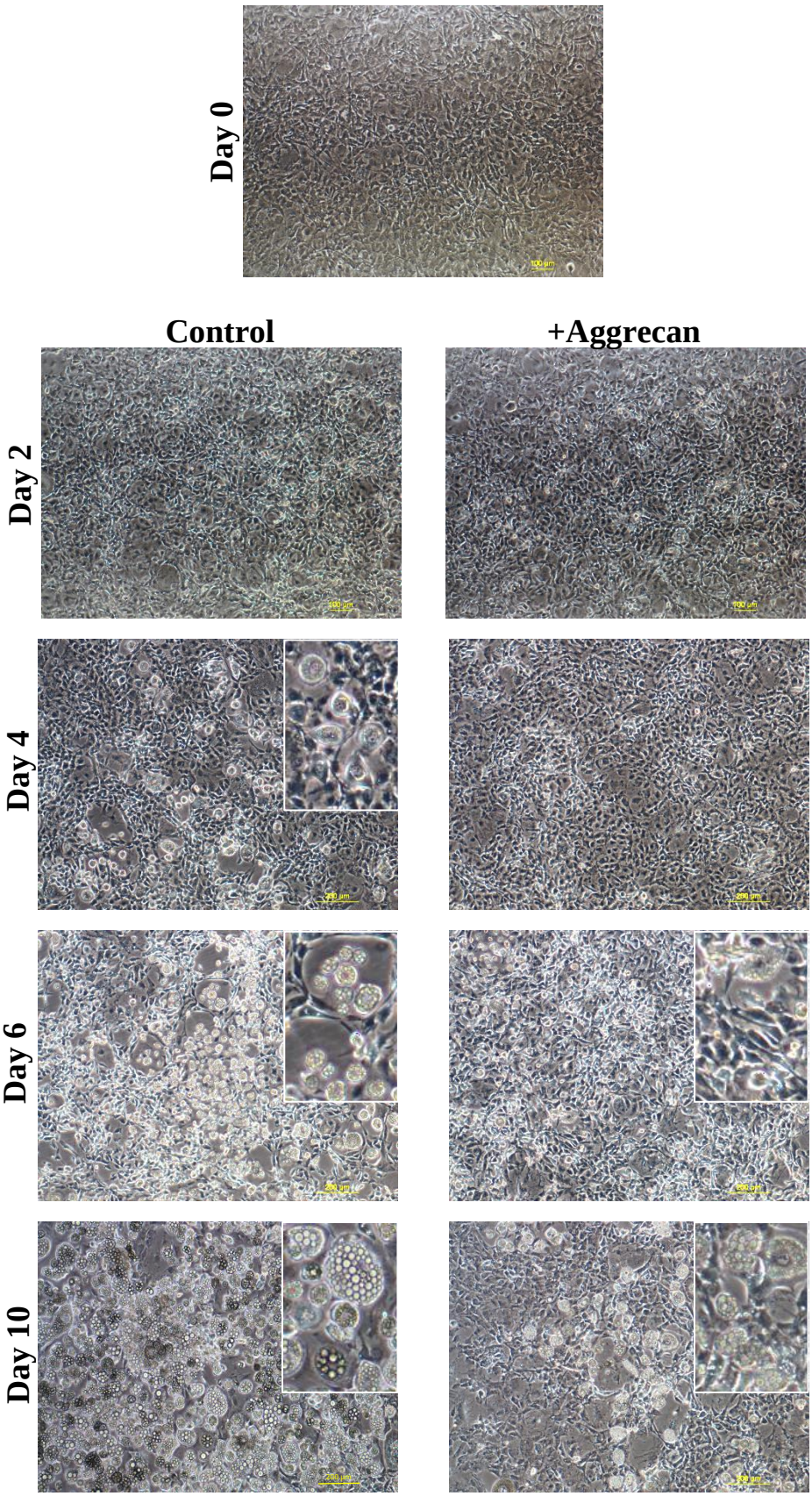
Day 0
Control
+Aggrecan
Day 2
Day 4
Day 6
Day 10

Figure 30. 3T3-L1 cells treated with exogenous aggrecan during adipogenesis. Representative micrographs are shown of 3T3-L1 monolayers 0, 2, 4, 6, and 10 days after induction with adipogenic media with and without treatment of 2 mg/ml exogenous aggrecan by phase contrast microscopy. Bars = 100 µm or 200 µm and are labeled as such (magnification is the same).

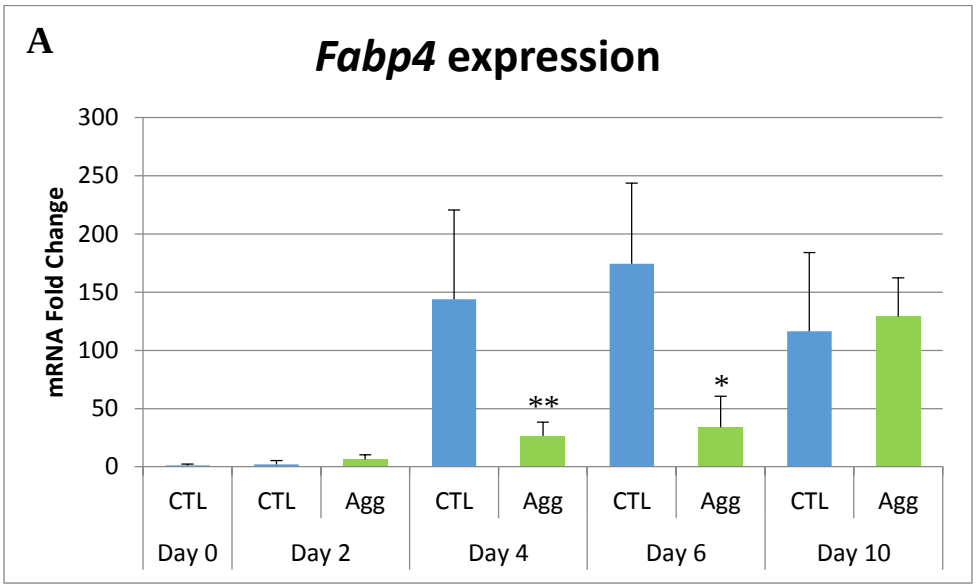
A
Fabp4 expression
mRNA Fold Change
300
250
200
150
100
50
0
**
*
CTL
CTL
Agg
CTL
Agg
CTL
Agg
CTL
Agg
Day 0
Day 2
Day 4
Day 6
Day 10

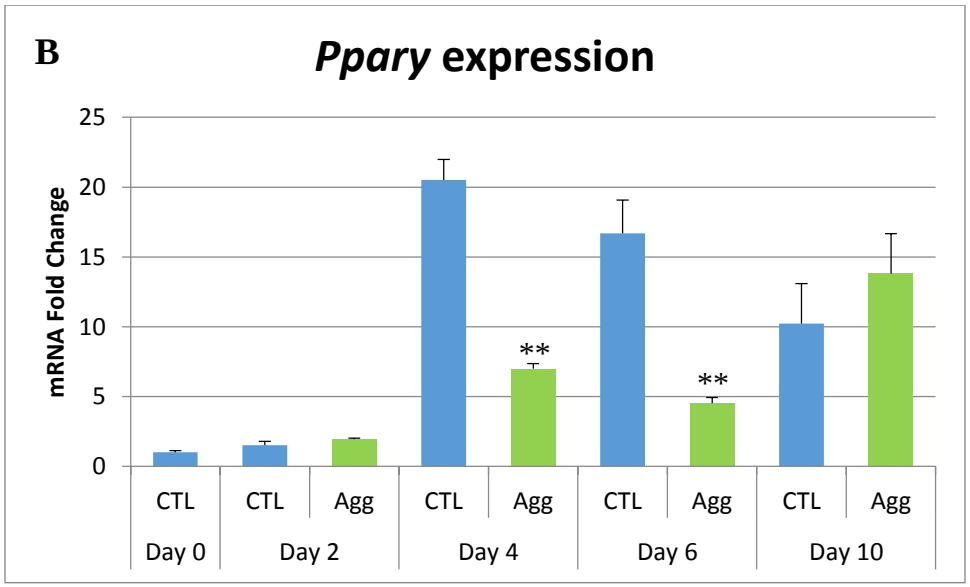
B
Ppary expression
mRNA Fold Change
25
20
15
10
5
0
**
**
CTL
CTL
Agg
CTL
Agg
CTL
Agg
CTL
Agg
Day 0
Day 2
Day 4
Day 6
Day 10

Figure 31. *Fabp4* and *Pparγ* expression during 3T3-L1 adipogenesis with and without addition of exogenous aggrecan. Total RNA was isolated from 3T3-L1 cells 0, 2, 4, 6, and 10 days after induction with adipogenic media with and without the addition of 2 mg/ml exogenous bovine aggrecan as shown in Figure 4. The relative fold change of *Fabp4* (A) and *Pparγ* (B) mRNA was quantified using the ΔΔCT method using Day 0 as the control and normalizing with *Gapdh* mRNA expression. Bars represent the mean $\pm$ standard deviation from 3 and 2 independent experiments for *Fabp4* and *Pparγ*, respectively, analyzed in duplicate.

*: p-value < 0.05, **: p-value < 0.01

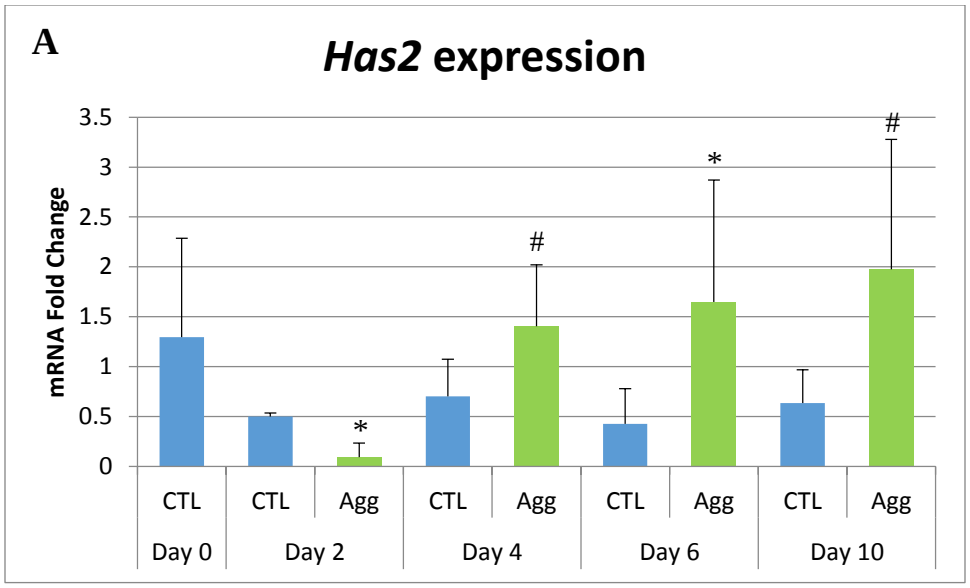
A
Has2 expression
mRNA Fold Change
3.5
3
2.5
2
1.5
1
0.5
0
*
#
*
#
CTL
CTL
Agg
CTL
Agg
CTL
Agg
CTL
Agg
Day 0
Day 2
Day 4
Day 6
Day 10

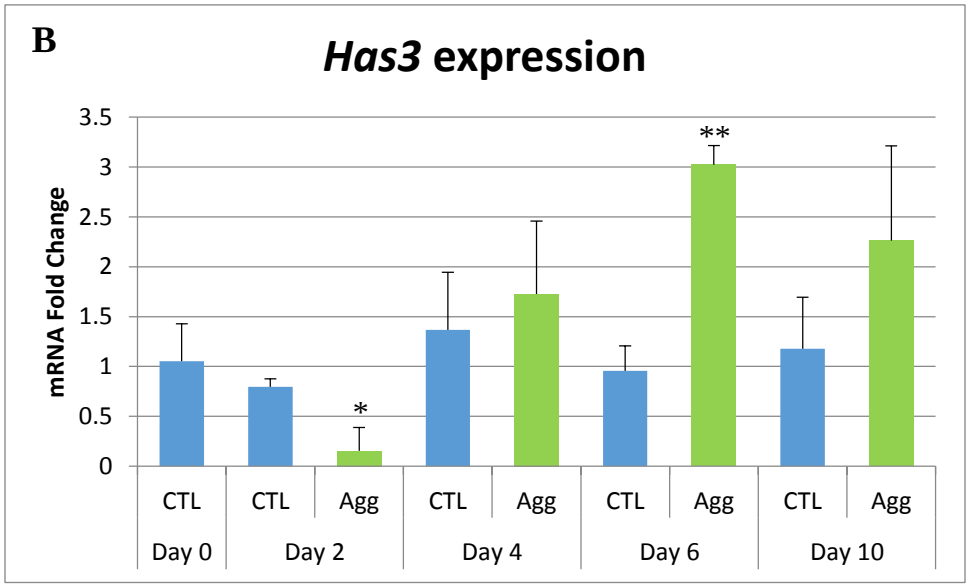
B
Has3 expression
mRNA Fold Change
3.5
3
2.5
2
1.5
1
0.5
0
*
**
CTL
CTL
Agg
CTL
Agg
CTL
Agg
CTL
Agg
Day 0
Day 2
Day 4
Day 6
Day 10

Figure 32. *Has2* and *Has3* expression during 3T3-L1 adipogenesis with and without addition of exogenous aggrecan. Total RNA was isolated from 3T3-L1 cells 0, 2, 4, 6, and 10 days after induction with adipogenic media with and without the addition of 2 mg/ml exogenous bovine aggrecan as shown in Figure 4. The relative fold change of *Has2* (A) and *Has3* (B) mRNA was quantified using the ΔΔCT method using Day 0 as the control and normalizing with *Gapdh* mRNA expression. Bars represent the mean ± standard deviation from 3 and 2 independent experiments for *Has2* and *Has3*, respectively, analyzed in duplicate.

#: p-value < 0.10, *: p-value < 0.05, **: p-value < 0.01

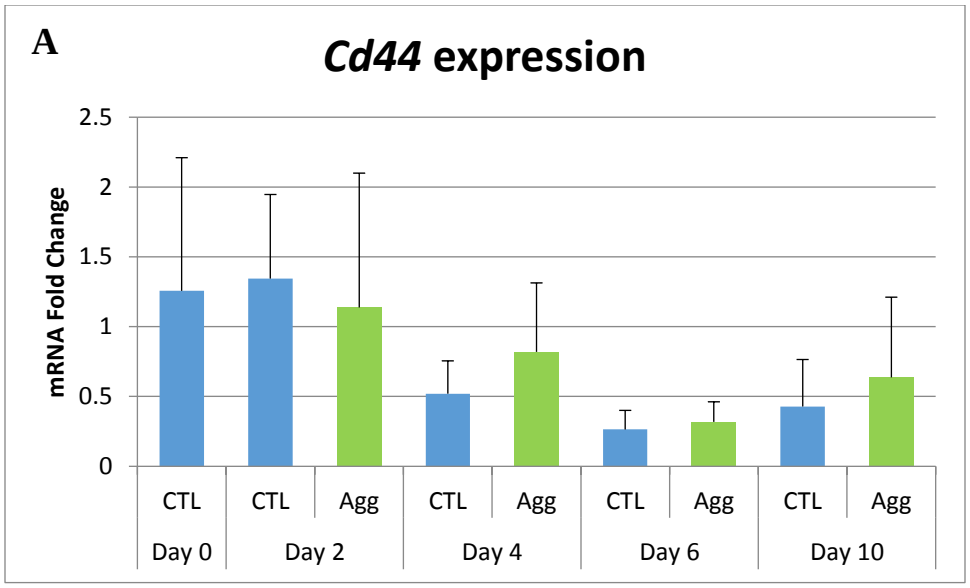
A
Cd44 expression
mRNA Fold Change
2.5
2
1.5
1
0.5
0
CTL
CTL
Agg
CTL
Agg
CTL
Agg
CTL
Agg
Day 0
Day 2
Day 4
Day 6
Day 10

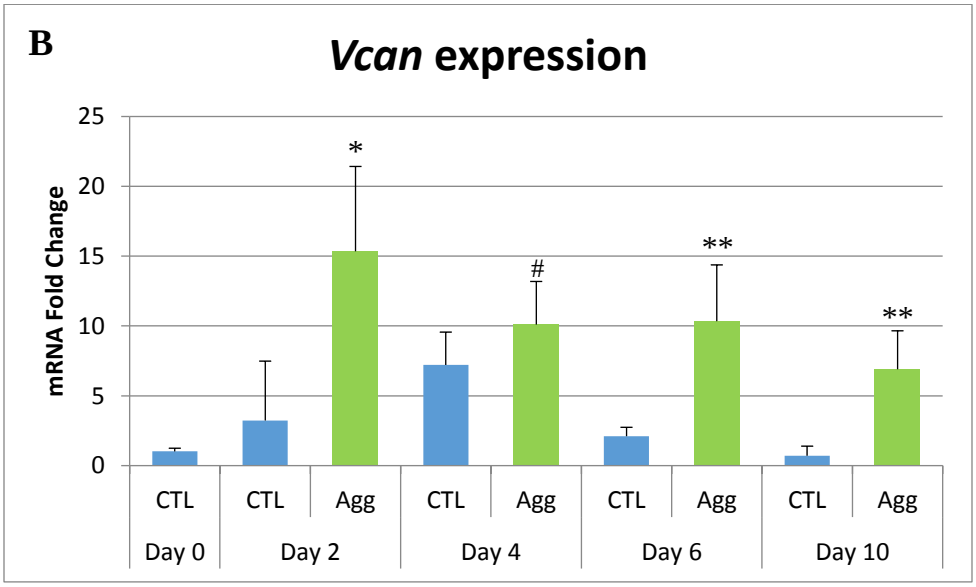
B
Vcan expression
mRNA Fold Change
25
20
15
10
5
0
*
#
**
**
CTL
CTL
Agg
CTL
Agg
CTL
Agg
CTL
Agg
Day 0
Day 2
Day 4
Day 6
Day 10

Figure 33. *Cd44* and *Vcan* expression during 3T3-L1 adipogenesis with and without addition of exogenous aggrecan. Total RNA was isolated from 3T3-L1 cells 0, 2, 4, 6, and 10 days after induction with adipogenic media with and without the addition of 2 mg/ml exogenous bovine aggrecan as shown in Figure 4. The relative fold change of *Cd44* (A) and *Vcan* (B) mRNA was quantified using the ΔΔCT method using Day 0 as the control and normalizing with *Gapdh* mRNA expression. Bars represent the mean $\pm$ standard deviation from 3 independent experiments analyzed in duplicate.

#: p-value < 0.10, *: p-value < 0.05, **: p-value < 0.01

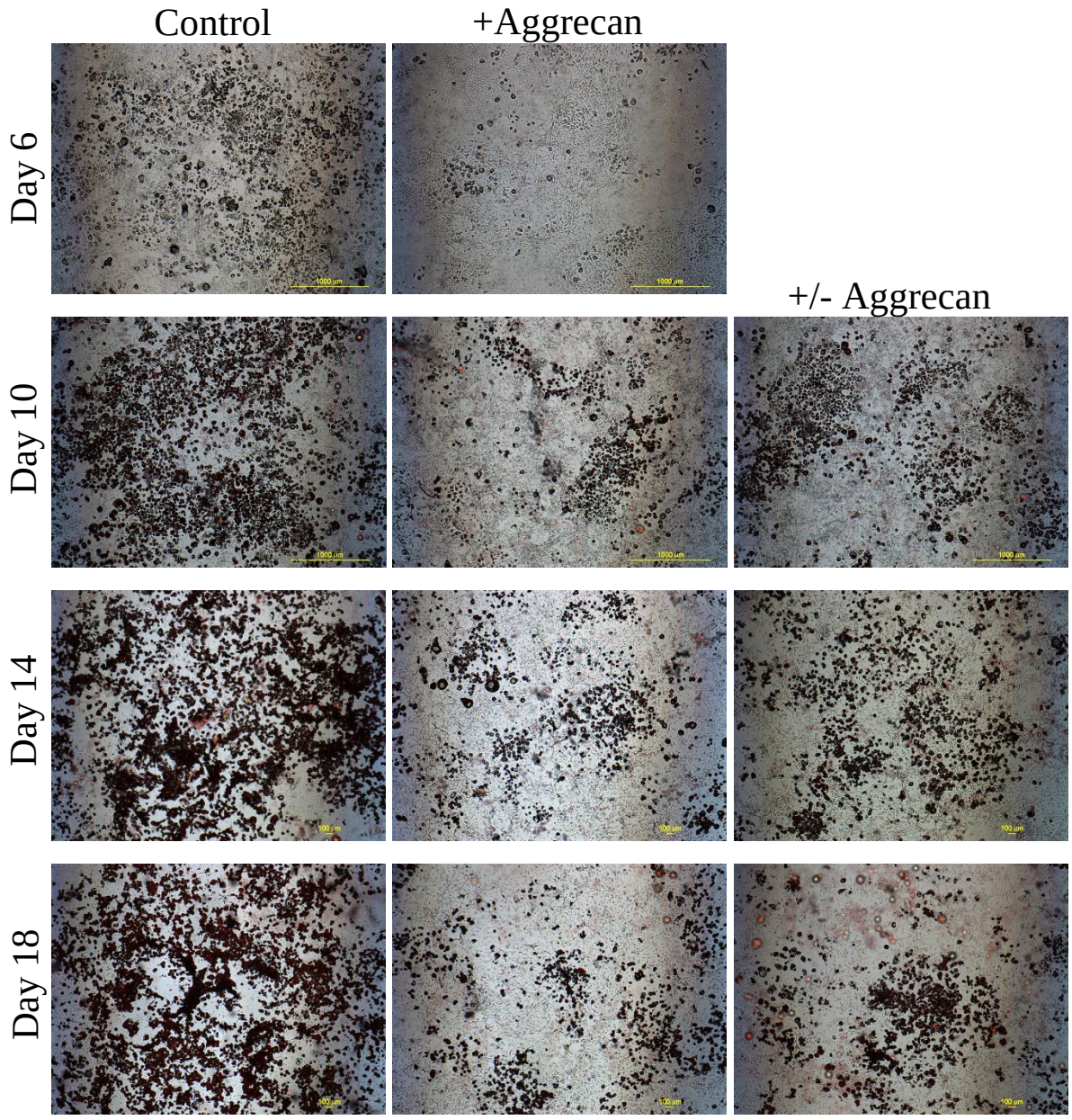
Control
+Aggrecan
+/- Aggrecan
Day 6
Day 10
Day 14
Day 18

Figure 34. Adipogenesis of 3T3-L1 cells in the presence or absence of exogenous aggrecan during adipogenic induction. 3T3-L1 cells were adipogenically induced in the presence or absence of 2 mg/ml exogenous aggrecan and then stained with Oil Red O. Micrographs for Day 6 depict 3T3-L1 cells that were adipogenically induced without (Control) or with (+Aggrecan) 2 mg/ml exogenous aggrecan. Day 10 micrographs display 3T3-L1 cells that were adipogenically induced without (Control) or with (+Aggrecan) 2 mg/ml exogenous aggrecan but include a culture where the aggrecan was excluded from the media change on Day 6 (+/-Aggrecan). Micrographs for Day 14 and Day 18 depict 3T3-L1 cells that were adipogenically induced without (Control) or with (+Aggrecan) 2 mg/ml exogenous aggrecan and include a culture where aggrecan was excluded from the media change on Day 10 (+/-Aggrecan). Micrographs are representative of 2 independent experiments. Bars = 1000 μm, original magnification, 40x.

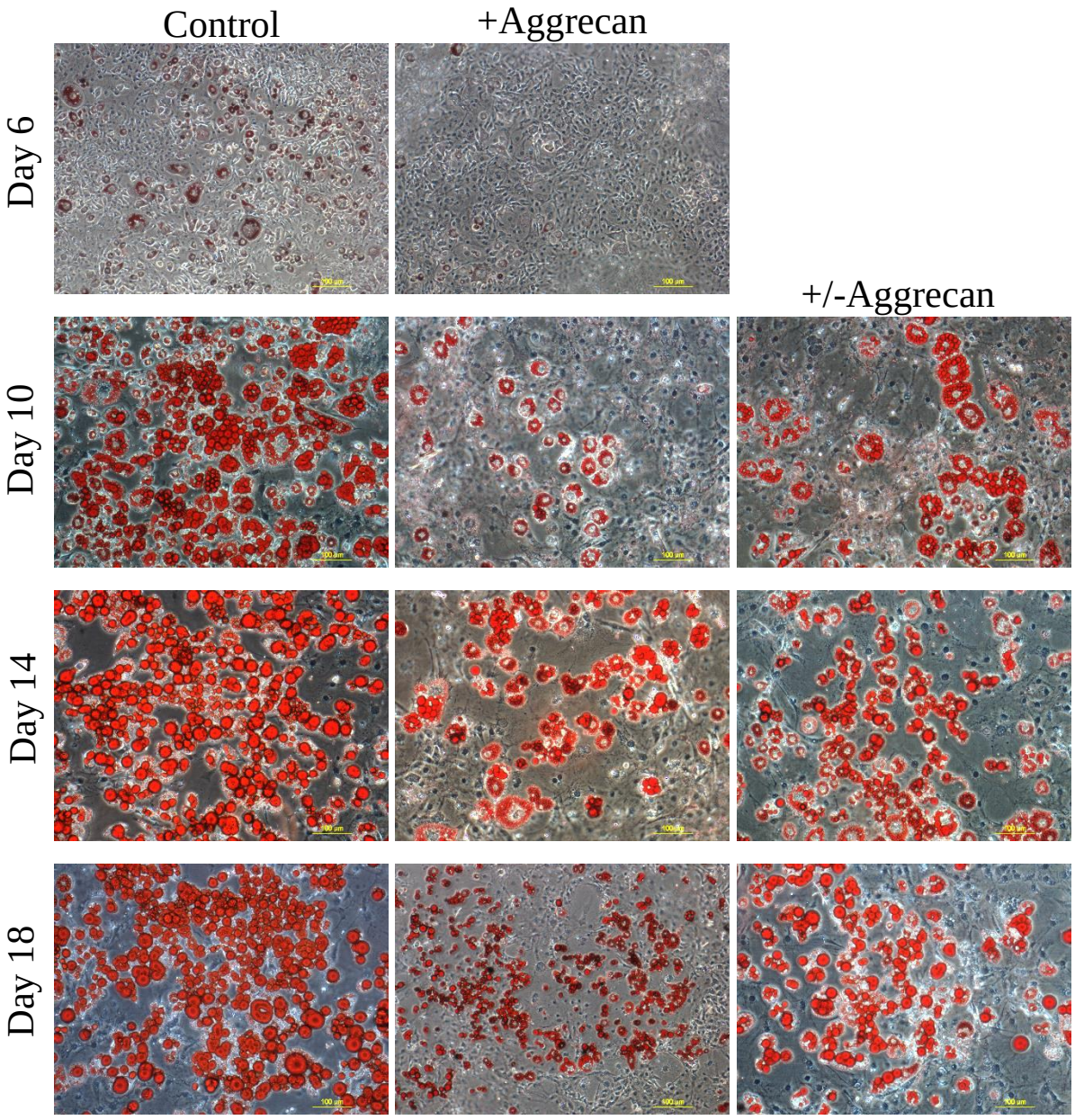
Control
+Aggrecan
+/-Aggrecan
Day 6
Day 10
Day 14
Day 18

Figure 35. Adipogenesis of 3T3-L1 cells in the presence or absence of exogenous aggrecan during adipogenic induction. 3T3-L1 cells were adipogenically induced in the presence or absence of 2 mg/ml exogenous aggrecan and then stained with Oil Red O. Micrographs for Day 6 depict 3T3-L1 cells that were adipogenically induced without (Control) or with (+Aggrecan) 2 mg/ml exogenous aggrecan. Day 10 micrographs display 3T3-L1 cells that were adipogenically induced without (Control) or with (+Aggrecan) 2 mg/ml exogenous aggrecan but include a culture where the aggrecan was excluded from the media change on Day 6 (+/-Aggrecan). Micrographs for Day 14 and Day 18 depict 3T3-L1 cells that were adipogenically induced without (Control) or with (+Aggrecan) 2 mg/ml exogenous aggrecan and include a culture where aggrecan was excluded from the media change on Day 10 (+/-Aggrecan). Micrographs are representative of 2 independent experiments. Bars = 100 μm, original magnification, 400x.

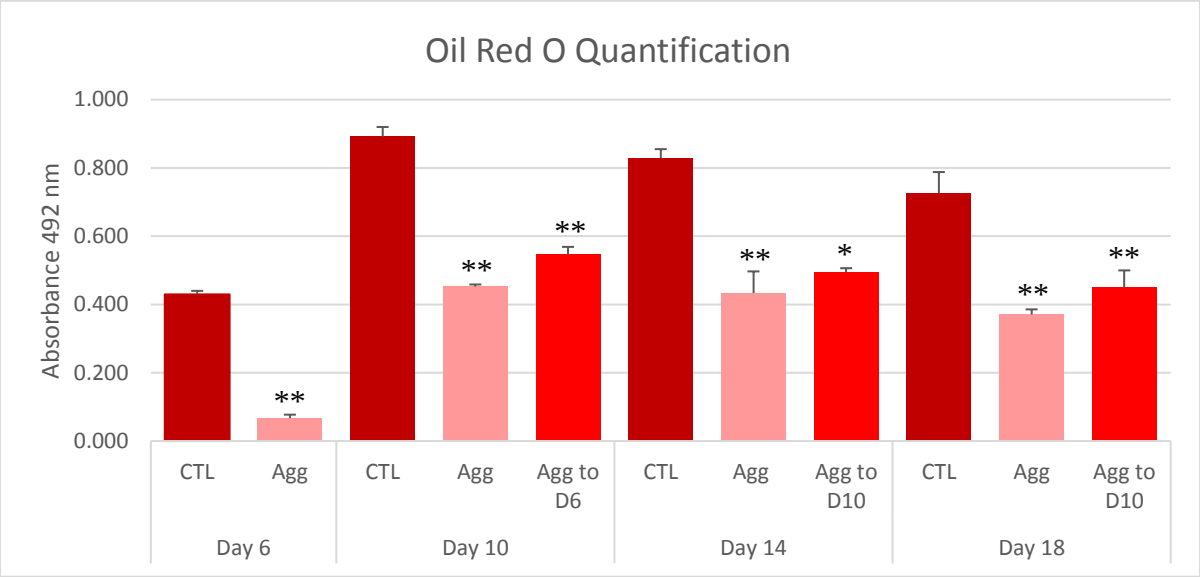
Oil Red O Quantification
Absorbance 492 nm
1.000
0.800
0.600
0.400
0.200
0.000
**
**
**
**
*
**
**
CTL
Agg
CTL
Agg
Agg to D6
CTL
Agg
Agg to D10
CTL
Agg
Agg to D10
Day 6
Day 10
Day 14
Day 18

Figure 36. Oil Red O stain quantification of 3T3-L1 cell adipogenesis in the presence or absence of exogenous aggrecan. 3T3-L1 cells were adipogenically induced in the presence or absence of 2 mg/ml exogenous aggrecan added at time points indicated in Figure 9A. Day 6 samples consist of 3T3-L1 cells that were adipogenically induced with (Agg) and without (CTL) 2 mg/ml exogenous aggrecan and stained with Oil Red O on day 6. Day 10 samples are 3T3-L1 cells that were adipogenically induced with (Agg) and without (CTL) 2 mg/ml exogenous aggrecan but include cultures where the aggrecan was excluded from the media change on Day 6 (Agg to D6) and stained for Oil Red O on day 10. Samples for Day 14 and Day 18 have 3T3-L1 cells that were adipogenically induced with (Agg) and without (CTL) 2 mg/ml exogenous aggrecan and include cultures where aggrecan was excluded from the media change on Day 10 (Agg to D10) and stained for Oil Red O on days 14 or 18, respectively. Oil Red O was extracted from samples with 100% ethanol and absorbance read at a 492 nm wavelength. Bars represent absorbance mean $\pm$ standard deviation of 2 independent experiments.

*: p-value <0.05, **: p-value <0.01

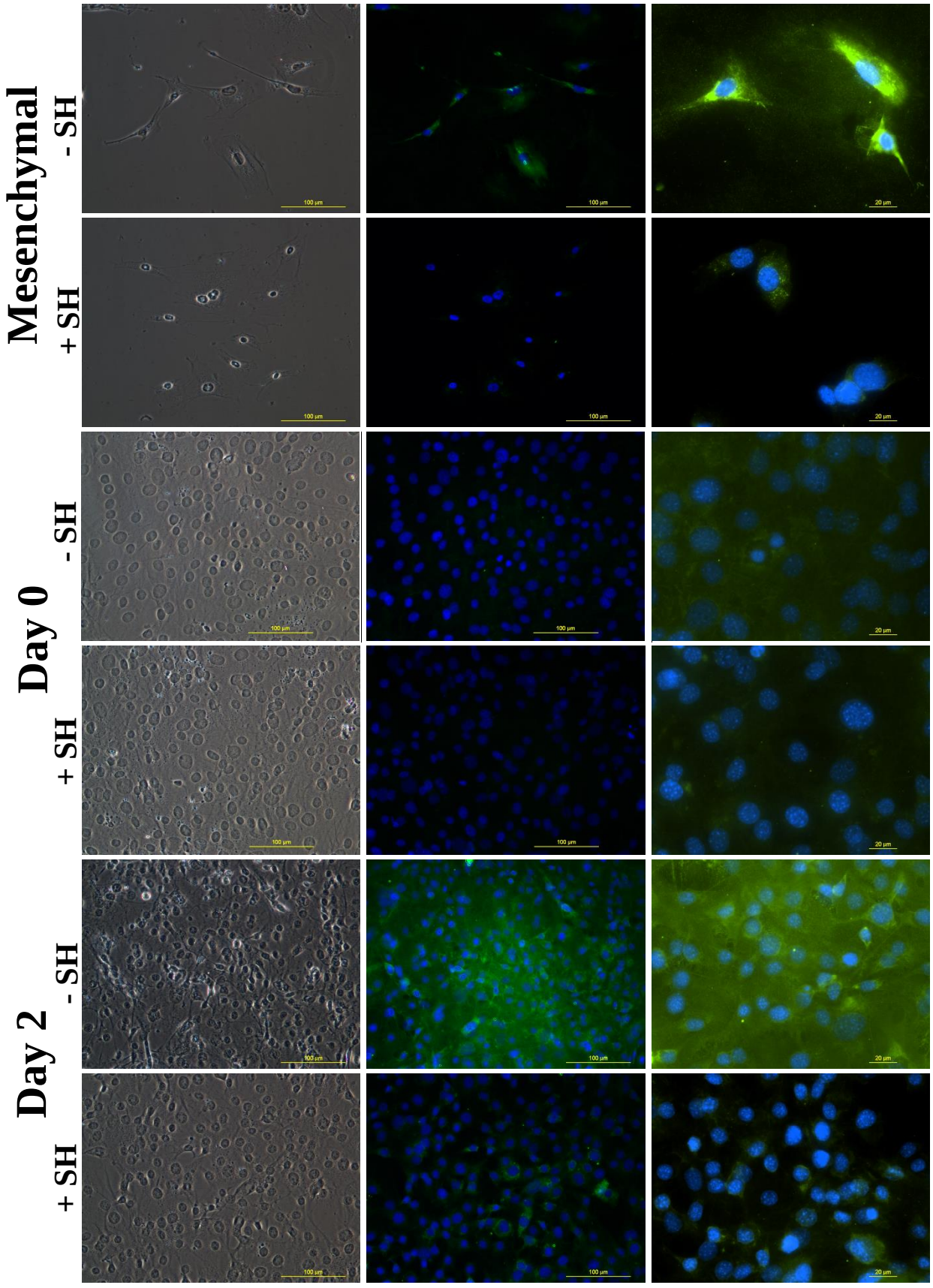
Mesenchymal
- SH
+ SH
Day 0
- SH
+ SH
Day 2
- SH
+ SH
100 µm
20 µm

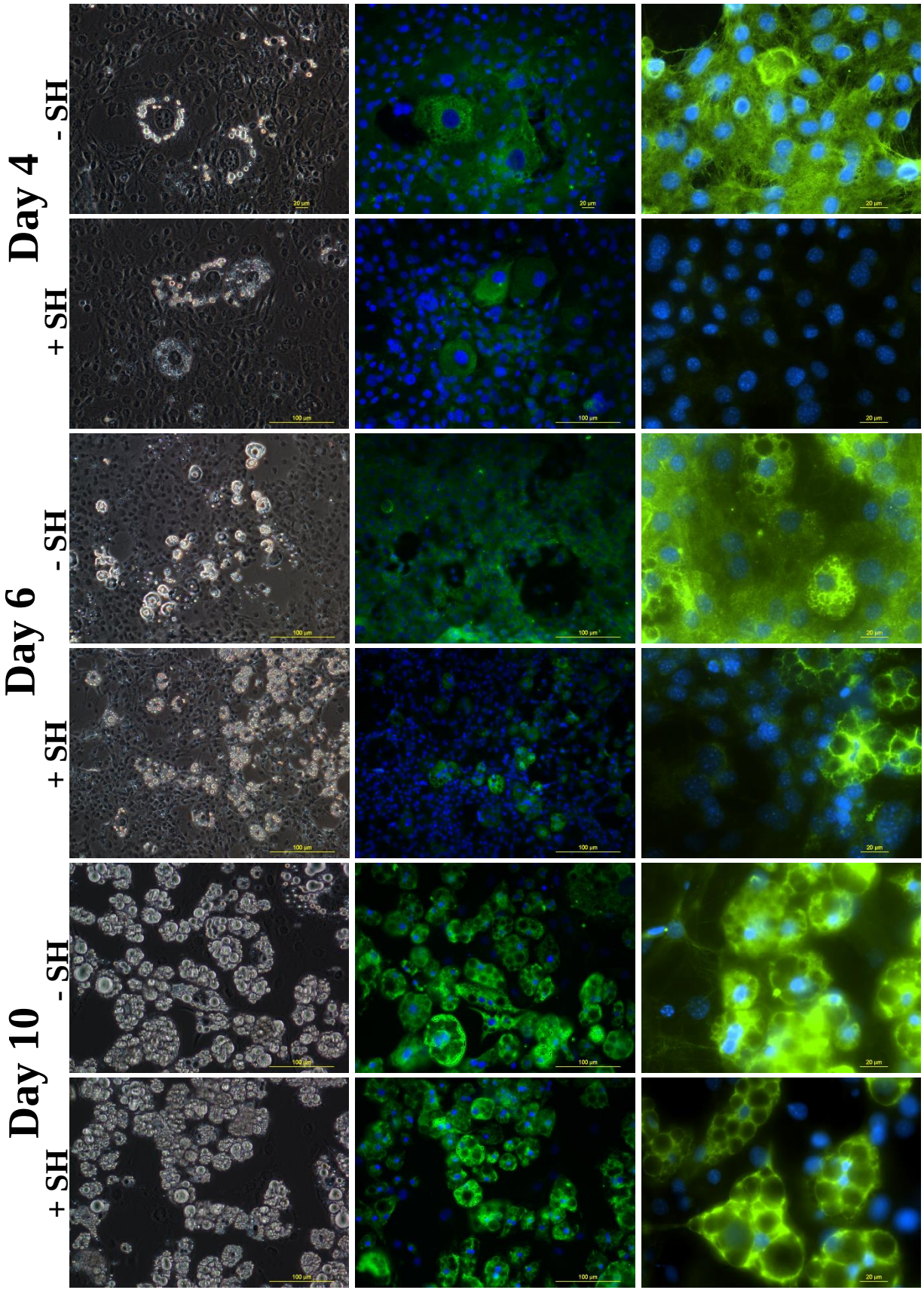
Day 4
- SH
+ SH
Day 6
- SH
+ SH
Day 10
- SH
+ SH

Figure 37. Detection of intracellular and extracellular hyaluronan (HA) associated with 3T3-L1 cells during adipogenesis. 3T3-L1 cells were fixed, permeablized and probed with a hyaluronan-binding protein during different stages of adipogenesis. To visualize internal HA, 3T3-L1 cells were enzymatically pre-treated with 20 U/ml *S. hyaluronidase* (+SH) for 3 hours prior to fixation. The 3T3-L1 cells monolayer is depicted by phase contrast imaging in the first column. Low magnification images of HA staining in green and nuclear staining in blue are depicted in the middle column with a scale bar of 1000 nm. Higher magnification images of HA staining in green and nuclear staining in blue are depicted in the last column with a scale bar of 20 nm.

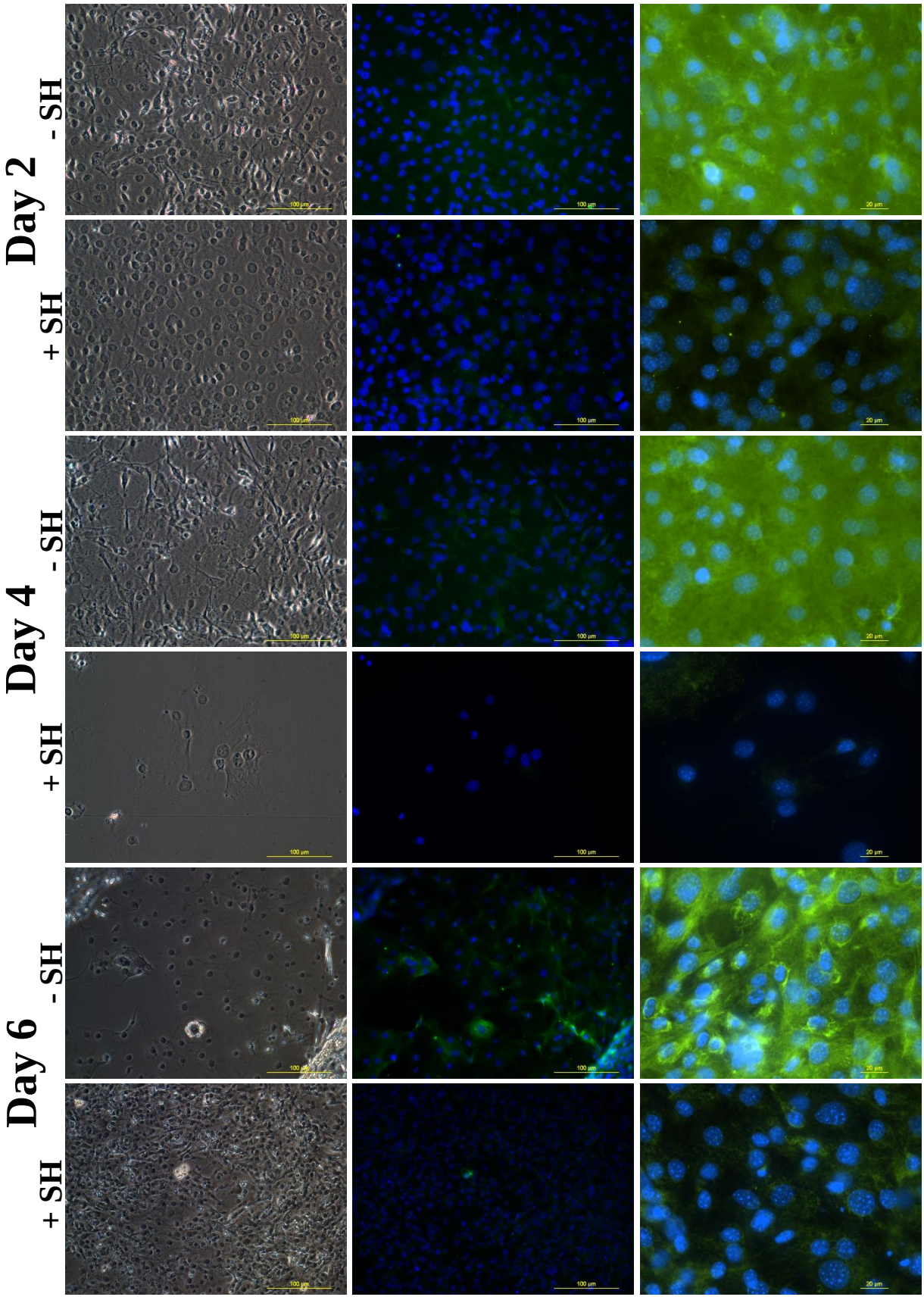
Day 2
- SH
+ SH
Day 4
- SH
+ SH
Day 6
- SH
+ SH

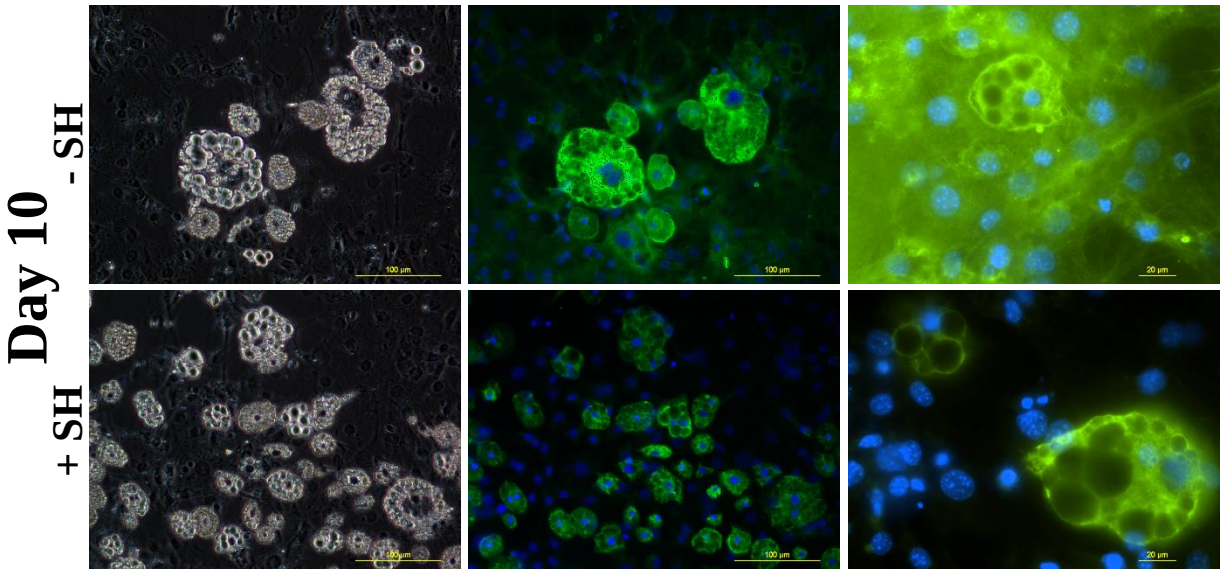
Day 10
- SH
+ SH

Figure 38. Detection of intracellular and extracellular hyaluronan (HA) associated with 3T3-L1 cells treated with exogenous aggrecan during adipogenesis. Representative micrographs show 3T3-L1 cells 2, 4, 6, and 10 days after induction with adipogenesis media containing 2 mg/ml exogenous aggrecan. 3T3-L1 cells were fixed, permeablized and probed with a hyaluronan-binding protein. To visualize internal HA, 3T3-L1 cells were enzymatically pre-treated with 20 U/ml *S. hyaluronidase* (+SH) for 3 hours prior to fixation. The 3T3-L1 cells monolayer is depicted by phase contrast imaging in the first column. Low magnification images of HA staining in green and nuclear staining in blue are depicted in the middle column with a scale bar of 1000 nm. Higher magnification images of HA staining in green and nuclear staining in blue are depicted in the last column with a scale bar of 20 nm.

CHAPTER 4: DISCUSSION

The goal of this dissertation was to gain insight into how hyaluronan-associated components of the extracellular/pericellular matrix participate in directing the differentiation fates of adult mesenchymal progenitor cells. This work began with attempts to isolate and study a primary mesenchymal progenitor population from adult bovine articular cartilage and progressed to the use of the mesenchymal progenitor cell line, 3T3-L1. The goal of characterizing the differentiation of a progenitor cell found in adult cartilage to become an adipocyte, as well as a mature chondrocyte, changed to following the differentiation of an adipocyte-favoring progenitor cell line into a chondrocyte, as well as a mature adipocyte. During adipogenesis, hyaluronan levels were observed to change dramatically. Experimental manipulation of these changes delayed or blocked adipogenesis. This study also demonstrates that the presence or absence of large proteoglycans, such as aggrecan or versican, may reflect the natural mechanism that cells/tissues use to control hyaluronan levels *in vivo*.

Articular cartilage has limited intrinsic repair and renewal potential once damaged [9]. Surgical regeneration methods are available but either produce inferior fibrocartilage that is not able to withstand mechanical stress over time [238] or require healthy tissue for transplantation that can be difficult to obtain [52, 54]. A population of cells recently found in articular cartilage was shown to have progenitor characteristics such as a high colony formation capacity, mesenchymal stem cell markers, and acquisition of chondrogenic phenotype after several passages [23, 24]. These specialized cells have been isolated based on enhanced binding to fibronectin and Hoechst 33342 dye exclusion [25, 26, 201, 239-241]. In other tissues, stem/progenitor cells

provide a renewable source of cells capable of replacing damaged differentiated cells. This discovery opens the possibility of targeting a resident progenitor cell population within articular cartilage for not only repair, but regeneration of damaged cartilage with hyaline cartilage. Results found here confirm a small population of cells isolated from bovine articular cartilage that has a unique staining pattern with Hoechst 33342 dye consistent with the so-called side population [222]. Hoechst 33342 staining was selectively inhibited in the presence of the potent P-glycoprotein inhibitor, verapamil, suggesting their dim Hoechst 33342 staining is due to the ABC-binding cassette family of transporters. Expression of these transporters is a major determinant of the progenitor side population profile and has been shown to be important in maintaining progenitor cell stemness [242-244]. However, the percentage of cells comprising the side population was very low, an average of 0.15%, but similar to other studies [26]. This means that out of every 100,000 cells analyzed, only 150 cells would be available for analysis. To circumvent this issue, other researchers expanded the side populations in culture until appropriate numbers were obtained [26, 239]. However, primary chondrocytes dedifferentiate in 2-dimensional culture, changing their function, gene expression, and cell morphology to resemble fibroblasts or mesenchymal cells [191, 223, 245, 246]. To avoid creating mesenchymal like cells with expansion and dedifferentiation that could be confused with the side population, it was decided to forgo expansion and focus on enriching the side population.

Studies have shown a greater number of progenitor cells reside in the superficial zones of articular cartilage compared to deeper zones [25, 26, 28] prompting an enrichment attempt by harvesting the superficial and middle/deep zones of the articular cartilage separately. However, there was only a modest increase in the side population of superficial cells detected compared to

deeper cells, 0.06% to 0.02%, respectively. Additionally, the ability to adhere to fibronectin through β1 receptors is also a stem cell characteristic that has been used to enrich mammalian progenitor cells from articular cartilage [25, 201, 247, 248]. In this dissertation, a portion of cells isolated from bovine articular cartilage adhered to fibronectin, however, we could not demonstrate any enhanced ability to efflux Hoechst 33342 dye in these cells through microscopic observation. Since attempts to increase the number of cells within the side population had failed, modifications of analyses were made in order to lower the number of cells needed.

The most common differentiation pathways used to demonstrate multipotency of putative articular cartilage progenitor cells are osteogenesis, chondrogenesis, and adipogenesis [249, 250]. Three different cell lines were chosen as positive controls for these pathways to ensure differentiation could occur under optimal conditions. CH310T1/2, MG-63, and 3T3-L1 cells were selected for chondrogenic [251], osteogenic [252], and adipogenic [76] differentiation, respectively. Because articular cartilage is populated with chondrocytes and hypertrophic chondrocytes have been shown to differentiate into osteocytes during ossification [253, 254], articular cartilage-derived cells differentiated to become chondrocytes and/or osteocytes alone would not be a convincing demonstration of multipotency, therefore, adipogenesis was the main focus. 3T3-L1 cells were analyzed to determine that adipogenesis could be completed on a miniature scale using only a tenth of the cells normally required (10^4 cells per well compared to 10^5). Unfortunately, while this was successful, it would still require more than 60 times the cells detected in 100,000 events per well. These cell numbers were just not feasible without expansion and expansion was undesirable. While we were able to confirm a side population of cells with a

unique Hoechst 33342 efflux profile that was isolated from bovine articular cartilage, we were unable to obtain enough side population progenitor cells for further analysis without expansion.

A few exciting observations made while working with 3T3-L1 cells led to some novel findings. The first observation was that 3T3-L1 cells showed the highest Hoechst 33342 efflux potential when compared to the other differentiation control cell lines, suggesting they might have multipotent potential beyond their designated "pre-adipocyte, unipotent" status [69, 70]. This hypothesis was tested by determining their chondrogenic potential in micromass cultures when exposed to chondrogenic inducers. The second observation was that between days 4 and 6 during 3T3-L1 adipogenic differentiation, aspirated medium was noticeably more viscous. This observation was originally made by Calvo *et al.* (1991) who identified hyaluronan as being partly responsible for the increase in viscosity [182]. Similarly, media conditioned by naked mole-rat fibroblasts were found to have increased viscosity after a few days of culture. When the media was tested, high-molecular mass hyaluronan was identified as the viscous substance [255]. Cell growth arrested by early contact inhibition is necessary for 3T3-L1 adipogenesis to occur [80] and Tian *et al*. established that hyaluronan was the extracellular signal that triggered the anticancer property of early contact inhibition found in naked mole-rat fibroblasts [255]. While a small handful of papers have addressed hyaluronan regulation during 3T3-L1 adipogenesis, how hyaluronan and its associated components as part of the pericellular matrix contribute to 3T3-L1 adipogenic differentiation remained unknown. We investigated the presence and properties of the pericellular matrix of mesenchymal 3T3-L1 and adipocyte 3T3-L1 cells in addition to the role of hyaluronan during 3T3-L1 adipogenesis.

3T3-L1 cells were grown in micromass cultures and treated with and without chondrogenic inducers to test their multipotent ability. To the best of our knowledge, we are the first to report that 3T3-L1 cells possess chondrogenic potential. Three independent lines of experimental evidence support this conclusion. First, uniform alcian blue staining throughout revealed a drastic increase in sulfated proteoglycans when 3T3-L1 cells were grown in micromass culture with a chondrogenic medium. Second, analysis of mRNA showed the increased sulfated proteoglycan to be the chondrocyte and cartilage specific proteoglycan, aggrecan [256]. This increase in aggrecan expression was concomitant with a decrease in versican, the proteoglycan associated with rapidly proliferating cells [257, 258] and pre-cartilage mesenchymal condensations [153, 259, 260]. This observation is consistent with a previous report in avian limb buds where versican expression is lost in the cartilage core, where cells have developed a more rounded, chondrogenic phenotype and aggrecan is up-regulated [261]. Third, we report here that *Has2* expression is significantly decreased in chondrogenic treated 3T3-L1 micormass cultures which is in agreement with previous studies that found *Has2* expression to be decreased in pre-cartilage condensations [153, 262]. These findings are not perhaps too surprising considering the recent discovery of adipose derived stem cells and their chondrogenic potential [58, 263]. While more research needs to be completed to fully explore the chondrogenic potential of 3T3-L1 cells, having an additional chondrogenic model for an adipogenic to chondrogenic system that doesn't involve an isolation step could aid in cartilage regeneration research.

Midway through 3T3-L1 adipogenesis, the culture medium became noticeably more viscous. Long, mucoid strings were formed with a Pasteur pipette during aspiration (Figure 16). Calvo *et al*. made a similar observation in 1991 and identified an increase in hyaluronan in culture

medium (not cell-associated) by ion exchange chromatography as a likely contributor to the increase in viscosity [182]. Hyaluronan is a negatively charged, non-sulfated glycosaminoglycan that is a major component of the extracellular matrix in multiple tissues and is roughly 100 times more viscous than water at biological concentrations [264, 265]. In spite of its simple structure of repeating disaccharides, hyaluronan plays a key role in many crucial cellular processes including tissue remodeling (wound repair), inflammation, tumorigenesis, angiogenesis, proliferation, motility and differentiation [133, 266-268]. We analyzed culture media throughout adipogenesis with a modified ELISA to quantify hyaluronan concentrations and found a significant increase during mid-late adipogenesis. Media collected during mid-late adipogenesis contained nearly 4 times the hyaluronan concentrations as media collected during early adipogenesis. This increase in hyaluronan is likely, at least, partially responsible for the increase in viscosity observed in conditioned media collected during mid-late adipogenesis, which is in agreement with findings from Calvo *et al*. [182].

Hyaluronan is synthesized by three different transmembrane hyaluronan synthases, HAS1, HAS2, and HAS3 [120]. We and others have found HAS2 to be the primary synthase used to make hyaluronan in 3T3-L1 cells [184]. Hyaluronan is polymerized at the inner surface of the plasma membrane and then extruded through the membrane into the extracellular space where it is assembled in the extracellular matrix or anchored to the cell surface by the synthase or by binding a cell surface receptor [117]. Once anchored, hyaluronan contributes to the organization, structural integrity, and hydrodynamic properties of the pericellular matrix by acting as a scaffold on which other hyaladherins can assemble [155]. We found that one such hyaladherin, versican, displays less than half a fold increase upon adipogenic induction as shown by relative mRNA

levels then decreases steadily through late adipogenesis. A similar pattern was observed by us and others for *Has2* expression [184]. This suggests that the increase in viscosity observed during mid-late adipogenesis is likely not due to an increase in versican or hyaluronan synthesis-but perhaps increased dissociation from the cell. This is in agreement with other studies that identified a "versican-like" chondroitin sulfate proteoglycan that interacted with hyaluronan in the culture medium of 3T3-L1 cells and was the same chondroitin sulfate proteoglycan that was mainly expressed in developing murine tissues [182, 183]. Versican has been shown to interact with endogenously produced hyaluronan via its G1 domain [269-271], similar to the articular cartilage proteoglycan, aggrecan [172, 272]. Both versican and aggrecan are capable of forming large aggregates of hyaluronan and link protein in the pericellular matrix of cultured cells [273]. However, 3T3-L1 adipocytes no longer have the capacity for pericellular matrix assembly and thus are distinctly different from 3T3-L1 mesenchymal cells.

In addition to its structural properties, the binding of hyaluronan to the surface receptor, CD44, plays a critical role in cell-cell/matrix adhesive interactions and signal transduction that affect cytoskeletal association. Regulation of various genes associated with the formation of the extracellular matrix and cytoskeletal elements is required for adipogenesis to occur [274, 275] and this association could be partly responsible for the drastic changes observed in cell morphology and cytoskeletal components during adipocyte differentiation. CD44 is a broadly distributed single pass, transmembrane glycoprotein that is found on a variety of cell types [276]. To our knowledge, we are the first to report that *Cd44* expression decreases after initial adipogenic induction and remains low throughout adipogenesis. CD44 anchors the pericellular matrix to the cell surface through its hyaluronan interactions, therefore its reduced expression could help explain why the

large pericellular matrices observed around mesenchymal 3T3-L1 cells are lost during differentiation to adipocytes. In addition, since hyaluronan internalization was detected concomitant with 3T3-L1 adipogenesis, CD44-mediated endocytosis of hyaluronan may be another mechanism to promote adipogenesis.

3T3-L1 cells with mesenchymal morphology retained pericellular matrices and those with adipocyte morphology were unable to synthesize or retain one. We show that the pericellular matrix of mesenchymal 3T3-L1 cells can be removed by treatment with *Streptomyces* hyaluronidase and short hyaluronan oligosaccharides. CD44 has a high affinity for large hyaluronan molecules but exhibits competition for high molecular hyaluronan binding with a minimum of six hyaluronan sugar oligosaccharides (or three disaccharide units) in high concentrations [277]. These results suggest mesenchymal 3T3-L1 cells have high molecular weight hyaluronan-dependent pericellular matrices that are receptor anchored similar to those found on chondrocytes [278]. Exogenous aggrecan increased the pericellular matrix size of mesenchymal 3T3-L1 cells. However, even when provided with exogenous hyaluronan and aggrecan, 3T3-L1 adipocytes were unable to assemble a detectable pericellular matrix (shown in Figure 19D). This most likely is partly due to the significant reduction in CD44 protein observed (Figure 18A) during late adipogenesis since CD44 serves as the critical link to the retention of hyaluronan-proteoglycan aggregates [279]. Similarly, COS-7 cells, which lack CD44, cannot assemble a pericellular matrix in the presence of exogenous aggrecan and/or hyaluronan until transfected with a CD44 expression plasmid [280]

In this study, several components of the pericellular matrix show an initial increase in expression directly after exposure to adipogenic inducers and then taper off to a consistent level. This suggests that regulation of the pericellular matrix is necessary for adipogenic differentiation, particularly the early stages. This is further illustrated by the significant reduction in 3T3-L1 adipogenesis when hyaluronan synthesis was inhibited with 4-MU treatment and with increased decoration of hyaluronan with exogenous aggrecan. While 4-MU interferes with the synthesis of hyaluronan, the addition of exogenous aggrecan increases the size of the pericellular matrix. Both treatments resulted in a relative increase in *Has2*, *Cd44*, and *Vcan* mRNA expression compared to untreated cultures. An alternative interpretation is that these treatments prevented the decreased expression of *Has2* and *Cd44* observed in untreated 3T3-L1 cultures during adipogenesis. There are some reports that show 4-MU treatment decreases *Has2* expression depending on the type of cells tested, but the results herein are consistent with studies performed in myofibroblasts [281, 282]. Our results show that inhibiting (1) hyaluronan synthesis with 4-MU or (2) access to hyaluronan by increased decoration with exogenous aggrecan causes these pericellular components to be retained at close to pre-induction levels and significantly reduces the number of cells that successfully undergo adipogenesis. Of course in this study exogenous aggrecan is a surrogate hyaladherin for endogenous versican. Interestingly, even though *Has2* levels were increased with exogenous aggrecan treatments (presumably causing an increase in hyaluronan synthesis), the viscosity of the culture medium remained unchanged. One would expect the culture medium to remain unchanged by 4-MU treatment regardless of the increase in *Has2* because 4-MU inhibits the availability of monosaccharide substrate of the enzyme resulting in the inhibition of hyaluronan synthesis. This suggests that any increase in hyaluronan synthesis is not being released into the culture medium and instead, is perhaps being retained at the cell surface as part

as the pericellular matrix. The increase in hyaluronan receptor, CD44, observed with exogenous aggrecan treatment supports this hypothesis because more receptors could bind more hyaluronan. With increased pericellular matrix components surrounding the cells, they are unable to efficiently undergo adipogenesis. These findings suggest hyaluronan released into the culture medium isn't merely a product of adipogenesis, but may be a requirement of 3T3-L1 adipogenesis. This is similar to both chondrogenesis and myogenesis in which high levels of hyaluronan must be cleared from around the cell in order for cellular condensation and migration to occur and differentiation to proceed [165].

Treatment with 4-MU effectively inhibits hyaluronan synthesis and has been shown to completely block pericellular matrix assembly in murine primary chondrocytes [214]. If loss of the pericellular matrix is required for 3T3-L1 adipogenesis to occur, why would 4-MU treatment inhibit adipogenesis? Several studies have determined that hyaluronan modulates TGF-β1 signaling to promote differentiation of myofibroblasts, although, they offer conflicting mechanisms as to how that modulation occurs [282, 283]. Webber *et al*. (2009) found that exogenous hyaluronan inhibited TGF-β1 signaling and suggested TGF-β1 required the synthesis of hyaluronan and not just its presence for proper signaling [283]. However, when Evanko *et al.* (2015) treated lung fibroblasts with 4-MU to inhibit hyaluronan synthesis, they observed an increase in myofibroblast differentiation [282]. Additionally, hyaluronan binding to CD44 led to a decrease in TGF-β1 mediated Smad signaling in renal epithelial cells while hyaluronan binding to CD44 led to an increase in TGF-β1 mediated Smad signaling in breast cancer cells [160, 284]. Different types of cells can have different responses to TGF-β1 which can be associated with differences in hyaluronan synthesis, turnover, different CD44 isoforms, and matrix integrity.

However, it has been reported that Smad3, which is activated by TGF-β through its receptor, binds to C/EBPβ to inhibit its transcriptional activity. This leads to a decrease in PPARγ transcription, a master regulator in adipogenesis, resulting in inhibition of adipocyte differentiation [90]. Knowing this, we propose the hypothesis that hyaluronan is required to initiate adipogenesis by binding to CD44, which binds TGF-β1 type I receptor, inhibiting the formation of TGF-β1 heterodimer receptor and its activation of Smad3, allowing transcription of early adipogenic genes (Figure 39A). Reduction of cell-associated hyaluronan would be associated with Smad 3 phosphorylation, blocking induction of adipogenesis (Figure 39B).

In addition to possible effects on TGF-β1, or other growth factor, signaling, adipogenesis may be modulated by the internalization of CD44 and hyaluronan. Cytoskeleton organization and organelle distribution are partially regulated by CD44 anchored to a hyaluronan dependent matrix [285]. This suggests that cytoskeleton-CD44-extracellular hyaluronan interactions might exert inside-out signaling, as suggested for chondrocytes [286]. The major method for hyaluronan elimination from the bloodstream by liver endothelial cells is by receptor-mediated endocytosis [287, 288]. Several studies found that CD44 facilitates a receptor-mediated uptake mechanism for hyaluronan internalization and degradation [150, 289]. In renal epithelial cells, hyaluronan bound to CD44 promotes TGF-β1 receptor trafficking to lipid rafts, which results in an increase in the association of TGF-β1 receptor with Smad7 [160]. Smad7 promotes receptor bound turnover located in lipid rafts via the caveolar internalization pathway. Endocytosis of cell surface receptors is an important regulatory event in signal transduction and this could partially explain the increase in intracellular hyaluronan in 3T3-L1 adipocytes and not mesenchymal cells. Allingham *et al*. (2006) showed expression of the hyaluronidase enzyme, *Hyal2*, was significantly increased during

adipogenesis in 3T3-L1 cells [184] and primarily localized in lysosomes [138]. Treatment with exogenous aggrecan causes the pericellular matrix to swell as aggrecan molecules fully decorate hyaluronan. The addition of exogenous aggrecan could block adipogenesis merely by steric hindrance. If highly aggrecan decorated hyaluronan cannot reach lysosomal HYAL2 through endocytosis, this may inhibit adipogenesis (Figure 40). Our lab has previously shown that hyaluronan highly decorated with exogenous aggrecan shows a significant reduction in endocytosis in rat chondrosarcoma cells [177]. It is unclear if the outcome of hyaluronan internalization is receptor turnover, internal hyaluronan signaling, or hyaluronan degradation but the inhibition of adipogenesis with exogenous aggrecan suggest access to hyaluronan for binding/cleaving and internalization is essential for adipogenesis to occur.

The control of cell shape, migration, proliferation, differentiation, and tissue development is regulated by the composition of the pericellular matrix, with adipocytes being no exception [290, 291]. Despite the recent growth of information regarding the effects of pericellular and extracellular components on adipogenesis, many questions still remain, and continued research is required to build and refine our current knowledge. However, our novel observations that the pericellular matrix and CD44 expression is lost during adipogenesis, and that blocking hyaluronan synthesis or increasing decoration of hyaluronan with exogenous aggrecan during the adipogenic differentiation protocol effectively inhibits 3T3-L1 adipogenesis further highlight the importance of the hyaluronan-dependent pericellular matrix in controlling adipocyte formation. Even though the clinical importance of these findings are not immediately evident, details of how the pericellular matrix is assembled and disassembled during adipogenesis could prove facilitative for clinical advancements in the future.

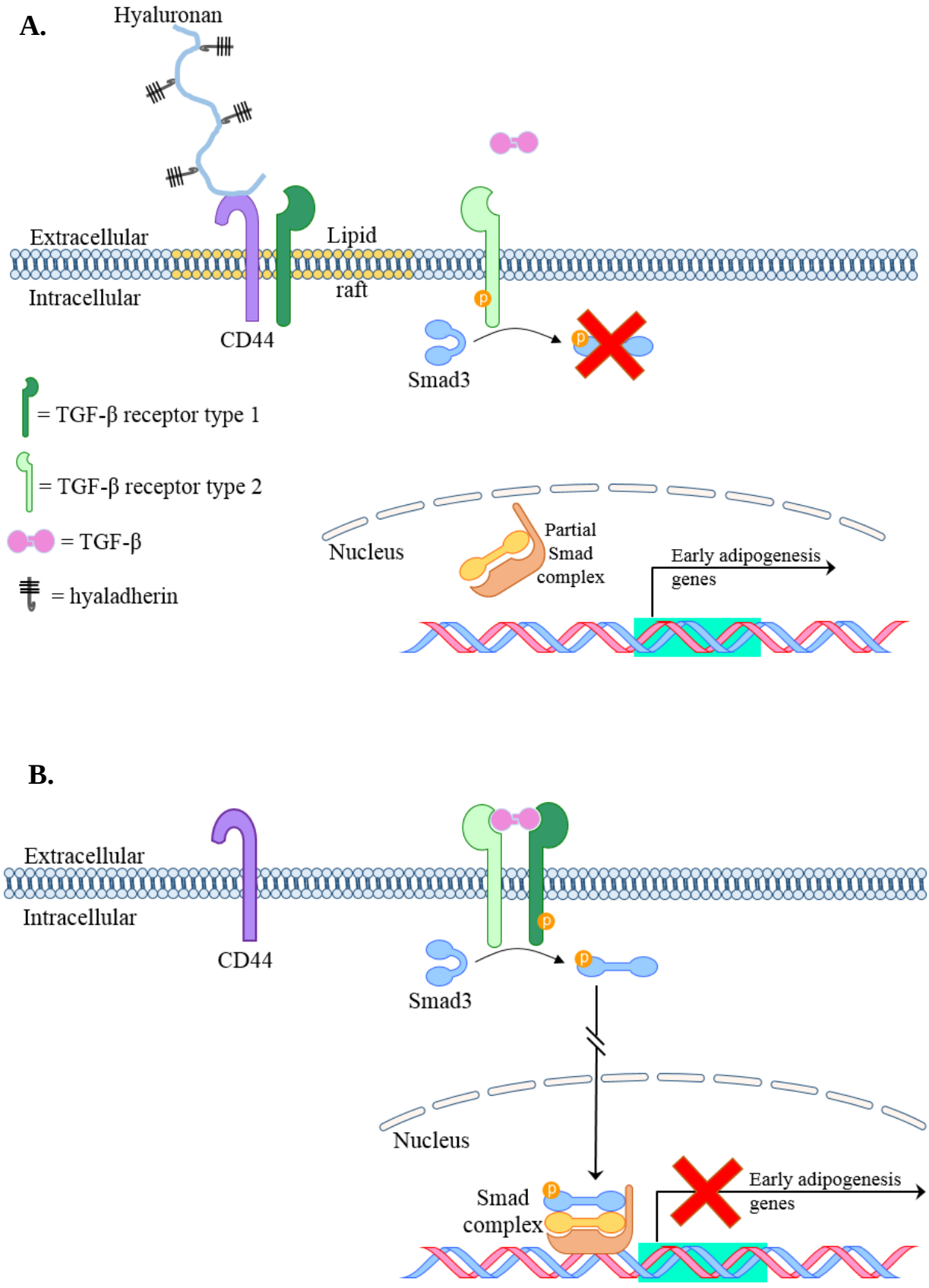
A.
Hyaluronan
Extracellular
Intracellular
Lipid
raft
CD44
Smad3
= TGF-β receptor type 1
= TGF-β receptor type 2
= TGF-β
= hyaladherin
Nucleus
Partial
Smad
complex
Early adipogenesis
genes
B.
Extracellular
Intracellular
CD44
Smad3
Nucleus
Smad
complex
Early adipogenesis
genes

Figure 39. Hyaluronan is required for initiation of adipogenesis. CD44 occupied with hyaluronan has increased affinity for TGF-β receptor type I [160]. CD44 associates with TGF-β receptor type I disassembling the heterodimer with TGF-β receptor type II resulting in the inability to bind its ligand [292]. Without ligand binding, Smad3 is not phosphorylated nor does it translocate to the nucleus as part of the Smad complex to block transcription of early adipogenesis genes (A). When hyaluronan synthesis is blocked with 4-MU treatment, there is little to no hyaluronan to bind CD44. The TGF-β receptor heterodimer is able to bind its ligand and phosphorylate Smad3. Active Smad3 associates with other Smad proteins and translocates to the nucleus where it binds to DNA and halts transcription of early adipogenesis genes (B).

A.

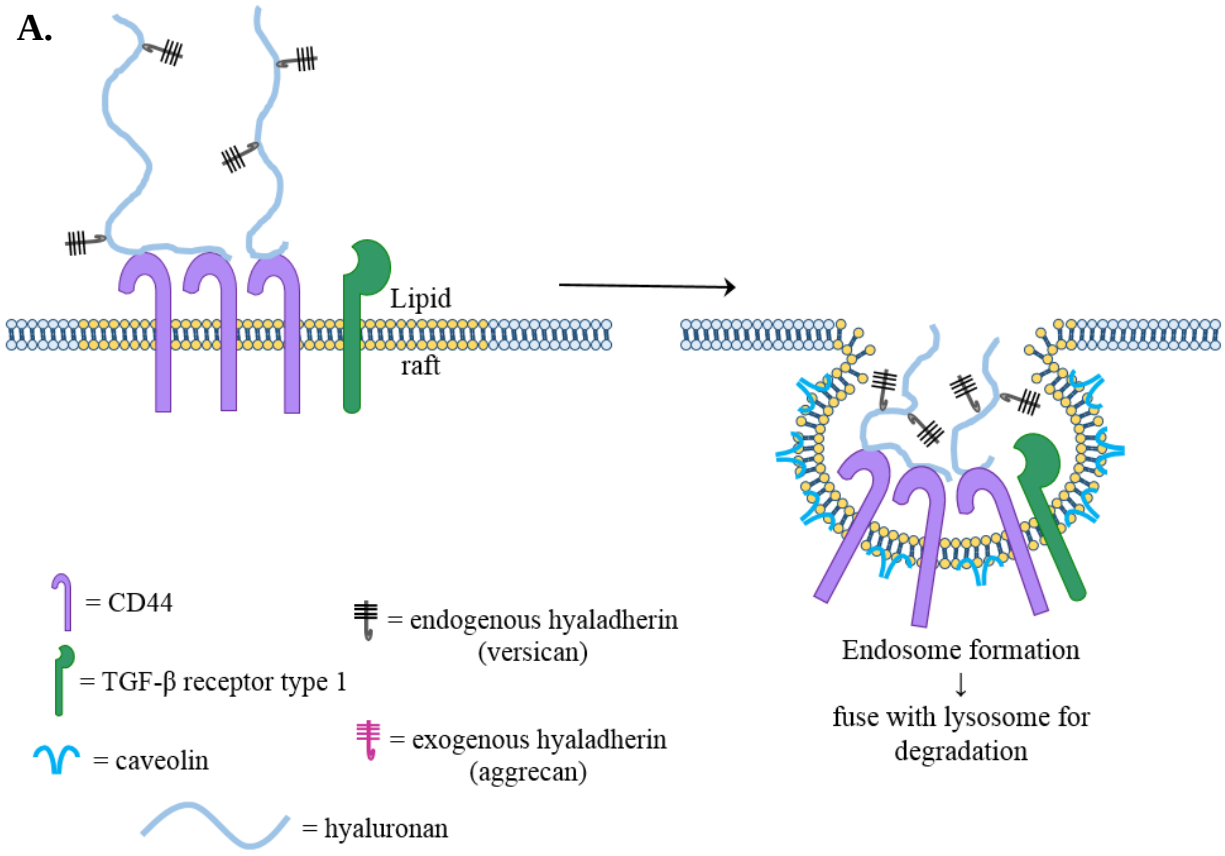
Lipid
raft
= CD44
= TGF-β receptor type 1
= caveolin
= hyaluronan
= endogenous hyaladherin
(versican)
= exogenous hyaladherin
(aggrecan)
Endosome formation
↓
fuse with lysosome for
degradation

B.

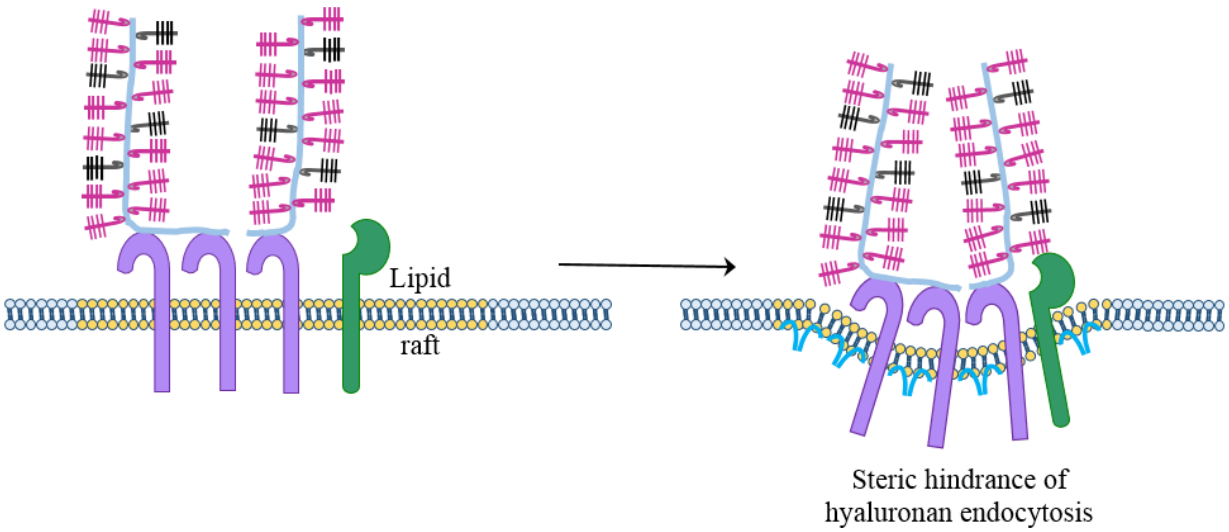
Lipid
raft
Steric hindrance of
hyaluronan endocytosis

Figure 40. Exogenous aggrecan inhibits CD44-mediated endocytosis required for adipogenesis. CD44 bound to hyaluronan lightly decorated with native versican clusters in lipid rafts. Caveolin protein binds to the lipid raft containing the cluster of CD44 and invaginates the membrane [161]. The lightly decorated hyaluronan is able to be surrounded by the invaginating membrane to form an endosomal vesicle that can be transported to a lysosome for degradation of the cargo (A). The addition of exogenous aggrecan fully decorates hyaluronan chains. These highly decorated hyaluronan chains prevent lipid raft clusters of CD44 from undergoing endocytosis likely due to steric hindrance based on the significant increase in volume of the additional aggrecan bound to hyaluronan. Without endocytosis of CD44 for both receptor degradation and reduction of the pericellular matrix, adipogenesis is inhibited.

REFERENCES

1. Hunziker, E.B., Michel, M., and Studer, D. (1997) *Ultrastructure of adult human articular cartilage matrix after cryotechnical processing.* Microsc Res Tech. **37**:271-284.
2. Pearle, A.D., Warren, R.F., and Rodeo, S.A. (2005) *Basic science of articular cartilage and osteoarthritis.* Clin Sports Med. **24**:1-12.
3. Mow, V.C., Kuei, S.C., Lai, W.M., and Armstrong, C.G. (1980) *Biphasic creep and stress relaxation of articular cartilage in compression? Theory and experiments.* J Biomech Eng. **102**:73-84.
4. Fernandes, R.J., Weis, M., Scott, M.A., Seegmiller, R.E., and Eyre, D.R. (2007) *Collagen XI chain misassembly in cartilage of the chondrodysplasia (cho) mouse.* Matrix Biol. **26**:597-603.
5. Hohenester, E. (2014) *Signalling complexes at the cell-matrix interface.* Curr Opin Struct Biol. **29**:10-16.
6. Bhosale, A.M. and Richardson, J.B. (2008) *Articular cartilage: structure, injuries and review of management.* Br Med Bull. **87**:77-95.
7. Aigner, T. and Stove, J. (2003) *Collagens--major component of the physiological cartilage matrix, major target of cartilage degeneration, major tool in cartilage repair.* Adv Drug Deliv Rev. **55**:1569-1593.
8. Jiang, Y., Hu, C., Yu, S., Yan, J., Peng, H., Ouyang, H.W., and Tuan, R.S. (2015) *Cartilage stem/progenitor cells are activated in osteoarthritis via interleukin-1beta/nerve growth factor signaling.* Arthritis Res Ther. **17**:327.
9. Becerra, J., Andrades, J.A., Guerado, E., Zamora-Navas, P., Lopez-Puertas, J.M., and Reddi, A.H. (2010) *Articular cartilage: structure and regeneration.* Tissue Eng Part B Rev. **16**:617-627.
10. Iwamoto, M., Ohta, Y., Larmour, C., and Enomoto-Iwamoto, M. (2013) *Toward regeneration of articular cartilage.* Birth Defects Res C Embryo Today. **99**:192-202.
11. Fujioka, R., Aoyama, T., and Takakuwa, T. (2013) *The layered structure of the articular surface.* Osteoarthritis Cartilage. **21**:1092-1098.
12. Buckwalter, J.A. and Mankin, H.J. (1998) *Articular cartilage: tissue design and chondrocyte-matrix interactions.* Instr Course Lect. **47**:477-486.

13. Poole, C.A. (1997) *Articular cartilage chondrons: form, function and failure.* J Anat. **191**:1-13.

14. Poole, C.A., Ayad, S., and Schofield, J.R. (1988) *Chondrons from articular cartilage: I. Immunolocalization of type VI collagen in the pericellular capsule of isolated canine tibial chondrons.* J Cell Sci. **90**:635-643.

15. Toole, B.P. (2004) *Hyaluronan: from extracellular glue to pericellular cue.* Nat Rev Cancer. **4**:528-539.

16. Knudson, C.B. (1993) *Hyaluronan receptor-directed assembly of chondrocyte pericellular matrix.* J Cell Biol. **120**:825-834.

17. Larson, C.M., Kelley, S.S., Blackwood, A.D., Banes, A.J., and Lee, G.M. (2002) *Retention of the native chondrocyte pericellular matrix results in significantly improved matrix production.* Matrix Biol. **21**:349-359.

18. Sandy, J.D. and Plaas, A.H. (1989) *Studies on the hyaluronate binding properties of newly synthesized proteoglycans purified from articular chondrocyte cultures.* Arch Biochem Biophys. **271**:300-314.

19. Poole, C.A., Matsuoka, A., and Schofield, J.R. (1991) *Chondrons from articular cartilage. III. Morphologic changes in the cellular microenvironment of chondrons isolated from osteoarthritic cartilage.* Arthritis Rheum. **34**:22-35.

20. Kuettner, K.E., Memoli, V.A., Pauli, B.U., Wrobel, N.C., Thonar, E.J., and Daniel, J.C. (1982) *Synthesis of cartilage matrix by mammalian chondrocytes in vitro. II. Maintenance of collagen and proteoglycan phenotype.* J Cell Biol. **93**:751-757.

21. Archer, C.W. and Francis-West, P. (2003) *The chondrocyte.* Int J Biochem Cell Biol. **35**:401-404.

22. Hardingham, T. and Bayliss, M. (1990) *Proteoglycans of articular cartilage: changes in aging and in joint disease.* Semin Arthritis Rheum. **20**:12-33.

23. Muinos-Lopez, E., Rendal-Vazquez, M.E., Hermida-Gomez, T., Fuentes-Boquete, I., Diaz-Prado, S., and Blanco, F.J. (2012) *Cryopreservation effect on proliferative and chondrogenic potential of human chondrocytes isolated from superficial and deep cartilage.* Open Orthop J. **6**:150-159.

24. Tallheden, T., Brittberg, M., Peterson, L., and Lindahl, A. (2006) *Human articular chondrocytes--plasticity and differentiation potential.* Cells Tissues Organs. **184**:55-67.

25. Dowthwaite, G.P., Bishop, J.C., Redman, S.N., Khan, I.M., Rooney, P., Evans, D.J., Haughton, L., Bayram, Z., Boyer, S., Thomson, B., Wolfe, M.S., and Archer, C.W. (2004) *The surface of articular cartilage contains a progenitor cell population.* J Cell Sci. **117**:889-897.

26. Hattori, S., Oxford, C., and Reddi, A.H. (2007) *Identification of superficial zone articular chondrocyte stem/progenitor cells.* Biochem Biophys Res Commun. **358**:99-103.

27. Grogan, S.P., Miyaki, S., Asahara, H., D'Lima, D.D., and Lotz, M.K. (2009) *Mesenchymal progenitor cell markers in human articular cartilage: normal distribution and changes in osteoarthritis.* Arthritis Res Ther. **11**:R85.

28. Pretzel, D., Linss, S., Rochler, S., Endres, M., Kaps, C., Alsalameh, S., and Kinne, R.W. (2011) *Relative percentage and zonal distribution of mesenchymal progenitor cells in human osteoarthritic and normal cartilage.* Arthritis Res Ther. **13**:R64.

29. Williams, R., Khan, I.M., Richardson, K., Nelson, L., McCarthy, H.E., Analbelsi, T., Singhrao, S.K., Dowthwaite, G.P., Jones, R.E., Baird, D.M., Lewis, H., Roberts, S., Shaw, H.M., Dudhia, J., Fairclough, J., Briggs, T., and Archer, C.W. (2014) *Identification and clonal characterisation of a progenitor cell sub-population in normal human articular cartilage.* PLoS One. **5**:e13246.

30. McCarthy, H.E., Bara, J.J., Brakspear, K., Singhrao, S.K., and Archer, C.W. (2012) *The comparison of equine articular cartilage progenitor cells and bone marrow-derived stromal cells as potential cell sources for cartilage repair in the horse.* Vet J. **192**:345-351.

31. Farr, J., Cole, B., Dhawan, A., Kercher, J., and Sherman, S. (2011) *Clinical cartilage restoration: evolution and overview.* Clin Orthop Relat Res. **469**:2696-2705.

32. Goldring, M.B. (2000) *Osteoarthritis and cartilage: the role of cytokines.* Curr Rheumatol Rep. **2**:459-465.

33. Naito, S., Shiomi, T., Okada, A., Kimura, T., Chijiiwa, M., Fujita, Y., Yatabe, T., Komiya, K., Enomoto, H., Fujikawa, K., and Okada, Y. (2007) *Expression of ADAMTS4 (aggrecanase-1) in human osteoarthritic cartilage.* Pathol Int. **57**:703-711.

34. Johansson, N., Ala-aho, R., Uitto, V., Grenman, R., Fusenig, N.E., Lopez-Otin, C., and Kahari, V.M. (2000) *Expression of collagenase-3 (MMP-13) and collagenase-1 (MMP-1) by transformed keratinocytes is dependent on the activity of p38 mitogen-activated protein kinase.* J Cell Sci. **113**:227-235.

35. Fosang, A.J. and Beier, F. (2011) *Emerging Frontiers in cartilage and chondrocyte biology.* Best Pract Res Clin Rheumatol. **25**:751-766.
36. Outerbridge, R.E. (1961) *The etiology of chondromalacia patellae.* J Bone Joint Surg Br. **43-B**:752-757.
37. Kellgren, J.H. and Lawrence, J.S. (1957) *Radiological assessment of osteo-arthrosis.* Ann Rheum Dis. **16**:494-502.
38. van der Kraan, P.M. and van den Berg, W.B. (2007) *Osteophytes: relevance and biology.* Osteoarthritis Cartilage. **15**:237-244.
39. Emrani, P.S., Katz, J.N., Kessler, C.L., Reichmann, W.M., Wright, E.A., McAlindon, T.E., and Losina, E. (2008) *Joint space narrowing and Kellgren-Lawrence progression in knee osteoarthritis: an analytic literature synthesis.* Osteoarthritis Cartilage. **16**:873-882.
40. Loeser, R.F. (2011) *Aging and osteoarthritis.* Curr Opin Rheumatol. **23**:492-496.
41. Loeser, R.F., Goldring, S.R., Scanzello, C.R., and Goldring, M.B. (2012) *Osteoarthritis: a disease of the joint as an organ.* Arthritis Rheum. **64**:1697-1707.
42. Felson, D.T., Lawrence, R.C., Dieppe, P.A., Hirsch, R., Helmick, C.G., Jordan, J.M., Kington, R.S., Lane, N.E., Nevitt, M.C., Zhang, Y., Sowers, M., McAlindon, T., Spector, T.D., Poole, A.R., Yanovski, S.Z., Ateshian, G., Sharma, L., Buckwalter, J.A., Brandt, K.D., and Fries, J.F. (2000) *Osteoarthritis: new insights. Part 1: the disease and its risk factors.* Ann Intern Med. **133**:635-646.
43. Bitton, R. (2009) *The economic burden of osteoarthritis.* Am J Manag Care. **15**:S230-235.
44. Wang, S.X., Ganguli, A.X., Macaulay, D., Reichmann, W., Medema, J.K., and Cifaldi, M.A. (2014) *The economic burden of osteoarthritis in americans: analysis from a privately insured population.* Osteoarthritis Cartilage. **22**:S210.
45. Dibonaventura, M., Gupta, S., McDonald, M., and Sadosky, A. (2011) *Evaluating the health and economic impact of osteoarthritis pain in the workforce: results from the National Health and Wellness Survey.* BMC Musculoskelet Disord. **12**:83.
46. Rutjes, A.W., Juni, P., da Costa, B.R., Trelle, S., Nuesch, E., and Reichenbach, S. (2012) *Viscosupplementation for osteoarthritis of the knee: a systematic review and meta-analysis.* Ann Intern Med. **157**:180-191.
47. Hochberg, M.C., Altman, R.D., April, K.T., Benkhalti, M., Guyatt, G., McGowan, J., Towheed, T., Welch, V., Wells, G., and Tugwell, P. (2012) *American College of*

Rheumatology 2012 recommendations for the use of nonpharmacologic and pharmacologic therapies in osteoarthritis of the hand, hip, and knee. Arthritis Care Res (Hoboken). **64**:465-474.

48. Grillet, B. and Dequeker, J. (1990) *Intra-articular steroid injection. A risk-benefit assessment.* Drug Saf. **5**:205-211.
49. Steadman, J.R., Rodkey, W.G., and Briggs, K.K. (2010) *Microfracture: Its History and Experience of the Developing Surgeon.* Cartilage. **1**:78-86.
50. Schurman, D.J. and Smith, R.L. (2004) *Osteoarthritis: current treatment and future prospects for surgical, medical, and biologic intervention.* Clin Orthop Relat Res. S183-189.
51. Hangody, L. and Fules, P. (2003) *Autologous osteochondral mosaicplasty for the treatment of full-thickness defects of weight-bearing joints: ten years of experimental and clinical experience.* J Bone Joint Surg Am. **85-A Suppl 2**:25-32.
52. Chahal, J., Gross, A.E., Gross, C., Mall, N., Dwyer, T., Chahal, A., Whelan, D.B., and Cole, B.J. (2013) *Outcomes of osteochondral allograft transplantation in the knee.* Arthroscopy. **29**:575-588.
53. Brittberg, M., Lindahl, A., Nilsson, A., Ohlsson, C., Isaksson, O., and Peterson, L. (1994) *Treatment of deep cartilage defects in the knee with autologous chondrocyte transplantation.* N Engl J Med. **331**:889-895.
54. Peterson, L., Minas, T., Brittberg, M., Nilsson, A., Sjogren-Jansson, E., and Lindahl, A. (2000) *Two- to 9-year outcome after autologous chondrocyte transplantation of the knee.* Clin Orthop Relat Res. **374**:212-234.
55. Marlovits, S., Zeller, P., Singer, P., Resinger, C., and Vecsei, V. (2006) *Cartilage repair: generations of autologous chondrocyte transplantation.* Eur J Radiol. **57**:24-31.
56. Kielpinski, G., Prinzi, S., Duguid, J., and du Moulin, G. (2005) *Roadmap to approval: use of an automated sterility test method as a lot release test for Carticel, autologous cultured chondrocytes.* Cytotherapy. **7**:531-541.
57. Caplan, A.I. (1991) *Mesenchymal stem cells.* J Orthop Res. **9**:641-650.
58. Ude, C.C., Sulaiman, S.B., Min-Hwei, N., Hui-Cheng, C., Ahmad, J., Yahaya, N.M., Saim, A.B., and Idrus, R.B. (2014) *Cartilage regeneration by chondrogenic induced adult stem cells in osteoarthritic sheep model.* PLoS One. **9**:e98770.

59. Seale, P., Bjork, B., Yang, W., Kajimura, S., Chin, S., Kuang, S., Scime, A., Devarakonda, S., Conroe, H.M., Erdjument-Bromage, H., Tempst, P., Rudnicki, M.A., Beier, D.R., and Spiegelman, B.M. (2008) *PRDM16 controls a brown fat/skeletal muscle switch.* Nature. **454**:961-967.

60. Saely, C.H., Geiger, K., and Drexel, H. (2012) *Brown versus white adipose tissue: a mini-review.* Gerontology. **58**:15-23.

61. Moro, C., Pillard, F., De Glisezinski, I., Harant, I., Riviere, D., Stich, V., Lafontan, M., Crampes, F., and Berlan, M. (2005) *Training enhances ANP lipid-mobilizing action in adipose tissue of overweight men.* Med Sci Sports Exerc. **37**:1126-1132.

62. Vitali, A., Murano, I., Zingaretti, M.C., Frontini, A., Ricquier, D., and Cinti, S. (2012) *The adipose organ of obesity-prone C57BL/6J mice is composed of mixed white and brown adipocytes.* J Lipid Res. **53**:619-629.

63. Jeanson, Y., Carriere, A., and Casteilla, L. (2015) *A new role for browning as a redox and stress adaptive mechanism?* Front Endocrinol (Lausanne). **6**:158.

64. Timmons, J.A., Wennmalm, K., Larsson, O., Walden, T.B., Lassmann, T., Petrovic, N., Hamilton, D.L., Gimeno, R.E., Wahlestedt, C., Baar, K., Nedergaard, J., and Cannon, B. (2007) *Myogenic gene expression signature establishes that brown and white adipocytes originate from distinct cell lineages.* Proc Natl Acad Sci U S A. **104**:4401-4406.

65. Cannon, B. and Nedergaard, J. (2004) *Brown adipose tissue: function and physiological significance.* Physiol Rev. **84**:277-359.

66. Wu, J., Bostrom, P., Sparks, L.M., Ye, L., Choi, J.H., Giang, A.H., Khandekar, M., Virtanen, K.A., Nuutila, P., Schaart, G., Huang, K., Tu, H., van Marken Lichtenbelt, W.D., Hoeks, J., Enerback, S., Schrauwen, P., and Spiegelman, B.M. (2012) *Beige adipocytes are a distinct type of thermogenic fat cell in mouse and human.* Cell. **150**:366-376.

67. Geloen, A., Roy, P.E., and Bukowiecki, L.J. (1989) *Regression of white adipose tissue in diabetic rats.* Am J Physiol. **257**:E547-553.

68. Ruiz-Ojeda, F.J., Ruperez, A.I., Gomez-Llorente, C., Gil, A., and Aguilera, C.M. (2016) *Cell models and their application for studying adipogenic differentiation in relation to obesity: a review.* Int J Mol Sci. **17**:1040.

69. Bortell, R., Owen, T.A., Ignotz, R., Stein, G.S., and Stein, J.L. (1994) *TGF beta 1 prevents the down-regulation of type I procollagen, fibronectin, and TGF beta 1 gene expression associated with 3T3-L1 pre-adipocyte differentiation.* J Cell Biochem. **54**:256-263.

70. Janssen, O.E. and Hilz, H. (1989) *Differentiation of 3T3-L1 pre-adipocytes induced by inhibitors of poly(ADP-ribose) polymerase and by related noninhibitory acids.* Eur J Biochem. **180**:595-602.

71. Green, H. and Meuth, M. (1974) *An established pre-adipose cell line and its differentiation in culture.* Cell. **3**:127-133.

72. Aoki, T. and Todaro, G.J. (1973) *Antigenic properties of endogenous type-C viruses from spontaneously transformed clones of BALB-3T3.* Proc Natl Acad Sci U S A. **70**:1598-1602.

73. Cortesi, E. and Dolara, P. (1983) *Neoplastic transformation of BALB 3T3 mouse embryo fibroblasts by the beef extract mutagen 2-amino-3-methylimidazo [4,5-d] quinoline.* Cancer Lett. **20**:43-47.

74. Rubin, H. (1981) *Growth regulation, reverse transformation, and adaptability of 3T3 cells in decreased Mg2+ concentration.* Proc Natl Acad Sci U S A. **78**:328-332.

75. Rubin, H. (1990) *On the nature of enduring modifications induced in cells and organisms.* Am J Physiol. **258**:L19-24.

76. Rosen, E.D., Walkey, C.J., Puigserver, P., and Spiegelman, B.M. (2000) *Transcriptional regulation of adipogenesis.* Genes Dev. **14**:1293-1307.

77. Green, H. and Kehinde, O. (1979) *Formation of normally differentiated subcutaneous fat pads by an established preadipose cell line.* J Cell Physiol. **101**:169-171.

78. Novikoff, A.B., Novikoff, P.M., Rosen, O.M., and Rubin, C.S. (1980) *Organelle relationships in cultured 3T3-L1 preadipocytes.* J Cell Biol. **87**:180-196.

79. Farmer, S.R. (2006) *Transcriptional control of adipocyte formation.* Cell Metab. **4**:263-273.

80. Cornelius, P., Enerback, S., Bjursell, G., Olivecrona, T., and Pekala, P.H. (1988) *Regulation of lipoprotein lipase mRNA content in 3T3-L1 cells by tumour necrosis factor.* Biochem J. **249**:765-769.

81. Dani, C., Amri, E.Z., Bertrand, B., Enerback, S., Bjursell, G., Grimaldi, P., and Ailhaud, G. (1990) *Expression and regulation of pOb24 and lipoprotein lipase genes during adipose conversion.* J Cell Biochem. **43**:103-110.

82. Student, A.K., Hsu, R.Y., and Lane, M.D. (1980) *Induction of fatty acid synthetase synthesis in differentiating 3T3-L1 preadipocytes.* J Biol Chem. **255**:4745-4750.

83. Summers, S.A., Yin, V.P., Whiteman, E.L., Garza, L.A., Cho, H., Tuttle, R.L., and Birnbaum, M.J. (1999) *Signaling pathways mediating insulin-stimulated glucose transport.* Ann N Y Acad Sci. **892**:169-186.

84. Bernlohr, D.A., Bolanowski, M.A., Kelly, T.J., Jr., and Lane, M.D. (1985) *Evidence for an increase in transcription of specific mRNAs during differentiation of 3T3-L1 preadipocytes.* J Biol Chem. **260**:5563-5567.

85. Cornelius, P., MacDougald, O.A., and Lane, M.D. (1994) *Regulation of adipocyte development.* Annu Rev Nutr. **14**:99-129.

86. Tanaka, T., Yoshida, N., Kishimoto, T., and Akira, S. (1997) *Defective adipocyte differentiation in mice lacking the C/EBPbeta and/or C/EBPdelta gene.* EMBO J. **16**:7432-7443.

87. Shan, T., Liu, W., and Kuang, S. (2013) *Fatty acid binding protein 4 expression marks a population of adipocyte progenitors in white and brown adipose tissues.* FASEB J. **27**:277-287.

88. Rosen, E.D., Hsu, C.H., Wang, X., Sakai, S., Freeman, M.W., Gonzalez, F.J., and Spiegelman, B.M. (2002) *C/EBPalpha induces adipogenesis through PPARgamma: a unified pathway.* Genes Dev. **16**:22-26.

89. Choy, L., Skillington, J., and Derynck, R. (2000) *Roles of autocrine TGF-beta receptor and Smad signaling in adipocyte differentiation.* J Cell Biol. **149**:667-682.

90. Choy, L. and Derynck, R. (2003) *Transforming growth factor-beta inhibits adipocyte differentiation by Smad3 interacting with CCAAT/enhancer-binding protein (C/EBP) and repressing C/EBP transactivation function.* J Biol Chem. **278**:9609-9619.

91. Hoshiba, T., Kawazoe, N., and Chen, G. (2012) *The balance of osteogenic and adipogenic differentiation in human mesenchymal stem cells by matrices that mimic stepwise tissue development.* Biomaterials. **33**:2025-2031.

92. Chavey, C., Mari, B., Monthouel, M.N., Bonnafous, S., Anglard, P., Van Obberghen, E., and Tartare-Deckert, S. (2003) *Matrix metalloproteinases are differentially expressed in adipose tissue during obesity and modulate adipocyte differentiation.* J Biol Chem. **278**:11888-11896.

93. Nagase, H. and Woessner, J.F., Jr. (1999) *Matrix metalloproteinases.* J Biol Chem. **274**:21491-21494.

94. Mott, J.D. and Werb, Z. (2004) *Regulation of matrix biology by matrix metalloproteinases.* Curr Opin Cell Biol. **16**:558-564.

95. Page-McCaw, A., Ewald, A.J., and Werb, Z. (2007) *Matrix metalloproteinases and the regulation of tissue remodelling.* Nat Rev Mol Cell Biol. **8**:221-233.

96. Shih, C.L. and Ajuwon, K.M. (2015) *Inhibition of MMP-13 prevents diet-induced obesity in mice and suppresses adipogenesis in 3T3-L1 preadipocytes.* Mol Biol Rep. **42**:1225-1232.

97. Bernot, D., Barruet, E., Poggi, M., Bonardo, B., Alessi, M.C., and Peiretti, F. (2010) *Down-regulation of tissue inhibitor of metalloproteinase-3 (TIMP-3) expression is necessary for adipocyte differentiation.* J Biol Chem. **285**:6508-6514.

98. Birzele, F., Fassler, S., Neubauer, H., Hildebrandt, T., and Hamilton, B.S. (2012) *Analysis of the transcriptome of differentiating and non-differentiating preadipocytes from rats and humans by next generation sequencing.* Mol Cell Biochem. **369**:175-181.

99. Han, J., Luo, T., Gu, Y., Li, G., Jia, W., and Luo, M. (2009) *Cathepsin K regulates adipocyte differentiation: possible involvement of type I collagen degradation.* Endocr J. **56**:55-63.

100. Ghatak, S., Misra, S., and Toole, B.P. (2002) *Hyaluronan oligosaccharides inhibit anchorage-independent growth of tumor cells by suppressing the phosphoinositide 3-kinase/Akt cell survival pathway.* J Biol Chem. **277**:38013-38020.

101. Ohno, S., Im, H.J., Knudson, C.B., and Knudson, W. (2005) *Hyaluronan oligosaccharide-induced activation of transcription factors in bovine articular chondrocytes.* Arthritis Rheum. **52**:800-809.

102. Tsukita, S., Oishi, K., Sato, N., Sagara, J., Kawai, A., and Tsukita, S. (1994) *ERM family members as molecular linkers between the cell surface glycoprotein CD44 and actin-based cytoskeletons.* J Cell Biol. **126**:391-401.

103. Lokeshwar, V.B., Fregien, N., and Bourguignon, L.Y. (1994) *Ankyrin-binding domain of CD44(GP85) is required for the expression of hyaluronic acid-mediated adhesion function.* J Cell Biol. **126**:1099-1109.

104. Mellor, L., Knudson, C.B., Hida, D., Askew, E.B., and Knudson, W. (2013) *Intracellular domain fragment of CD44 alters CD44 function in chondrocytes.* J Biol Chem. **288**:25838-25850.

105. Titushkin, I., Sun, S., Paul, A., and Cho, M. (2013) *Control of adipogenesis by ezrin, radixin and moesin-dependent biomechanics remodeling.* J Biomech. **46**:521-526.

106. Arisawa, K., Ichi, I., Yasukawa, Y., Sone, Y., and Fujiwara, Y. (2013) *Changes in the phospholipid fatty acid composition of the lipid droplet during the differentiation of 3T3-L1 adipocytes.* J Biochem. **154**:281-289.

107. Shoham, N., Girshovitz, P., Katzengold, R., Shaked, N.T., Benayahu, D., and Gefen, A. (2014) *Adipocyte stiffness increases with accumulation of lipid droplets.* Biophys J. **106**:1421-1431.

108. Spiegelman, B.M. and Farmer, S.R. (1982) *Decreases in tubulin and actin gene expression prior to morphological differentiation of 3T3 adipocytes.* Cell. **29**:53-60.

109. Smas, C.M. and Sul, H.S. (1995) *Control of adipocyte differentiation.* Biochem J. **309**:697-710.

110. Meyer, K. and Palmer, J.W. (1934) *The polysaccharide of the vitreous humor.* J Biol Chem. **107**:629-634.

111. Meyer, K. (1958) *Chemical structure of hyaluronic acid.* Fed Proc. **17**:1075-1077.

112. Balazs, E.A., Laurent, T.C., and Jeanloz, R.W. (1986) *Nomenclature of hyaluronic acid.* Biochem J. **235**:903.

113. Almond, A. (2007) *Hyaluronan.* Cell Mol Life Sci. **64**:1591-1596.

114. Hascall, V.C., Majors, A.K., De La Motte, C.A., Evanko, S.P., Wang, A., Drazba, J.A., Strong, S.A., and Wight, T.N. (2004) *Intracellular hyaluronan: a new frontier for inflammation?* Biochim Biophys Acta. **1673**:3-12.

115. Toole, B.P., Wight, T.N., and Tammi, M.I. (2002) *Hyaluronan-cell interactions in cancer and vascular disease.* J Biol Chem. **277**:4593-4596.

116. Chen, W.Y. and Abatangelo, G. (1999) *Functions of hyaluronan in wound repair.* Wound Repair Regen. **7**:79-89.

117. Prehm, P. (1984) *Hyaluronate is synthesized at plasma membranes.* Biochem J. **220**:597-600.

118. Coutinho, P.M., Deleury, E., Davies, G.J., and Henrissat, B. (2003) *An evolving hierarchical family classification for glycosyltransferases.* J Mol Biol. **328**:307-317.

119. Lee, J.Y. and Spicer, A.P. (2000) *Hyaluronan: a multifunctional, megaDalton, stealth molecule.* Curr Opin Cell Biol. **12**:581-586.

120. Weigel, P.H., Hascall, V.C., and Tammi, M. (1997) *Hyaluronan synthases.* J Biol Chem. **272**:13997-14000.

121. Prehm, P. (1989) *Identification and regulation of the eukaryotic hyaluronate synthase.* Ciba Found Symp. **143**:21-30; discussion 30-40, 281-285.

122. Weigel, P.H. (2015) *Hyaluronan synthase: the mechanism of initiation at the reducing end and a pendulum model for polysaccharide translocation to the cell exterior.* Int J Cell Biol. **2015**:367579.

123. Jiang, D., Liang, J., and Noble, P.W. (2007) *Hyaluronan in tissue injury and repair.* Annu Rev Cell Dev Biol. **23**:435-461.

124. Itano, N., Sawai, T., Yoshida, M., Lenas, P., Yamada, Y., Imagawa, M., Shinomura, T., Hamaguchi, M., Yoshida, Y., Ohnuki, Y., Miyauchi, S., Spicer, A.P., McDonald, J.A., and Kimata, K. (1999) *Three isoforms of mammalian hyaluronan synthases have distinct enzymatic properties.* J Biol Chem. **274**:25085-25092.

125. Stern, R. (2008) *Hyaluronidases in cancer biology.* Semin Cancer Biol. **18**:275-280.

126. Greenwald, R.A. and Moy, W.W. (1980) *Effect of oxygen-derived free radicals on hyaluronic acid.* Arthritis Rheum. **23**:455-463.

127. Horton, M.R., Shapiro, S., Bao, C., Lowenstein, C.J., and Noble, P.W. (1999) *Induction and regulation of macrophage metalloelastase by hyaluronan fragments in mouse macrophages.* J Immunol. **162**:4171-4176.

128. Ohno, S., Im, H.J., Knudson, C.B., and Knudson, W. (2006) *Hyaluronan oligosaccharides induce matrix metalloproteinase 13 via transcriptional activation of NFkappaB and p38 MAP kinase in articular chondrocytes.* J Biol Chem. **281**:17952-17960.

129. West, D.C. and Kumar, S. (1989) *Hyaluronan and angiogenesis.* Ciba Found Symp. **143**:187-201; discussion 201-187, 281-185.

130. Noble, P.W., McKee, C.M., Cowman, M., and Shin, H.S. (1996) *Hyaluronan fragments activate an NF-kappa B/I-kappa B alpha autoregulatory loop in murine macrophages.* J Exp Med. **183**:2373-2378.

131. Turino, G.M. and Cantor, J.O. (2003) *Hyaluronan in respiratory injury and repair.* Am J Respir Crit Care Med. **167**:1169-1175.

132. Toole, B.P. (2001) *Hyaluronan in morphogenesis.* Semin Cell Dev Biol. **12**:79-87.

133. Huang, L., Cheng, Y.Y., Koo, P.L., Lee, K.M., Qin, L., Cheng, J.C., and Kumta, S.M. (2003) *The effect of hyaluronan on osteoblast proliferation and differentiation in rat calvarial-derived cell cultures.* J Biomed Mater Res A. **66**:880-884.

134. Evanko, S.P., Angello, J.C., and Wight, T.N. (1999) *Formation of hyaluronan- and versican-rich pericellular matrix is required for proliferation and migration of vascular smooth muscle cells.* Arterioscler Thromb Vasc Biol. **19**:1004-1013.

135. Camenisch, T.D., Spicer, A.P., Brehm-Gibson, T., Biesterfeldt, J., Augustine, M.L., Calabro, A., Jr., Kubalak, S., Klewer, S.E., and McDonald, J.A. (2000) *Disruption of hyaluronan synthase-2 abrogates normal cardiac morphogenesis and hyaluronan-mediated transformation of epithelium to mesenchyme.* J Clin Invest. **106**:349-360.

136. Kakizaki, I., Kojima, K., Takagaki, K., Endo, M., Kannagi, R., Ito, M., Maruo, Y., Sato, H., Yasuda, T., Mita, S., Kimata, K., and Itano, N. (2004) *A novel mechanism for the inhibition of hyaluronan biosynthesis by 4-methylumbelliferone.* J Biol Chem. **279**:33281-33289.

137. Csoka, A.B., Frost, G.I., and Stern, R. (2001) *The six hyaluronidase-like genes in the human and mouse genomes.* Matrix Biol. **20**:499-508.

138. Chow, G. and Knudson, W. (2005) *Characterization of promoter elements of the human HYAL-2 gene.* J Biol Chem. **280**:26904-26912.

139. Rai, S.K., Duh, F.M., Vigdorovich, V., Danilkovitch-Miagkova, A., Lerman, M.I., and Miller, A.D. (2001) *Candidate tumor suppressor HYAL2 is a glycosylphosphatidylinositol (GPI)-anchored cell-surface receptor for jaagsiekte sheep retrovirus, the envelope protein of which mediates oncogenic transformation.* Proc Natl Acad Sci U S A. **98**:4443-4448.

140. Duterme, C., Mertens-Strijthagen, J., Tammi, M., and Flamion, B. (2009) *Two novel functions of hyaluronidase-2 (Hyal2) are formation of the glycocalyx and control of CD44-ERM interactions.* J Biol Chem. **284**:33495-33508.

141. Hida, D., Danielson, B.T., Knudson, C.B., and Knudson, W. (2015) *CD44 knock-down in bovine and human chondrocytes results in release of bound HYAL2.* Matrix Biol. **48**:42-54.

142. Embry Flory, J.J., Fosang, A.J., and Knudson, W. (2006) *The accumulation of intracellular ITEGE and DIPEN neoepitopes in bovine articular chondrocytes is mediated by CD44 internalization of hyaluronan.* Arthritis Rheum. **54**:443-454.

143. Knudson, W., Chow, G., and Knudson, C.B. (2002) *CD44-mediated uptake and degradation of hyaluronan.* Matrix Biol. **21**:15-23.

144. Harada, H. and Takahashi, M. (2007) *CD44-dependent intracellular and extracellular catabolism of hyaluronic acid by hyaluronidase-1 and -2.* J Biol Chem. **282**:5597-5607.

145. Harrisson, F., van Hoof, J., and Vanroelen, C. (1986) *On the presence of proteolytic activity in glycosaminoglycan-degrading enzyme preparations.* J Histochem Cytochem. **34**:1231-1235.

146. Liu, L.F., Kodama, K., Wei, K., Tolentino, L.L., Choi, O., Engleman, E.G., Butte, A.J., and McLaughlin, T. (2015) *The receptor CD44 is associated with systemic insulin resistance and proinflammatory macrophages in human adipose tissue.* Diabetologia. **58**:1579-1586.

147. Knudson, W., Aguiar, D.J., Hua, Q., and Knudson, C.B. (1996) *CD44-anchored hyaluronan-rich pericellular matrices: an ultrastructural and biochemical analysis.* Exp Cell Res. **228**:216-228.

148. Okamoto, I., Kawano, Y., Murakami, D., Sasayama, T., Araki, N., Miki, T., Wong, A.J., and Saya, H. (2001) *Proteolytic release of CD44 intracellular domain and its role in the CD44 signaling pathway.* J Cell Biol. **155**:755-762.

149. Gunthert, U., Hofmann, M., Rudy, W., Reber, S., Zoller, M., Haussmann, I., Matzku, S., Wenzel, A., Ponta, H., and Herrlich, P. (1991) *A new variant of glycoprotein CD44 confers metastatic potential to rat carcinoma cells.* Cell. **65**:13-24.

150. Hua, Q., Knudson, C.B., and Knudson, W. (1993) *Internalization of hyaluronan by chondrocytes occurs via receptor-mediated endocytosis.* J Cell Sci. **106**:365-375.

151. Bourguignon, L.Y., Lokeshwar, V.B., Chen, X., and Kerrick, W.G. (1993) *Hyaluronic acid-induced lymphocyte signal transduction and HA receptor (GP85/CD44)-cytoskeleton interaction.* J Immunol. **151**:6634-6644.

152. Peterson, R.S., Andhare, R.A., Rousche, K.T., Knudson, W., Wang, W., Grossfield, J.B., Thomas, R.O., Hollingsworth, R.E., and Knudson, C.B. (2004) *CD44 modulates Smad1 activation in the BMP-7 signaling pathway.* J Cell Biol. **166**:1081-1091.

153. Knudson, C.B. and Toole, B.P. (1985) *Changes in the pericellular matrix during differentiation of limb bud mesoderm.* Dev Biol. **112**:308-318.

154. Clarris, B.J. and Fraser, J.R. (1968) *On the pericellular zone of some mammalian cells in vitro.* Exp Cell Res. **49**:181-193.

155. Laurent, T.C. and Fraser, J.R. (1992) *Hyaluronan.* FASEB J. **6**:2397-2404.

156. Thankamony, S.P. and Knudson, W. (2006) *Acylation of CD44 and its association with lipid rafts are required for receptor and hyaluronan endocytosis.* J Biol Chem. **281**:34601-34609.

157. Greyner, H.J., Wiraszka, T., Zhang, L.S., Petroll, W.M., and Mummert, M.E. (2010) *Inducible macropinocytosis of hyaluronan in B16-F10 melanoma cells.* Matrix Biol. **29**:503-510.

158. Collis, L., Hall, C., Lange, L., Ziebell, M., Prestwich, R., and Turley, E.A. (1998) *Rapid hyaluronan uptake is associated with enhanced motility: implications for an intracellular mode of action.* FEBS Lett. **440**:444-449.

159. Tammi, R., Rilla, K., Pienimaki, J.P., MacCallum, D.K., Hogg, M., Luukkonen, M., Hascall, V.C., and Tammi, M. (2001) *Hyaluronan enters keratinocytes by a novel endocytic route for catabolism.* J Biol Chem. **276**:35111-35122.

160. Ito, T., Williams, J.D., Fraser, D.J., and Phillips, A.O. (2004) *Hyaluronan regulates transforming growth factor-beta1 receptor compartmentalization.* J Biol Chem. **279**:25326-25332.

161. Fra, A.M., Williamson, E., Simons, K., and Parton, R.G. (1995) *De novo formation of caveolae in lymphocytes by expression of VIP21-caveolin.* Proc Natl Acad Sci U S A. **92**:8655-8659.

162. Le Lay, S., Hajduch, E., Lindsay, M.R., Le Liepvre, X., Thiele, C., Ferre, P., Parton, R.G., Kurzchalia, T., Simons, K., and Dugail, I. (2006) *Cholesterol-induced caveolin targeting to lipid droplets in adipocytes: a role for caveolar endocytosis.* Traffic. **7**:549-561.

163. Damm, E.M., Pelkmans, L., Kartenbeck, J., Mezzacasa, A., Kurzchalia, T., and Helenius, A. (2005) *Clathrin- and caveolin-1-independent endocytosis: entry of simian virus 40 into cells devoid of caveolae.* J Cell Biol. **168**:477-488.

164. Choi, S.I., Maeng, Y.S., Kim, T.I., Lee, Y., Kim, Y.S., and Kim, E.K. (2015) *Lysosomal trafficking of TGFBIp via caveolae-mediated endocytosis.* PLoS One. **10**:e0119561.

165. Knudson, C.B. and Knudson, W. (1993) *Hyaluronan-binding proteins in development, tissue homeostasis, and disease.* FASEB J. **7**:1233-1241.

166. Yang, B., Yang, B.L., Savani, R.C., and Turley, E.A. (1994) *Identification of a common hyaluronan binding motif in the hyaluronan binding proteins RHAMM, CD44 and link protein.* EMBO J. **13**:286-296.

167. Kohda, D., Morton, C.J., Parkar, A.A., Hatanaka, H., Inagaki, F.M., Campbell, I.D., and Day, A.J. (1996) *Solution structure of the link module: a hyaluronan-binding domain involved in extracellular matrix stability and cell migration.* Cell. **86**:767-775.

168. Day, A.J. and Prestwich, G.D. (2002) *Hyaluronan-binding proteins: tying up the giant.* J Biol Chem. **277**:4585-4588.

169. Stern, R., Asari, A.A., and Sugahara, K.N. (2006) *Hyaluronan fragments: an information-rich system.* Eur J Cell Biol. **85**:699-715.

170. Turley, E.A., Noble, P.W., and Bourguignon, L.Y. (2002) *Signaling properties of hyaluronan receptors.* J Biol Chem. **277**:4589-4592.

171. Hardingham, T.E., Fosang, A.J., and Dudhia, J., *Aggrecan, the chondroitin sulfate/keratan sulfate proteoglycan from cartilage.*, in *Articular Cartilage and Osteoarthritis*, K.E. Kuettner, et al., Editors. 1992, Raven Press: New York. p. 5-20.

172. Hardingham, T.E. and Muir, H. (1972) *The specific interaction of hyaluronic acid with cartillage proteoglycans.* Biochim Biophys Acta. **279**:401-405.

173. Hascall, V.C. and Heinegard, D. (1974) *Aggregation of cartilage proteoglycans. II. Oligosaccharide competitors of the proteoglycan-hyaluronic acid interaction.* J Biol Chem. **249**:4242-4249.

174. LeBaron, R.G., Zimmermann, D.R., and Ruoslahti, E. (1992) *Hyaluronate binding properties of versican.* J Biol Chem. **267**:10003-10010.

175. Koob, T.J. and Vogel, K.G. (1987) *Site-related variations in glycosaminoglycan content and swelling properties of bovine flexor tendon.* J Orthop Res. **5**:414-424.

176. Heldin, P., Suzuki, M., Teder, P., and Pertoft, H. (1995) *Chondroitin sulfate proteoglycan modulates the permeability of hyaluronan-containing coats around normal human mesothelial cells.* J Cell Physiol. **165**:54-61.

177. Danielson, B.T., Knudson, C.B., and Knudson, W. (2015) *Extracellular processing of the cartilage proteoglycan aggregate and its effect on CD44-mediated internalization of hyaluronan.* J Biol Chem. **290**:9555-9570.

178. Bitter, T. and Muir, H.M. (1962) *A modified uronic acid carbazole reaction.* Anal Biochem. **4**:330-334.

179. Knudson, C.B. and Toole, B.P. (1985) *Fluorescent morphological probe for hyaluronate.* J Cell Biol. **100**:1753-1758.

180. Li, X.Q., Thonar, E.J., and Knudson, W. (1989) *Accumulation of hyaluronate in human lung carcinoma as measured by a new hyaluronate ELISA.* Connect Tissue Res. **19**:243-253.

181. Melrose, J., Tammi, M., and Smith, S. (2002) *Visualisation of hyaluronan and hyaluronan-binding proteins within ovine vertebral cartilages using biotinylated aggrecan G1-link complex and biotinylated hyaluronan oligosaccharides.* Histochem Cell Biol. **117**:327-333.

182. Calvo, J.C., Rodbard, D., Katki, A., Chernick, S., and Yanagishita, M. (1991) *Differentiation of 3T3-L1 preadipocytes with 3-isobutyl-1-methylxanthine and dexamethasone stimulates cell-associated and soluble chondroitin 4-sulfate proteoglycans.* J Biol Chem. **266**:11237-11244.

183. Zizola, C.F., Julianelli, V., Bertolesi, G., Yanagishita, M., and Calvo, J.C. (2007) *Role of versican and hyaluronan in the differentiation of 3T3-L1 cells into preadipocytes and mature adipocytes.* Matrix Biol. **26**:419-430.

184. Allingham, P.G., Brownlee, G.R., Harper, G.S., Pho, M., Nilsson, S.K., and Brown, T.J. (2006) *Gene expression, synthesis and degradation of hyaluronan during differentiation of 3T3-L1 adipocytes.* Arch Biochem Biophys. **452**:83-91.

185. Ji, E., Jung, M.Y., Park, J.H., Kim, S., Seo, C.R., Park, K.W., Lee, E.K., Yeom, C.H., and Lee, S. (2014) *Inhibition of adipogenesis in 3T3-L1 cells and suppression of abdominal fat accumulation in high-fat diet-feeding C57BL/6J mice after downregulation of hyaluronic acid.* Int J Obes (Lond). **38**:1035-1043.

186. Spiegelman, B.M., Choy, L., Hotamisligil, G.S., Graves, R.A., and Tontonoz, P. (1993) *Regulation of adipocyte gene expression in differentiation and syndromes of obesity/diabetes.* J Biol Chem. **268**:6823-6826.

187. Singh, P., Carraher, C., and Schwarzbauer, J.E. (2010) *Assembly of fibronectin extracellular matrix.* Annu Rev Cell Dev Biol. **26**:397-419.

188. Chun, T.H., Hotary, K.B., Sabeh, F., Saltiel, A.R., Allen, E.D., and Weiss, S.J. (2006) *A pericellular collagenase directs the 3-dimensional development of white adipose tissue.* Cell. **125**:577-591.

189. Monslow, J., Govindaraju, P., and Pure, E. (2015) *Hyaluronan - a functional and structural sweet spot in the tissue microenvironment.* Front Immunol. **6**:231.

190. Wu, Y.J., La Pierre, D.P., Wu, J., Yee, A.J., and Yang, B.B. (2005) *The interaction of versican with its binding partners.* Cell Res. **15**:483-494.

191. Takahashi, N., Knudson, C.B., Thankamony, S., Ariyoshi, W., Mellor, L., Im, H.J., and Knudson, W. (2010) *Induction of CD44 cleavage in articular chondrocytes.* Arthritis Rheum. **62**:1338-1348.

192. Brooks, S.C., Locke, E.R., and Soule, H.D. (1973) *Estrogen receptor in a human cell line (MCF-7) from breast carcinoma.* J Biol Chem. **248**:6251-6253.

193. Reznikoff, C.A., Brankow, D.W., and Heidelberger, C. (1973) *Establishment and characterization of a cloned line of C3H mouse embryo cells sensitive to postconfluence inhibition of division.* Cancer Res. **33**:3231-3238.

194. Heremans, H., Billiau, A., Cassiman, J.J., Mulier, J.C., and de Somer, P. (1978) *In vitro cultivation of human tumor tissues. II. Morphological and virological characterization of three cell lines.* Oncology. **35**:246-252.

195. Billiau, A., Edy, V.G., Heremans, H., Van Damme, J., Desmyter, J., Georgiades, J.A., and De Somer, P. (1977) *Human interferon: mass production in a newly established cell line, MG-63.* Antimicrob Agents Chemother. **12**:11-15.

196. Kimura, J.H., Hardingham, T.E., Hascall, V.C., and Solursh, M. (1979) *Biosynthesis of proteoglycans and their assembly into aggregates in cultures of chondrocytes from the Swarm rat chondrosarcoma.* J Biol Chem. **254**:2600-2609.

197. Choi, H.U., Meyer, K., and Swarm, R. (1971) *Mucopolysaccharide and protein--polysaccharide of a transplantable rat chondrosarcoma.* Proc Natl Acad Sci U S A. **68**:877-879.

198. Kucharska, A.M., Kuettner, K.E., and Kimura, J.H. (1990) *Biochemical characterization of long-term culture of the Swarm rat chondrosarcoma chondrocytes in agarose.* J Orthop Res. **8**:781-792.

199. Eaker, S.S., Hawley, T.S., Ramezani, A., and Hawley, R.G. (2004) *Detection and enrichment of hematopoietic stem cells by side population phenotype.* Methods Mol Biol. **263**:161-180.

200. Wang, Y., Yin, C., Feng, L., Ma, L., Wei, Y., and Sheng, G. (2013) *Sorting, identification and enrichment of side population cells in THP-1 acute monocytic leukemia cells.* Oncol Rep. **29**:1923-1931.

201. Williams, R., Khan, I.M., Richardson, K., Nelson, L., McCarthy, H.E., Analbelsi, T., Singhrao, S.K., Dowthwaite, G.P., Jones, R.E., Baird, D.M., Lewis, H., Roberts, S., Shaw, H.M., Dudhia, J., Fairclough, J., Briggs, T., and Archer, C.W. (2010) *Identification and clonal characterisation of a progenitor cell sub-population in normal human articular cartilage.* PLoS One. **5**:e13246.

202. Jones, P.H. and Watt, F.M. (1993) *Separation of human epidermal stem cells from transit amplifying cells on the basis of differences in integrin function and expression.* Cell. **73**:713-724.

203. Lee, H.G. and Cowman, M.K. (1994) *An agarose gel electrophoretic method for analysis of hyaluronan molecular weight distribution.* Anal Biochem. **219**:278-287.

204. Jain, R.G., Andrews, L.G., McGowan, K.M., Pekala, P.H., and Keene, J.D. (1997) *Ectopic expression of Hel-N1, an RNA-binding protein, increases glucose transporter (GLUT1) expression in 3T3-L1 adipocytes.* Mol Cell Biol. **17**:954-962.

205. Stephens, J.M. and Pekala, P.H. (1991) *Transcriptional repression of the GLUT4 and C/EBP genes in 3T3-L1 adipocytes by tumor necrosis factor-alpha.* J Biol Chem. **266**:21839-21845.

206. Ahrens, P.B., Solursh, M., and Reiter, R.S. (1977) *Stage-related capacity for limb chondrogenesis in cell culture.* Dev Biol. **60**:69-82.

207. Maleski, M.P. and Knudson, C.B. (1996) *Hyaluronan-mediated aggregation of limb bud mesenchyme and mesenchymal condensation during chondrogenesis.* Exp Cell Res. **225**:55-66.

208. Roux, C., Pisani, D.F., Yahia, H.B., Djedaini, M., Beranger, G.E., Chambard, J.C., Ambrosetti, D., Michiels, J.F., Breuil, V., Ailhaud, G., Euller-Ziegler, L., and Amri, E.Z. (2013) *Chondrogenic potential of stem cells derived from adipose tissue: a powerful pharmacological tool.* Biochem Biophys Res Commun. **440**:786-791.

209. Ibrahim, A.M., Elgharabawi, N.M., Makhlouf, M.M., and Ibrahim, O.Y. (2015) *Chondrogenic differentiation of human umbilical cord blood-derived mesenchymal stem cells in vitro.* Microsc Res Tech. **78**:667-675.

210. Cao, B., Li, Z., Peng, R., and Ding, J. (2015) *Effects of cell-cell contact and oxygen tension on chondrogenic differentiation of stem cells.* Biomaterials. **64**:21-32.

211. Knudson, W., Casey, B., Nishida, Y., Eger, W., Kuettner, K.E., and Knudson, C.B. (2000) *Hyaluronan oligosaccharides perturb cartilage matrix homeostasis and induce chondrocytic chondrolysis.* Arthritis Rheum. **43**:1165-1174.

212. Rasmussen, T.B., Uttenthal, A., de Stricker, K., Belak, S., and Storgaard, T. (2003) *Development of a novel quantitative real-time RT-PCR assay for the simultaneous detection of all serotypes of foot-and-mouth disease virus.* Arch Virol. **148**:2005-2021.

213. Livak, K.J. and Schmittgen, T.D. (2001) *Analysis of relative gene expression data using real-time quantitative PCR and the 2(-Delta Delta C(T)) Method.* Methods. **25**:402-408.

214. Luo, N., Knudson, W., Askew, E.B., Veluci, R., and Knudson, C.B. (2014) *CD44 and hyaluronan promote the bone morphogenetic protein 7 signaling response in murine chondrocytes.* Arthritis Rheumatol. **66**:1547-1558.

215. Jackson, K.A., Majka, S.M., Wang, H., Pocius, J., Hartley, C.J., Majesky, M.W., Entman, M.L., Michael, L.H., Hirschi, K.K., and Goodell, M.A. (2001) *Regeneration of ischemic cardiac muscle and vascular endothelium by adult stem cells.* J Clin Invest. **107**:1395-1402.

216. Shimano, K., Satake, M., Okaya, A., Kitanaka, J., Kitanaka, N., Takemura, M., Sakagami, M., Terada, N., and Tsujimura, T. (2003) *Hepatic oval cells have the side population phenotype defined by expression of ATP-binding cassette transporter ABCG2/BCRP1.* Am J Pathol. **163**:3-9.

217. Majka, S.M., Beutz, M.A., Hagen, M., Izzo, A.A., Voelkel, N., and Helm, K.M. (2005) *Identification of novel resident pulmonary stem cells: form and function of the lung side population.* Stem Cells. **23**:1073-1081.

218. Yano, S., Ito, Y., Fujimoto, M., Hamazaki, T.S., Tamaki, K., and Okochi, H. (2005) *Characterization and localization of side population cells in mouse skin.* Stem Cells. **23**:834-841.

219. Ergen, A.V., Jeong, M., Lin, K.K., Challen, G.A., and Goodell, M.A. (2013) *Isolation and characterization of mouse side population cells.* Methods Mol Biol. **946**:151-162.

220. Calcagno, A.M., Salcido, C.D., Gillet, J.P., Wu, C.P., Fostel, J.M., Mumau, M.D., Gottesman, M.M., Varticovski, L., and Ambudkar, S.V. (2010) *Prolonged drug selection of breast cancer cells and enrichment of cancer stem cell characteristics.* J Natl Cancer Inst. **102**:1637-1652.

221. Ashkani-Esfahani, S., Hosseinabadi, O.K., Moezzi, P., Moafpourian, Y., Kardeh, S., Rafiee, S., Fatheazam, R., Noorafshan, A., Nadimi, E., Mehrvarz, S., Khoshneviszadeh, M., and Khoshneviszadeh, M. (2016) *Verapamil, a calcium-channel blocker, improves the wound healing process in rats with excisional full-thickness skin wounds based on stereological parameters.* Adv Skin Wound Care. **29**:271-274.

222. Goodell, M.A., Brose, K., Paradis, G., Conner, A.S., and Mulligan, R.C. (1996) *Isolation and functional properties of murine hematopoietic stem cells that are replicating in vivo.* J Exp Med. **183**:1797-1806.

223. Benya, P.D. and Shaffer, J.D. (1982) *Dedifferentiated chondrocytes reexpress the differentiated collagen phenotype when cultured in agarose gels.* Cell. **30**:215-224.

224. McSheehy, P.M. and Chambers, T.J. (1986) *Osteoblast-like cells in the presence of parathyroid hormone release soluble factor that stimulates osteoclastic bone resorption.* Endocrinology. **119**:1654-1659.

225. Green, H. and Kehinde, O. (1975) *An established preadipose cell line and its differentiation in culture. II. Factors affecting the adipose conversion.* Cell. **5**:19-27.

226. Goodell, M.A., Rosenzweig, M., Kim, H., Marks, D.F., DeMaria, M., Paradis, G., Grupp, S.A., Sieff, C.A., Mulligan, R.C., and Johnson, R.P. (1997) *Dye efflux studies suggest that hematopoietic stem cells expressing low or undetectable levels of CD34 antigen exist in multiple species.* Nat Med. **3**:1337-1345.

227. Taylor, S.M. and Jones, P.A. (1979) *Multiple new phenotypes induced in 10T1/2 and 3T3 cells treated with 5-azacytidine.* Cell. **17**:771-779.

228. Green, H. and Kehinde, O. (1976) *Spontaneous heritable changes leading to increased adipose conversion in 3T3 cells.* Cell. **7**:105-113.

229. Rubin, C.S., Hirsch, A., Fung, C., and Rosen, O.M. (1978) *Development of hormone receptors and hormonal responsiveness in vitro. Insulin receptors and insulin sensitivity in the preadipocyte and adipocyte forms of 3T3-L1 cells.* J Biol Chem. **253**:7570-7578.

230. Smas, C.M. and Sul, H.S. (1997) *Molecular mechanisms of adipocyte differentiation and inhibitory action of pref-1.* Crit Rev Eukaryot Gene Expr. **7**:281-298.

231. Derby, M.A. and Pintar, J.E. (1978) *The histochemical specificity of Streptomyces hyaluronidase and chondroitinase ABC.* Histochem J. **10**:529-547.

232. Spicer, A.P., Olson, J.S., and McDonald, J.A. (1997) *Molecular cloning and characterization of a cDNA encoding the third putative mammalian hyaluronan synthase.* J Biol Chem. **272**:8957-8961.

233. Kosaki, R., Watanabe, K., and Yamaguchi, Y. (1999) *Overproduction of hyaluronan by expression of the hyaluronan synthase Has2 enhances anchorage-independent growth and tumorigenicity.* Cancer Res. **59**:1141-1145.

234. Kudo, D., Kon, A., Yoshihara, S., Kakizaki, I., Sasaki, M., Endo, M., and Takagaki, K. (2004) *Effect of a hyaluronan synthase suppressor, 4-methylumbelliferone, on B16F-10 melanoma cell adhesion and locomotion.* Biochem Biophys Res Commun. **321**:783-787.

235. Nakamura, T., Takagaki, K., Shibata, S., Tanaka, K., Higuchi, T., and Endo, M. (1995) *Hyaluronic-acid-deficient extracellular matrix induced by addition of 4-methylumbelliferone to the medium of cultured human skin fibroblasts.* Biochem Biophys Res Commun. **208**:470-475.

236. Dastagir, K., Reimers, K., Lazaridis, A., Jahn, S., Maurer, V., Strauss, S., Dastagir, N., Radtke, C., Kampmann, A., Bucan, V., and Vogt, P.M. (2014) *Murine embryonic fibroblast cell lines differentiate into three mesenchymal lineages to different extents: new models to investigate differentiation processes.* Cell Reprogram. **16**:241-252.

237. Shao, H.Y., Hsu, H.Y., Wu, K.S., Hee, S.W., Chuang, L.M., and Yeh, J.I. (2013) *Prolonged induction activates Cebpalpha independent adipogenesis in NIH/3T3 cells.* PLoS One. **8**:e51459.

238. Schurman, D.J. and Smith, R.L. (2004) *Osteoarthritis: current treatment and future prospects for surgical, medical, and biologic intervention.* Clin Orthop Relat Res. **427**:S183-189.

239. Yu, Y., Zheng, H., Buckwalter, J.A., and Martin, J.A. (2014) *Single cell sorting identifies progenitor cell population from full thickness bovine articular cartilage.* Osteoarthritis Cartilage. **22**:1318-1326.

240. Williams, R.J., 3rd and Harnly, H.W. (2007) *Microfracture: indications, technique, and results.* Instr Course Lect. **56**:419-428.

241. Teramura, T., Fukuda, K., Kurashimo, S., Hosoi, Y., Miki, Y., Asada, S., and Hamanishi, C. (2008) *Isolation and characterization of side population stem cells in articular synovial tissue.* BMC Musculoskelet Disord. **9**:86.

242. Zhou, S., Schuetz, J.D., Bunting, K.D., Colapietro, A.M., Sampath, J., Morris, J.J., Lagutina, I., Grosveld, G.C., Osawa, M., Nakauchi, H., and Sorrentino, B.P. (2001) *The ABC transporter Bcrp1/ABCG2 is expressed in a wide variety of stem cells and is a molecular determinant of the side-population phenotype.* Nat Med. **7**:1028-1034.

243. Bhattacharya, S., Das, A., Mallya, K., and Ahmad, I. (2007) *Maintenance of retinal stem cells by Abcg2 is regulated by notch signaling.* J Cell Sci. **120**:2652-2662.

244. Apati, A., Orban, T.I., Varga, N., Nemeth, A., Schamberger, A., Krizsik, V., Erdelyi-Belle, B., Homolya, L., Varady, G., Padanyi, R., Karaszi, E., Kemna, E.W., Nemet, K., and Sarkadi, B. (2008) *High level functional expression of the ABCG2 multidrug transporter in undifferentiated human embryonic stem cells.* Biochim Biophys Acta. **1778**:2700-2709.

245. Kon, E., Verdonk, P., Condello, V., Delcogliano, M., Dhollander, A., Filardo, G., Pignotti, E., and Marcacci, M. (2009) *Matrix-assisted autologous chondrocyte transplantation for the repair of cartilage defects of the knee: systematic clinical data review and study quality analysis.* Am J Sports Med. **37 Suppl 1**:156S-166S.

246. Nehrer, S., Domayer, S., Dorotka, R., Schatz, K., Bindreiter, U., and Kotz, R. (2006) *Three-year clinical outcome after chondrocyte transplantation using a hyaluronan matrix for cartilage repair.* Eur J Radiol. **57**:3-8.

247. Nelson, L., McCarthy, H.E., Fairclough, J., Williams, R., and Archer, C.W. (2014) *Evidence of a viable pool of stem cells within human osteoarthritic cartilage.* Cartilage. **5**:203-214.

248. Marcus, P., De Bari, C., Dell'Accio, F., and Archer, C.W. (2014) *Articular chondroprogenitor cells maintain chondrogenic potential but fail to form a functional matrix when implanted into muscles of SCID mice.* Cartilage. **5**:231-240.

249. Jiang, Y., Jahagirdar, B.N., Reinhardt, R.L., Schwartz, R.E., Keene, C.D., Ortiz-Gonzalez, X.R., Reyes, M., Lenvik, T., Lund, T., Blackstad, M., Du, J., Aldrich, S., Lisberg, A., Low, W.C., Largaespada, D.A., and Verfaillie, C.M. (2002) *Pluripotency of mesenchymal stem cells derived from adult marrow.* Nature. **418**:41-49.

250. Alsalameh, S., Amin, R., Gemba, T., and Lotz, M. (2004) *Identification of mesenchymal progenitor cells in normal and osteoarthritic human articular cartilage.* Arthritis Rheum. **50**:1522-1532.

251. Denker, A.E., Haas, A.R., Nicoll, S.B., and Tuan, R.S. (1999) *Chondrogenic differentiation of murine C3H10T1/2 multipotential mesenchymal cells: I. Stimulation by bone morphogenetic protein-2 in high-density micromass cultures.* Differentiation. **64**:67-76.

252. Clover, J. and Gowen, M. (1994) *Are MG-63 and HOS TE85 human osteosarcoma cell lines representative models of the osteoblastic phenotype?* Bone. **15**:585-591.

253. Yang, L., Tsang, K.Y., Tang, H.C., Chan, D., and Cheah, K.S. (2014) *Hypertrophic chondrocytes can become osteoblasts and osteocytes in endochondral bone formation.* Proc Natl Acad Sci U S A. **111**:12097-12102.

254. Zhou, X., von der Mark, K., Henry, S., Norton, W., Adams, H., and de Crombrugghe, B. (2014) *Chondrocytes transdifferentiate into osteoblasts in endochondral bone during development, postnatal growth and fracture healing in mice.* PLoS Genet. **10**:e1004820.

255. Tian, X., Azpurua, J., Hine, C., Vaidya, A., Myakishev-Rempel, M., Ablaeva, J., Mao, Z., Nevo, E., Gorbunova, V., and Seluanov, A. (2013) *High-molecular-mass hyaluronan mediates the cancer resistance of the naked mole rat.* Nature. **499**:346-349.

256. Luo, W., Guo, C., Zheng, J., Chen, T.L., Wang, P.Y., Vertel, B.M., and Tanzer, M.L. (2000) *Aggrecan from start to finish.* J Bone Miner Metab. **18**:51-56.

257. Bode-Lesniewska, B., Dours-Zimmermann, M.T., Odermatt, B.F., Briner, J., Heitz, P.U., and Zimmermann, D.R. (1996) *Distribution of the large aggregating proteoglycan versican in adult human tissues.* J Histochem Cytochem. **44**:303-312.

258. Zimmermann, D.R., Dours-Zimmermann, M.T., Schubert, M., and Bruckner-Tuderman, L. (1994) *Versican is expressed in the proliferating zone in the epidermis and in association with the elastic network of the dermis.* J Cell Biol. **124**:817-825.

259. Kimata, K., Oike, Y., Tani, K., Shinomura, T., Yamagata, M., Uritani, M., and Suzuki, S. (1986) *A large chondroitin sulfate proteoglycan (PG-M) synthesized before chondrogenesis in the limb bud of chick embryo.* J Biol Chem. **261**:13517-13525.

260. Shinomura, T., Jensen, K.L., Yamagata, M., Kimata, K., and Solursh, M. (1990) *The distribution of mesenchyme proteoglycan (PG-M) during wing bud outgrowth.* Anat Embryol (Berl). **181**:227-233.

261. Shepard, J.B., Krug, H.A., LaFoon, B.A., Hoffman, S., and Capehart, A.A. (2007) *Versican expression during synovial joint morphogenesis.* Int J Biol Sci. **3**:380-384.

262. Kosher, R.A. and Savage, M.P. (1981) *Glycosaminoglycan synthesis by the apical ectodermal ridge of chick limb bud.* Nature. **291**:231-232.

263. Dragoo, J.L., Carlson, G., McCormick, F., Khan-Farooqi, H., Zhu, M., Zuk, P.A., and Benhaim, P. (2007) *Healing full-thickness cartilage defects using adipose-derived stem cells.* Tissue Eng. **13**:1615-1621.

264. Fraser, J.R., Laurent, T.C., and Laurent, U.B. (1997) *Hyaluronan: its nature, distribution, functions and turnover.* J Intern Med. **242**:27-33.

265. Balazs, E.A., Watson, D., Duff, I.F., and Roseman, S. (1967) *Hyaluronic acid in synovial fluid. I. Molecular parameters of hyaluronic acid in normal and arthritis human fluids.* Arthritis Rheum. **10**:357-376.

266. Sironen, R.K., Tammi, M., Tammi, R., Auvinen, P.K., Anttila, M., and Kosma, V.M. (2011) *Hyaluronan in human malignancies.* Exp Cell Res. **317**:383-391.

267. Sherman, L., Sleeman, J., Herrlich, P., and Ponta, H. (1994) *Hyaluronate receptors: key players in growth, differentiation, migration and tumor progression.* Curr Opin Cell Biol. **6**:726-733.

268. Kujawa, M.J., Carrino, D.A., and Caplan, A.I. (1986) *Substrate-bonded hyaluronic acid exhibits a size-dependent stimulation of chondrogenic differentiation of stage 24 limb mesenchymal cells in culture.* Dev Biol. **114**:519-528.

269. Merrilees, M.J., Zuo, N., Evanko, S.P., Day, A.J., and Wight, T.N. (2016) *G1 domain of versican regulates hyaluronan organization and the phenotype of cultured human dermal fibroblasts.* J Histochem Cytochem. **64**:353-363.

270. Shinomura, T., Nishida, Y., Ito, K., and Kimata, K. (1993) *cDNA cloning of PG-M, a large chondroitin sulfate proteoglycan expressed during chondrogenesis in chick limb buds. Alternative spliced multiforms of PG-M and their relationships to versican.* J Biol Chem. **268**:14461-14469.

271. Hudson, K.S., Andrews, K., Early, J., Mjaatvedt, C.H., and Capehart, A.A. (2010) *Versican G1 domain and V3 isoform overexpression results in increased chondrogenesis in the developing chick limb in ovo.* Anat Rec (Hoboken). **293**:1669-1678.

272. Meyer-Puttlitz, B., Milev, P., Junker, E., Zimmer, I., Margolis, R.U., and Margolis, R.K. (1995) *Chondroitin sulfate and chondroitin/keratan sulfate proteoglycans of nervous tissue: developmental changes of neurocan and phosphacan.* J Neurochem. **65**:2327-2337.

273. Matsumoto, K., Shionyu, M., Go, M., Shimizu, K., Shinomura, T., Kimata, K., and Watanabe, H. (2003) *Distinct interaction of versican/PG-M with hyaluronan and link protein.* J Biol Chem. **278**:41205-41212.

274. Soukas, A., Socci, N.D., Saatkamp, B.D., Novelli, S., and Friedman, J.M. (2001) *Distinct transcriptional profiles of adipogenesis in vivo and in vitro.* J Biol Chem. **276**:34167-34174.

275. Gregoire, F.M., Smas, C.M., and Sul, H.S. (1998) *Understanding adipocyte differentiation.* Physiol Rev. **78**:783-809.

276. Underhill, C.B., Green, S.J., Comoglio, P.M., and Tarone, G. (1987) *The hyaluronate receptor is identical to a glycoprotein of Mr 85,000 (gp85) as shown by a monoclonal antibody that interferes with binding activity.* J Biol Chem. **262**:13142-13146.

277. Underhill, C.B., Chi-Rosso, G., and Toole, B.P. (1983) *Effects of detergent solubilization on the hyaluronate-binding protein from membranes of simian virus 40-transformed 3T3 cells.* J Biol Chem. **258**:8086-8091.

278. Knudson, w., Casey, B., Nishida, Y., Eger, W., Kuettner, K.E., and Knudson, C.B. (2000) *Hyaluronan oligosaccharides perturb cartilage matrix homeostasis and induce chondrocytic chondrolysis.* Arthritis Rheum. **43**:1165-1174.

279. Jiang, H., Peterson, R.S., Wang, W., Bartnik, E., Knudson, C.B., and Knudson, W. (2002) *A requirement for the CD44 cytoplasmic domain for hyaluronan binding, pericellular matrix assembly, and receptor-mediated endocytosis in COS-7 cells.* J Biol Chem. **277**:10531-10538.

280. Knudson, W., Bartnik, E., and Knudson, C.B. (1993) *Assembly of pericellular matrices by COS-7 cells transfected with CD44 lymphocyte-homing receptor genes.* Proc Natl Acad Sci U S A. **90**:4003-4007.

281. Kultti, A., Pasonen-Seppanen, S., Jauhiainen, M., Rilla, K.J., Karna, R., Pyoria, E., Tammi, R.H., and Tammi, M.I. (2009) *4-Methylumbelliferone inhibits hyaluronan synthesis by depletion of cellular UDP-glucuronic acid and downregulation of hyaluronan synthase 2 and 3.* Exp Cell Res. **315**:1914-1923.

282. Evanko, S.P., Potter-Perigo, S., Petty, L.J., Workman, G.A., and Wight, T.N. (2015) *Hyaluronan controls the deposition of fibronectin and collagen and modulates TGF-beta1 induction of lung myofibroblasts.* Matrix Biol. **42**:74-92.

283. Webber, J., Jenkins, R.H., Meran, S., Phillips, A., and Steadman, R. (2009) *Modulation of TGFbeta1-dependent myofibroblast differentiation by hyaluronan.* Am J Pathol. **175**:148-160.

284. Bourguignon, L.Y., Singleton, P.A., Zhu, H., and Zhou, B. (2002) *Hyaluronan promotes signaling interaction between CD44 and the transforming growth factor beta receptor I in metastatic breast tumor cells.* J Biol Chem. **277**:39703-39712.

285. Underhill, C.B. and Toole, B.P. (1979) *Binding of hyaluronate to the surface of cultured cells.* J Cell Biol. **82**:475-484.

286. Knudson, C.B., Nofal, G.A., Pamintuan, L., and Aguiar, D.J. (1999) *The chondrocyte pericellular matrix: a model for hyaluronan-mediated cell-matrix interactions.* Biochem Soc Trans. **27**:142-147.

287. McCourt, P.A., Ek, B., Forsberg, N., and Gustafson, S. (1994) *Intercellular adhesion molecule-1 is a cell surface receptor for hyaluronan.* J Biol Chem. **269**:30081-30084.

288. Zhou, B., Weigel, J.A., Fauss, L., and Weigel, P.H. (2000) *Identification of the hyaluronan receptor for endocytosis (HARE).* J Biol Chem. **275**:37733-37741.

289. Culty, M., Nguyen, H.A., and Underhill, C.B. (1992) *The hyaluronan receptor (CD44) participates in the uptake and degradation of hyaluronan.* J Cell Biol. **116**:1055-1062.

290. Musil, K.J., Malmstrom, A., and Donner, J. (1991) *Alteration of proteoglycan metabolism during the differentiation of 3T3-L1 fibroblasts into adipocytes.* J Cell Biol. **114**:821-826.

291. Kubo, Y., Kaidzu, S., Nakajima, I., Takenouchi, K., and Nakamura, F. (2000) *Organization of extracellular matrix components during differentiation of adipocytes in long-term culture.* In Vitro Cell Dev Biol Anim. **36**:38-44.

292. Heldin, C.H., Miyazono, K., and ten Dijke, P. (1997) *TGF-beta signalling from cell membrane to nucleus through SMAD proteins.* Nature. **390**:465-471.

APPENDIX A: Biological Safety Protocol

The Brody School of Medicine
Office of Prospective Health
East Carolina University
188 Warren Life Sciences Building • Greenville, NC 27834
252-744-2070 office • 252-744-2417 fax

EAST CAROLINA UNIVERSITY

Occupational Medicine
Employee Health
Radiation Safety
Infection Control
Biological Safety

TO: Dr. Cheryl B Knudson
Department Anatomy and Cell Biology

FROM: Eddie Johnson
Chad Spruill CJS
Biological Safety Officers

RE: Registration Final Approval

Date: February 11, 2016

Your Biological Safety Protocol, Knudson C, 09-01; 12-01; 15-01, **Hyaluronan-Cell Interactions in Cartilage** has received **final approval** to be conducted at Biosafety Level in based on your registration/revisions submitted,

using: A. Biohazards

- ☐ Infectious Agent(s)
- ☐ Biotoxin(s)
- ☐ Allergen(s)
- ☐ Prion(s)
- ☒ Human blood, fluid, cells, tissue or cell cultures
- ☐ Transformed cells
- ☐ Other

and/or B. ☒ NIH Use of Recombinant DNA (or RNA) molecules, microorganisms use or breeding transgenic or techniques (plasmids, viral vectors, transfection); of transgenic animals or plants at NIH Category III-F.

This approval is effective for a period of 3 years and may be renewed with an updated registration if needed at that time. Your laboratory will be inspected periodically (every 1-3 years) depending upon the materials/techniques used.

Please notify the Animal Care staff before beginning work with Biohazard agents in animals. Also please keep in mind all individuals who will be exposed to or handle human-derived biohazardous agents will be due for Blood Borne Pathogens refresher training annually.

Please do not hesitate to contact Biological Safety at 744-2070 if you have any questions, concerns, or need any additional information. Best wishes on your research.

cc: Dr. Jeff Smith, Chair, Biosafety Committee
Janine Davenport, IACUC
Dale Aycock, Comparative Medicine

East Carolina University
The Brody School of Medicine • Department of Anatomy and Cell Biology
7N-100 Brody Medical Sciences Building • 600 Moye Boulevard • Greenville, NC 27834
252-744-2849 office • **252-744-2850** fax • **http://www.ecu.edu/anatomy/**

May 12, 2015

To: Office of Prospective Health
Brody School of Medicine, East Carolina University

From: Cheryl B Knudson, Ph.D., PI
Department of Anatomy and Cell Biology
Brody School of Medicine

RE: Changes in Personnel
Biological Safety Registration, Protocol Knudson 09-01; 12-01
Hyaluronan-Cell Interactions in Cartilage
Laboratory Location(s): Brody 7E-118, 7N-94, 7N-86, 7W-39A

Laboratory Personnel:

Remaining the same:
Cheryl B. Knudson, PI
Warren Knudson, co-PI
Joan Zary Oswald
Emily Askew, Ph.D., Investigator

Personnel to be added:
Karen Michelle Cobb
Samantha Sellers
Shinya Ishizuka

Personnel to be Removed: (no longer working at ECU)
Kayla Britton
Yohei Ohno
Roberta Veluci

All three of the individuals to be added have had lab-specific training and have demonstrated proficiency on use of the agents and procedure-specific laboratory safety practices and containment procedures and precautions for the Biosafety Level 2. They also have completed the Blood Borne Pathogens Training in 2015. Please contact me if you need any additional information.

Sincerely yours,